Electrodynamics of high-T_c superconductors

D. N. Basov

Department of Physics, University of California San Diego, La Jolla, California 92093-0319, USA

T. Timusk

Department of Physics and Astronomy, McMaster University, Hamilton, Ontario, Canada L8S 4M1

(Published 26 August 2005)

Recent studies of the electromagnetic response of high-T_c superconductors using terahertz, infrared, and optical spectroscopies are reviewed. In combination these experimental techniques provide a comprehensive picture of the low-energy excitations and charge dynamics in this class of materials. These results are discussed with an emphasis on conceptual issues, including evolution of the electronic spectral weight in doped Mott-Hubbard insulators, the *d*-wave superconducting energy gap and the normal-state pseudogap, anisotropic superfluid response, electronic phase segregation, emergence of coherent electronic state as a function of both temperature and doping, the vortex state, and the energetics of the superconducting transition. Because the theoretical understanding of these issues is still evolving the review is focused on the analysis of the universal trends that are emerging out of a large body of work carried on by many research teams. Where possible data generated by infrared/optical techniques are compared with the data from other spectroscopic and transport methods.

CONTENTS

I. INTRODUCTION

The phenomenon of high-temperature superconductivity in the cuprate perovskites (Bednorz and Müller, 1986) has been at the focus of condensed-matter physics for nearly 20 years. Despite an unprecedented effort the central issue—the mechanism of high-T_c superconductivity—still remains unsolved.

Several important experimental advances have led to a deeper understanding of these complex materials. Over the past decade the research has been dominated by experiments on well-characterized specimens afforded by immense progress in crystal preparation using both better inert crucibles for flux growth and optical floating zone furnaces. High-quality crystals and crystalline films have been characterized by a comprehensive set of experimental tools. Available spectroscopic data generated with complementary probes provide a detailed experimental picture of excitations as a function of both frequency and momentum.

Spectroscopic studies of electrodynamics are emerging as the premier experimental tool of high-T_c superconductivity. In combination, terahertz (THz) and infrared (IR) and/or optical methods make possible experimental access to the optical constants in the frequency range critical for the understanding of physics underlying strongly correlated phenomena in solids. Optical spectroscopy of metals and semiconductors has provided invaluable insights into their electronic band structure and elementary excitations. The validity of theoretical descriptions of electronic bands in solids as well as of electron dynamics is routinely verified against optical data. Moreover, in situations where the theoretical guidance for data interpretation is insufficient, quantitative information can still be extracted from the spectroscopic measurements through model-independent analysis of optical constants based on a variety of sum rules (Sec. IV.E). This latter forte of the IR/optical approach is indispensable for high-T_c research, since properties of these novel superconductors signal a breakdown of standard theories of metals. Therefore a knowledge of the optical constants establishes an experimental foundation for crucial tests of proposed models and also motivates the development of novel theoretical constructs. THz-IR and/or optical results generated by many research teams worldwide facilitate inference of universal patterns in the electromagnetic response of high-T_c cuprates that are not specific to a particular family of materials but instead reflect intrinsic properties of the CuO_2 planes along with genuine features of the interplane conductivity. The primary goal of this review is to present an analysis of the generic trends seen in the optical constants.

The parent, undoped, compounds of high-T_c cuprates are *Mott-Hubbard* (MH) *insulators*. When a moderate density of charge carriers is introduced into a MH system, all of its physical properties are radically modified. This leads to complex phase diagrams that have been methodically studied in many materials using THz and/or IR optics (Sec. II.A). This work has uncovered common attributes of the cuprates and other classes of MH insulators (Imada *et al.*, 1998). One region of the phase diagram that has captured unparalleled attention is the so-called pseudogap state realized primarily in moderately doped materials with a T_c lower than $T_{c,\max}$ for a given series (Timusk and Statt, 1999). A variety of physical probes reveal a captivating feature of this state, a partial or incomplete gap already in the normal state that resembles the superconducting gap, in both magnitude and symmetry, leading to a view accepted by many theorists and experimentalists that the origin of the pseudogap may be intimately related to superconducting pairing at $T > T_c$. An alternate point of view holds that the pseudogap represents a state that competes with superconductivity. Infrared spectroscopy has an outstanding track record in probing various gapped states in solids, and this research has provided important contributions to the experimental picture of the pseudogap state in cuprates (Sec. VII).

The region in the phase diagram that yields the highest superconducting transition temperatures, the optimal doping region, is also the region with the most unconventional electromagnetic properties. Also termed the strange-metal region it is characterized by unusual power-law behaviors of most of the optical constants. At higher doping levels (the so-called overdoped regime) the systems are similar to ordinary metals in many respects while at lower doping levels they are dominated by the pseudogap and two-component behavior. This transition region has been discussed in terms of a quantum critical point near optimal doping (Sec. VII).

Underdoped cuprates are characterized by the appearance of several crossover phenomena that signal increasing coherence of in-plane properties. These include the appearance of a bosonic resonance mode leading to a gap in the scattering rate of the in-plane currents. The resonance can be seen with a variety of probes including neutron scattering, angle-resolved photoemission (ARPES), and dc transport. However, in many ways the optical conductivity, analyzed within the picture of the extended Drude model (Secs. VII.A–VII.E), has proven to be the most informative way of studying the presence of the resonance mode in the broadest range of cuprate systems as a function of temperature and doping.

As of today, there is no generally accepted picture of the electromagnetic response of the CuO_2 planes in superconducting phases of the cuprates. Significant progress in the understanding of the carrier dynamics has been achieved starting from the perspective of Eliashberg analysis with the assumption of a strong interaction between quasiparticles and spin fluctuations. A

remarkable advantage of this approach is that it potentially provides a unified description of the complex conductivity data and results extracted from single-particle spectroscopies including tunneling and ARPES. This analysis, when applied to several cuprates, points to coupling of the charge carriers to a continuous spectrum of excitations extending to well over 0.5 eV and, at low temperatures, to the resonance mode. We shall review several aspects of the Eliashberg framework pertinent to discussion of the experimental situation in Secs. IV.B and IV.C.

It is now widely accepted that doping of MH insulators does not necessarily result in a spatially homogeneous distribution of charge carriers in a conducting phase. Instead, doping often initiates the appearance of self-organization in real space, where charge-rich regions are separated by regions with strongly depleted carrier density (Tranquada *et al.*, 1995). A particularly interesting form of this effect is the so-called stripe phase. The stripes paradigm opens new approaches to elucidate the high-T_c phenomenon in a fashion radically departing from models based on interacting quasiparticles (Emery *et al.*, 1997). The relevance of the stripes and other forms of spin/charge ordered states to electronic properties and to the phenomenon of high-temperature superconductivity itself is debated. A number of recent experimental and theoretical studies have been aimed at the investigation of the infrared and optical properties attributable to stripes (Sec. VI.C).

The normal state of high-T_c cuprates is anomalous and is not compatible with the standard treatment of excitations in terms of Landau quasiparticles. This challenges the applicability of the Bardeen-Cooper-Schrieffer (BCS) scheme, which described superconductivity in terms of the pairing instability of an ensemble of quasiparticles. Spectroscopic experiments indicate that the origin of high-T_c superconductivity may be related to lowering of the electronic kinetic energy (Basov, Woods, *et al.*, 1999; Molegraaf *et al.*, 2002) and not of the potential energy as in the conventional BCS scheme. This conclusion is inferred from subjecting the optical constants of several classes of high-T_c materials to the scrutiny of sum rules (Sec. VIII.F).

Numerous advances both in the spectroscopy of microsamples and in the preparation of high-quality single crystals have facilitated studies of the interlayer electrodynamics in many families of cuprates. These measurements provide straightforward experimental access to properties directly related to the quasi-two-dimensional nature of the electronic transport. The *c*-axis experiments probe the conductivity channels associated with single-particle and Cooper pair propagation between the CuO_2 layers. In this fashion, *c*-axis experiments offer a unique perspective on the electronic state of the CuO_2 layers that is complementary to the studies of the in-plane conductivity (Secs. VII and VIII).

Microwave studies of the electromagnetic response were instrumental in unraveling the *d*-wave nature of the order parameter in high-T_c superconductors (Hardy *et al.*, 1993), a conclusion later supported by phase-sensitive experiments. The electrodynamics of a $d_{x^2-y^2}$ superconductor is controlled by quasiparticle excitations near the nodes of the gap function. Since microwave and IR methods are sensitive to dissipative processes in a superconductor even at $T \ll T_c$, these experiments have been instrumental in exploring the details of the nodal quasiparticle dynamics under the superconducting dome in the phase diagram. These studies will be surveyed in Sec. VII.

The vortex state in high-T_c cuprates has been systematically investigated using a combination of microwave, coherent terahertz, and infrared methods in high magnetic fields. These technically demanding experiments as well as measurements of the ac Hall effect, both above and below T_c, will be reviewed in Sec. IX.

The problem of high-T_c superconductivity is arguably one of the most difficult problems in contemporary physics. It is therefore not surprising that this problem has prompted development and refinements of relevant experimental techniques. Advances in THz-IR instrumentation motivated (at least in part) by various aspects of high-T_c research include development methods suitable for low-temperature studies of microcrystals, further sophistication of the THz time-domain spectroscopy, synchrotron-based IR ellipsometry, and polarimetry in magnetic fields. A brief survey of the experimental techniques actively employed to tackle the high-T_c mystery will be presented in Sec. III.

This review is an attempt to present a snapshot of our current understanding of the electrodynamics of high-T_c cuprates. In view of the abundant literature on the subject, this review is bound to be incomplete both in terms of topics covered and references cited. We conclude this account by outlining unresolved issues.

II. UNIVERSAL TRENDS

A. Phase diagram

High-T_c superconductivity is achieved when a moderate density of electrons or holes is introduced into the parent antiferromagnetic phases of the cuprates. This is realized either by chemical substitution (e.g., $La_2CuO_4 \rightarrow La_{2-x}Sr_xCuO_4$) or by significant deviations from stoichiometry (e.g., $La_2CuO_4 \rightarrow La_{2-x}CuO_{4+\delta}$).

Both the electron- and hole-doped sides of the phase diagram displayed in Fig. 1 show a number of common elements:

(1) an antiferromagnetism in the undoped parent compound that is transformed by doping into a fairly good conducting system in the carrier density range of $n = 10^{20}-10^{21}$ cm^{-3};

(2) a critical doping level that is needed to trigger superconductivity;

(3) a transition temperature that first increases with doping (underdoped region), then reaches a maximum value for a given series (optimal doping) but is

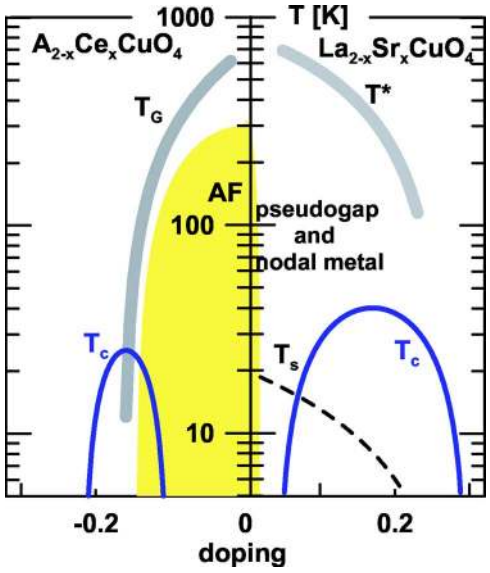

FIG. 1. (Color in online edition) Schematic phase diagram displaying characteristic temperatures for electron-doped $A_{2-x}CeCuO_4$ and its hole-doped counterpart $La_{2-x}Sr_xCuO_4$. The pseudogap temperature T^* is from Timusk and Statt (1999). A variety of experimental probes suggest that some form of spin ordering at $T<T_s$ can coexist with superconductivity for $x<0.2$ (Yamada *et al.*, 1998; Julien, 2003; Panagopoulos *et al.*, 2004). Electron-doped materials reveal the coexistence of superconductivity and long-range antiferromagnetic (AF) order (Matsuda *et al.*, 2002). T_G signifies an optical gap observed by Onose *et al.* (2001) and by Zimmers *et al.* (2004) reminiscent of the pseudogap on the hole-doped side of the phase diagram.

suppressed with further increases in the doping level (overdoped regime);

(4) a superconducting state that is preceded by the formation of the enigmatic pseudogap with an onset temperature T^* that decreases with doping;

(5) a narrow region of high in-plane coherence above the superconducting transition temperature dominated by the bosonic resonance mode.

The above features of the phase diagrams are not in dispute, with the exception of the pseudogap and the bosonic mode in electron-doped materials. Despite the fact that signatures of the pseudogap are evident in the charge response of electron-doped materials, the characteristic features of this state are yet to be observed in the magnetic properties of any of $A_{2-x}Ce_xCuO_4$ ($A=$Nd, La, Sm, Pr) compounds. The pseudogap boundary is rather blurred and its location is quite uncertain and depends on which particular experimental probe is being used (Batlogg *et al.*, 1994; Batlogg and Emery, 1996; Timusk and Statt, 1999) as well as on the particular high-T_c system. For example, while the pseudogap joins the superconducting gap at or close to optimal doping in $YBa_2Cu_3O_y$ (Y-123), it extends well into the overdoped state in $Bi_2Sr_2CaCu_2O_8$ (Bi-2212) according to Shibauchi *et al.* (2001). Part of the difficulty in locating the pseudogap boundary results from the confusion in the literature between the *pseudogap in the density of states* that occurs at a rather large temperature in the underdoped cuprates and *a pseudogap in the excitation spectrum*, which actually causes an increase in the density of states, as a result of the mass renormalization associated with a bosonic resonance mode. This lower pseudogap is not shown in Fig. 1 since it may not be generic to all cuprates (Timusk, 2003).

The region in the phase diagram below T^*, which corresponds to the onset of the depression of the NMR Knight shift at around 300 K in underdoped samples (Warren *et al.*, 1989; Yoshinari *et al.*, 1990), is generally called *the pseudogap region*. It appears to be the result of the development of a gap in the density of states. There is evidence for other, lower temperature scales that correspond to various crossover phenomena. The earliest of these is the temperature scale T_s associated with the depression in the NMR relaxation rate $1/T_1T$; see the review by Timusk and Statt (1999) and by Timusk (2003) for details. In underdoped samples T_s is a few tens of degrees above T_c, but in optimally and overdoped samples the two temperatures merge and there is only one transition at T_c. Other evidence of a highly coherent state above the superconducting transition include terahertz measurements in Bi-2212 by Corson *et al.* (1999) and the Nernst effect in La-214 of Xu *et al.* (2000) and Wang *et al.* (2001). The enhanced in-plane coherence also leads to the development of a resonance in the *c*-axis conductivity of bilayered systems, to be discussed in Sec. VII.C.

Figure 2 shows the temperature-doping phase diagram of Bi-2212 based on transport and IR measurements. The highest-temperature region designated in the diagram is the *strange-metal region* (Emery and Kivelson, 1995a, 1995b). This region is characterized by linear *ab*-plane resistivity and a linear scattering rate variation with frequency. The interplane conductivity is frequency independent in this region. The region below it is the *pseudogap region*. The resistivity in the *c*-axis direction develops a semiconducting dependence in this region, and the line separating the two regions has been based on *c*-axis transport measurements of Shibauchi *et al.* (2001). Below the pseudogap region, and just a few tens of degrees above the superconducting state, is the *coherent spin-gap region*. The dashed line separating the pseudogap region from the coherent region has been based on recent *ab*-plane infrared data by Hwang, Timusk, Puchkov, *et al.* (2004). Finally, the lowest-temperature region is that of long-range superconductivity. The line separating it from the normal state is the parabolic approximation of Presland *et al.* (1991).

In dc transport properties the pseudogap and the spin gap act differently. The pseudogap primarily affects the states near the antinode and has less effect on the nodal states which remain ungapped. The result is that the *c*-axis conductivity decreases as the pseudogap develops at T^*. The in-plane dc conductivity shows no discontinuity at this temperature but becomes anomalous below

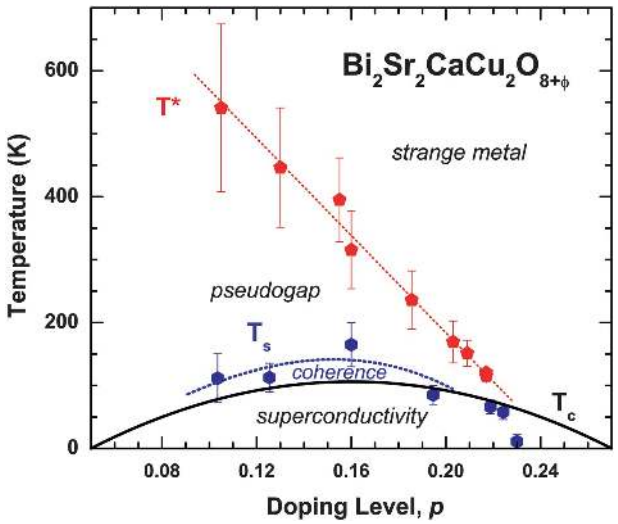

FIG. 2. (Color) The phase diagram of Bi-2212 based on transport and infrared measurements. The dashed line labeled T^* is the boundary between the high-temperature strange-metal region and the pseudogap region. Its position is based on *c*-axis transport measurements of Shibauchi *et al.* (2001). The region below it is the pseudogap region. The line denoted T_s separates the pseudogap region from the coherent region just above T_c, the superconducting transition temperature. Blue dots indicate temperature at which the resonance mode emerges in the data. Adapted from Hwang *et al.*, 2004.

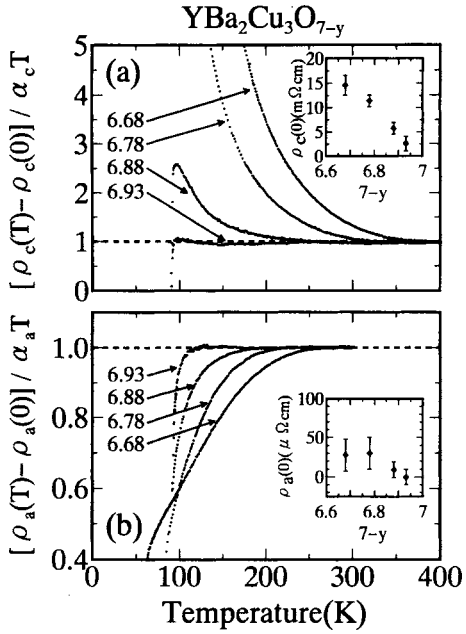

FIG. 3. The effect of the normal-state gaps on dc resistivity. The upper panel shows that the *c*-axis resistivity begins to increase at around 300 K in the sample with the lowest doping level. This is due to the formation of the pseudogap. In the same sample the *ab*-plane resistivity decreases faster than linear but at a lower temperature. This is due to the development of in-plane coherence. Insets show the doping dependence of the *c*-axis and *a*-axis resistivities. Adapted from Takenaka *et al.*, 1994.

T_s, where it begins to increase. These effects are illustrated in Fig. 3 from dc transport measurements of Takenaka *et al.* (1994). The figure shows that in these underdoped samples of Y-123 as the temperature is lowered, the *c*-axis resistivity is enhanced above the linear trend while the in-plane resistivity is suppressed.

B. Crystal structure, bonds and bands

The key structural element of all high-T_c superconductors is the set of n CuO_2 planes separated by the so-called charge reservoirs. Materials such as $La_{2-x}Sr_xCuO_4$ (La-214) and $Nd_{2-x}Sr_xCuO_4$ (Nd-214) contain one plane per unit cell and are referred to as *single-layered compounds*. The most commonly studied Bi-2212 and Y-123 systems are *double-layered systems* with $n=2$ planes per unit cell. The electron transport and processes responsible for superconductivity at high T_c are believed to be intimately connected to CuO_2 planes. Several families of cuprates can be synthesized with $n=1,2,3$. Within each given family the transition temperature increases with increasing number of layers.

In La_2CuO_4 the CuO_2 planes are formed by CuO_6 octahedra. As a result of the Jahn-Teller distortion of the octahedra, the degeneracy of the Cu *d* orbitals is partially lifted, leading to the appearance of $e_g = d_{x^2-y^2}, d_{z^2-r^2}$ and $t_{2g} = d_{xy}, d_{xz}, d_{yz}$ states. Similarly, the O $2p$ levels are also split. As a result, all Cu states hybridize with the O states. Since the $pd\sigma$ interaction is most prominent, the CuO bonding and antibonding σ states show the largest energy separation, with a complex of other bands in between (Pickett, 1989).

Local-density-approximation (LDA) calculations of the electronic band structure capture the gross features of the high-energy behavior of many cuprates (say, for $\hbar\omega > 0.5$–1 eV) (for a review see Pickett, 1989) as well as the important characteristics of the Fermi surface in doped compounds (Pickett *et al.*, 1992). However, LDA calculations fail to account for the two principal features of undoped materials: the insulating gap and the antiferromagnetic ordering. The above inconsistencies signal the breakdown of the independent-particle picture underlying the LDA. In fact, the failures of LDA-type calculations also apply to the broader class of the Mott-Hubbard insulators. Band theory ignores the on-site Coulomb repulsion U and as a consequence falsely predicts a paramagnetic metallic state in several transition-metal oxides. Since the electronic bandwidth W in many transition-metal oxides, including the cuprates, is much smaller than the magnitude of U, the conduction band splits to form a large energy gap of the order of U. The predominant role of U in defining the ground state of parent insulating compounds suggests that the doped cuprates including superconducting phases should be viewed as doped Mott-Hubbard insulators.

A more realistic view of the electronic structure of cuprates requires an account of the Cu-O charge-transfer energy. Since the energy difference between

oxygen p levels and copper d levels is much smaller than the on-site Coulomb energy, the lowest energy excitation will be of the order of the charge-transfer energy. Following the classification of Zaanen *et al.* (1985) cuprates can be characterized as charge-transfer insulators. One important accomplishment of IR and optical studies of cuprates is that they provide valuable information on the changes of the electronic structure as a result of the doping process. A detailed examination of the evolution of the optical constants with doping reveals that the absorption attributable to free carriers originates at the expense of the suppression of the charge-transfer excitations. The electronic state responsible for superconductivity appears to be made up from O $2p$ and Cu $3d$ orbitals which are separated by a charge-transfer gap in undoped systems (Orenstein, Thomas, *et al.*, 1990; Uchida *et al.*, 1991). Useful insights into the evolution of the electronic structure of doped Mott-Hubbard insulators are provided by the dynamical mean field theory (Georges *et al.*, 1996) and t-J model (Dagotto, 1994; Jaklic and Prelovsek, 2000).

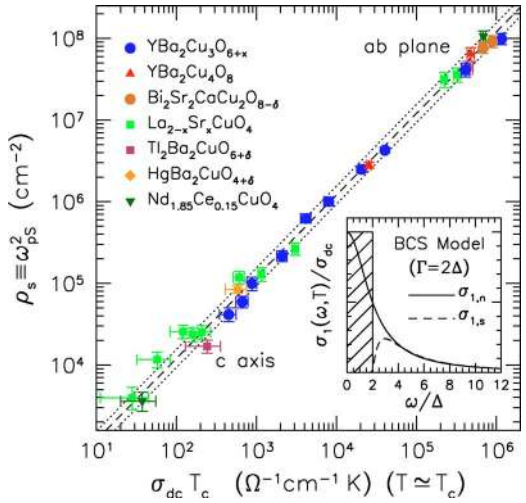

FIG. 4. (Color in online edition) The superfluid density (ρ_s) vs the product of the dc conductivity and T_c. Inset illustrates a relationship between the superfluid density (shaded area) and the optical conductivity of a superconductor. Adapted from Homes, Dordevic, *et al.*, 2004.

C. Doping

The suppression of the antiferromagnetic correlations and the emergence of a conducting state in the doped cuprates is accompanied by an increase of the electronic spectral weight proportional to n/m^*, where n is the carrier density and m^* is their effective mass. The n/m^* ratio increases linearly with doping at moderate doping levels thus supporting the notion of the doped MH insulators (Cooper *et al.*, 1990; Orenstein, Thomas, *et al.*, 1990; Rotter *et al.*, 1991). At doping levels near optimal doping, further doping does not result in increased Drude spectral weight and the n/m^* ratio flattens out (Puchkov, Fournier, *et al.*, 1996). Recent LDA calculations are consistent with these observations (Ambrosch-Draxl *et al.*, 2003). However, there is evidence in the Bi-2212 system of increasing spectral weight in the overdoped region (Kendziora *et al.*, 1997; Hwang, Timusk, Puchkov, *et al.*, 2004). Not only is the electronic structure of conducting phases modified compared to that of insulating hosts but also the character of the low-energy electronic excitations is altered in doped materials. In particular, a growing fraction of the spectral weight confined within the charge-transfer gap appears in the coherent channel characterized by a Drude-like ω dependence of the optical constants, whereas the relative weight of the incoherent component spread out through the mid-IR region is reduced (Secs. V and VI).

A gradual development of coherence with doping has paramount consequences for superconductivity. Experiments described in Sec. VIII show that the superconducting condensate is primarily drawn from the coherent component of the electromagnetic response. A steady increase of the coherent spectral weight (at least in the underdoped regime) yields an increased superfluid density. The latter correlates with an increase of the superconducting transition temperature, a result encompassed by the celebrated "Uemura plot." Homes, Dordevic, *et al.* (2004) found that the relationship $\rho_s \propto T_c \sigma_{dc}$, where σ_{dc} is the normal-state resistivity, held over a wide range of doping for all high-temperature superconductors (Fig. 4). Surprisingly both ab-plane and c-axis properties followed the same universal curve. A somewhat similar correlation between the superfluid density and the dc conductivity had been noticed previously for c-axis properties by Basov, Timusk, *et al.* (1994).

A hint of the physics behind $\rho_s \propto T_c \sigma_{dc}$ can be seen from an application of the conductivity sum rule to a dirty-limit BCS superconductor in which the scattering rate $\Gamma = 1/\tau$ exceeds the magnitude of the energy gap 2Δ. In such a system the spectral weight in a frequency region of the gap is transferred to the superconducting condensate according to the Ferrell-Glover-Tinkham sum rule (Ferrell and Glover, 1958; Tinkham and Ferrell, 1959). The magnitude of the conductivity is σ_{dc} and the width of the gap is $2\Delta \propto T_c$. Then the spectral weight of the condensate is given by $\rho_s \propto \sigma_{dc} T_c$. Since the ab-plane transport of the cuprates is in the clean limit, this argument will have to be modified. It seems that the coherent Drude part of the spectral weight is transferred to the condensate, leaving the incoherent sideband behind. The universal scaling relation implies that the width of the Drude peak $\hbar/\tau \propto T_c$. This follows directly from the well-known linear variation of the scattering rate with temperature $\hbar/\tau \propto T$ (Varma *et al.*, 1989; Schlesinger *et al.*, 1990). The implications of Homes's plot are discussed in Sec. VIII and by Zaanen (2004).

D. Anisotropy

The layered crystal structure leads to a strong anisotropy in the electronic properties. A qualitative difference in the charge dynamics along the conducting CuO_2

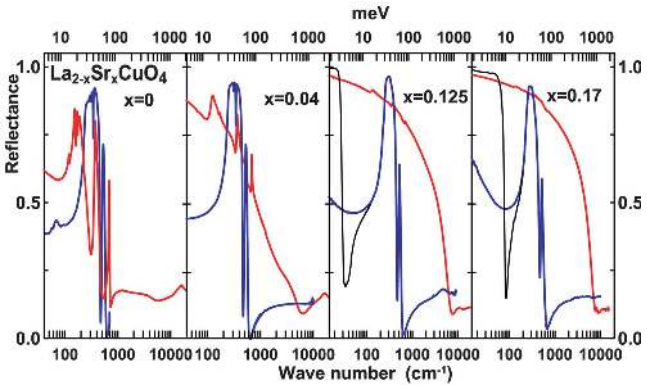

FIG. 5. (Color) Reflectance spectra for La-214 crystals at various dopings. Red lines, $R_{ab}(\omega)$ spectra at 300 K; blue lines, $R_c(\omega)$ spectra at 300 K. The interlayer response is nearly insulating even in superconducting phases. This behavior is modified at $T<T_c$: black lines (10-K data) show a sharp plasma edge, discussed in Sec. VII.A. Data from Dumm *et al.* (2002, 2003), Dordevic, Komiya, *et al.* (2003b), and Padilla *et al.* (2005a).

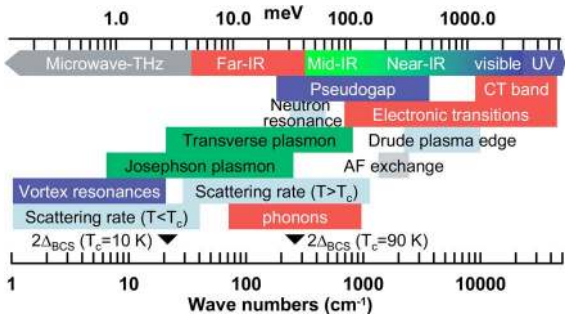

FIG. 6. (Color in online edition) Characteristic energy scales in high-T_c superconductors. Infrared and optical spectroscopies allow one to probe electronic excitations in the frequency range from $\simeq$20 cm^{-1} to at least 50 000 cm^{-1}. Several other techniques described in this section are suitable for extending the low-energy boundary down to microwave frequencies.

planes and along the nearly insulating interlayer direction can be readily seen in the raw reflectance data in Fig. 5. Here we plot the representative results for the La-214 family. The in-plane ($\mathbf{E}\|CuO_2$) reflectance $R_{ab}(\omega)$ is characterized by relatively high absolute values in the far-IR region and shows a distinctive plasma edge behavior in the near-IR with a minimum close to 10 000 cm^{-1}. The phonon features which dominate the response of the parent insulating compounds (left panel) appear to be depressed even at very mild doping levels (as low as $x=0.04$). On the other hand, the interlayer spectra $R_c(\omega)$ displayed in Fig. 5 are dominated by strong phonon structures at all dopings. The electronic contribution, which ought to produce an upturn of $R_c(\omega)$ in the far-IR, is barely noticeable even in the $x=0.125$ sample but is becoming stronger at higher dopings. A quantitative analysis of the data shows that the electronic anisotropy is reduced with increasing doping level (Cooper and Gray, 1994). Other cuprates show a similar evolution of both $R_{ab}(\omega)$ and $R_c(\omega)$.

The degree of both electronic and optical anisotropy varies strongly from one family of cuprates to the other. Most anisotropic single-layered $Bi_2Sr_2CuO_6$ (Bi-2201) compounds show ratios between the in-plane and interplane conductivities exceeding 10^4, whereas in the most isotropic $YBa_2Cu_3O_7$ system this factor drops down to $\simeq$10 (Cooper and Gray, 1994). Not surprisingly, the superfluid density is also strongly anisotropic in cuprates and reveals gigantic variations from one family of cuprates to the other. Typical values of the condensate plasma frequency inferred from the in-plane conductivity $\omega_{s,ab}$ range between 4000 and 10 000 cm^{-1} in different systems whereas the interlayer plasma frequency $\omega_{s,c}$ shows much more dramatic variation between different families ranging from $\simeq$1 to 1000 cm^{-1}.

E. Spin-charge self-organization and inhomogeneities

Numerous experiments indicate that carriers doped in the CuO_2 planes form hole-rich and hole-depleted regions (Tranquada *et al.*, 1996). Such electronic phase separation occurring on diverse length scales appears to be an intrinsic attribute of doped Mott-Hubbard (MH) insulators (Kivelson *et al.*, 2003). In several classes of layered transition-metal oxides the spins and/or the charges tend to segregate in one-dimensional (1D) self-organized regions commonly referred to as *stripes*. Stripes can be static or fluctuating on relatively short time scales. Coexistence of spin and/or charge modulation with superconductivity in the presence of a magnetic field has been recently detected using a variety of spectroscopic methods (Lake *et al.*, 2001; Mitrovic *et al.*, 2001; Hoffman *et al.*, 2002). A comprehensive understanding of spin and/or charge self-organization in oxides is a challenging task. A broad interest in this task within the condensed-matter community signifies a novel phase in the survey of strongly correlated phenomena in solids that until recently has been primarily focused on the properties of nominally homogeneous systems. Neutron-scattering experiments are best suited to examine periodic spin and charge modulations. Ordered states lead to the development of an additional incommensurate structure in magnetic and nuclear scattering with a correlation between the incommensurability factor δ and T_c ("Yamada plot"; Yamada *et al.*, 1998). The implications of spin-charge self-organization for the dynamical properties of charges have been investigated by several groups and will be discussed in Secs. VI.C and VIII.D.

III. ENERGY SCALES AND EXPERIMENTAL TECHNIQUES

Figure 6 summarizes characteristic energy scales involved in the study of high-temperature superconductors. Traditional IR and optical spectroscopy probe excitations and collective modes in the energy region from about 20 up to 50 000 cm^{-1}. In this range the far-infrared region is of special interest to superconductivity, since it

includes both the superconducting gap and the energies of the excitations believed to be relevant to the formation of the superconducting state. Also, by integrating the optical conductivity and applying sum rules one can evaluate the superconducting penetration depth λ.

The workhorse technique has been the use of a Michelson interferometer, with a range of sources, detectors, and beam splitters to extend the measurement range from the millimeter wave region to the ultraviolet and in some cases, with the aid of synchrotron radiation, to the vacuum ultraviolet (Homes, Reedyk, *et al.*, 1993; Basov, Dordevic, *et al.*, 2003). Added to this wide range of reflectance data one has the dc conductivity at zero frequency. It is then possible to obtain any of the optical constants through Kramers-Kronig analysis of reflectance. With polarizers one can also measure the anisotropic optical constants along the three principal directions of single crystals or oriented films. Reflectance $R(\omega)$ measurements on single crystals are the most popular but occasionally thin-film transmission $T(\omega)$ is also used, although one is always faced with the difficulty of finding transparent substrates.

New and interesting materials often come in the form of very small crystals of irregular shape. A first step in dealing with small samples is the use of an overfilling technique in which geometrical effects are corrected by reference to spectra of the same sample coated with a metal with known optical properties such as gold (Homes, Reedyk, *et al.*, 1993). Further improvements result in replacing the low-brightness laboratory sources with synchrotrons which have a much greater brightness (Forro *et al.*, 1990; Williams *et al.*, 1990; Romero *et al.*, 1992; Boris *et al.*, 2002; Carr *et al.*, 2002; Abo-Bakr *et al.*, 2003; Singley, Abo-Bakr, *et al.*, 2004).

Spectroscopic ellipsometry is an old technique mostly used in the visible, but in recent years it has been extended to the infrared, where the access to high-brightness synchrotron sources have made it a practical technique that in many cases rivals the more traditional reflectance spectroscopy (Kircher *et al.*, 1997). A combination of ellipsometers and synchrotron light has produced numerous results on both in-plane and interplane electrodynamics of high-T_c cuprates (Bernhard *et al.*, 2001; Boris *et al.*, 2002, 2004; Kovaleva *et al.*, 2004).

Terahertz time-domain spectroscopy (Grishkovsky *et al.*, 1990) is a powerful technique that extends the range of far-infrared spectroscopy to the difficult region of frequencies between microwaves and traditional far infrared. The radiation is generated and detected using Hertz dipoles—metal stripes with a narrow gap prepared on the surface of an amorphous semiconducting substrate or through optical rectification in optical media that lack inversion symmetry, such as ZnTe. Terahertz techniques have been used mainly in the transmission mode on thin-film samples. They have provided valuable insights into the dynamics of nodal quasiparticles in cuprates (Nuss *et al.*, 1991; Buhleier *et al.*, 1994; Corson *et al.*, 1999, 2000) and the vortex state in high-T_c materials (Parks *et al.*, 1995; Mallozzi *et al.*, 1998, Thorsmølle *et al.*, 2002).

Apart from THz time-domain spectroscopy, microwave techniques have been employed to probe the electrodynamics of high-T_c superconductors below 20–30 cm^{-1} (Hardy and Bonn, 1996). The traditional microwave approach is to use a resonant cavity to measure very accurately the real and imaginary parts of the surface impedance at a single frequency, typically as a function of temperature. Spectroscopy is possible with this approach but it involves the time-consuming work of combining the measurements of many discrete cavity systems, each tuned to a different frequency with a different microwave source (Degiorgi *et al.*, 1991; Hosseini *et al.*, 1999). To overcome these problems, several groups are pursuing the use of tunable microwave sources and nonresonant quasioptical layouts (Gaifullin *et al.*, 2000a, 2000b; Turner *et al.*, 2003). Backward wave oscillators have been used this way for the investigation of the low-energy electrodynamics in cuprates (Kozlov and Volkov, 1998). Backward wave oscillators are compact microwave vacuum tube devices that emit tunable monochromatic radiation with an output power of the order of 10–100 mW in the frequency range between 3 and 33 cm^{-1}. Apart from enabling both $R(\omega)$ and $T(\omega)$ measurements in this difficult frequency interval (Dulic *et al.*, 2001; Kakeshita *et al.*, 2001; Fudamoto *et al.*, 2003), backward wave oscillator sources can be incorporated into the layout of a Mach-Zehnder interferometer. The interferometric scheme makes possible a direct determination of both attenuation and phase change of radiation transmitted through a sample. This is sufficient to determine the optical constants of semitransparent samples without the use of Kramers-Kronig (KK) analysis (Pronin *et al.*, 1998).

An examination of the ac Hall effect in different frequency ranges has provided a wealth of information on the anomalous features of the low-energy dynamics of high-T_c superconductors (Drew *et al.*, 1996; Parks *et al.*, 1997). These experiments are aimed at determining the Hall angle $\tan\theta_H = \sigma_{xy}/\sigma_{xx}$. The magnitude of nondiagonal conductivity σ_{xy} tends to be small in metals and superconductors. However, it can be accurately measured using a sensitive photoelastic polarization modulation technique (Cerne *et al.*, 2000). The IR Hall angle cannot be measured directly but must be deduced from transmission studies of polarized light. The experimentally accessible quantity is the Faraday angle θ_F, which is the angle of rotation of the polarization in a magnetic field in the direction parallel to the propagation of the electromagnetic radiation. In the thin-film limit (the film thickness d is much smaller than both the wavelength and the penetration depth) the Hall angle can be related to θ_F using Maxwell's equation:

$$\theta_H = \left(\frac{1+n}{Z_0\sigma_{xx}} + 1\right)\theta_F, \tag{1}$$

where Z_0 is the free-space impedance and n is the refractive index of the substrate (Grayson *et al.*, 2002). These measurements have been accomplished using far-IR interferometers (Kaplan *et al.*, 1996; Grayson *et*

al., 2002) as well as the technique of time-domain THz spectroscopy (Spielman *et al.*, 1994).

IV. DYNAMICAL CONDUCTIVITY OF SOLIDS

The optical constants of solids are introduced in the context of "materials parameters" entering Maxwell's equations and the wave equation (Wooten, 1972). It is customary to discuss electrodynamics of metals and superconductors in terms of the complex dielectric function $\epsilon=\epsilon_1(\omega)+i\epsilon_2(\omega)$ and the complex conductivity $\sigma(\omega)=\sigma_1(\omega)+i\sigma_2(\omega)$. The real and imaginary parts of these two sets of optical constants are trivially related as $\sigma_1(\omega)=(\omega/4\pi)\epsilon_2(\omega)$ and $\sigma_2(\omega)=-(\omega/4\pi)[\epsilon_1(\omega)-1]$. In the case of isotropic materials the direction of polarization and induced currents coincides, leading to a simple relation between the displacement field $\vec{D}$, electric current density $\vec{J}$, and the electric field: $\vec{D}=\epsilon(\omega)\vec{E}$ and $\vec{J}=\sigma(\omega)\vec{E}$. In more complicated uniaxial crystals (e.g., La_2CuO_4) or biaxial crystals (e.g., $YBa_2Cu_3O_7$), the response of a system has to be described with third-rank tensors of $\epsilon(\omega)$ or $\sigma(\omega)$. Experimentally accessible quantities [$R(\omega)$ or $T(\omega)$] are uniquely determined by the optical constants. Causality of the electromagnetic response implies that the real and imaginary parts of the optical constants are connected by KK relations (Toll, 1956). This fundamental connection allows one to work out algorithms to infer both real and imaginary parts of $\sigma(\omega)$ or $\varepsilon(\omega)$ from the raw data. Analytical properties of the optical constants constitute the foundation for the sum rules that will be reviewed in this section. In addition, we shall describe several standard models most commonly employed for the analysis of electrodynamics of metals and superconductors.

A. The Drude-Lorentz and Kubo formulas

The average rate of dissipation of electromagnetic energy density W is proportional to the imaginary part of the dielectric function or equivalently to the real part of the complex conductivity: $W=[\omega\epsilon_2(\omega)/2\pi]E^2=2\sigma_1(\omega)E^2$. Therefore the structure seen in the spectra of the "dissipative" part of the optical constants $\epsilon_2(\omega)$ or $\sigma_1(\omega)$ uncovers the allowed absorption channels in a system associated with various excitations. A classical model that describes the multichannel aspect of radiation interaction with a solid is the *Drude-Lorentz oscillator model*:

$$4\pi\sigma(\omega)=\frac{\omega_{pD}^2\tau_D}{1-i\omega\tau_D}+\frac{\sum\omega_{pj}^2\omega}{i(\omega_j^2-\omega^2)+\omega/\tau_j}. \tag{2}$$

In this expression, which is obtained by solving the equations of motion separately for free and bound charges, the first term stands for the Drude response of the free carriers, ω_{pD} is the Drude plasma frequency, and $1/\tau_D$ is the scattering rate of the free carriers. The second term stands for the response of bound charges and has the form of multiple oscillators, each centered at ω_j with a plasma frequency ω_{pj} and scattering rate $1/\tau_j$. Particular microscopic scenarios leading to these terms include, but are not restricted to, absorption by infrared active phonons and interband transitions.

The classical Drude formula for the dynamical conductivity [first term in Eq. (2)] can be obtained by using a standard Boltzmann equation and approximating the collision integral with a single collision frequency $1/\tau_D$. The Drude formula describes the free-carrier contribution to $\sigma_1(\omega)$ as a Lorentzian peak centered at zero frequency with an oscillator strength ω_{pD}^2, where $\omega_{pD}^2=(e^2/3\pi^2\hbar)\int\mathbf{v}\cdot d\mathbf{S}_F$ and $\mathbf{v}$ is the electron velocity and $\mathbf{S}_F$ is an element of the Fermi surface. For a spherical Fermi surface $\omega_{pD}^2=4\pi ne^2/m_B$, where n is the free-carrier density and m_B is the electronic band mass. The Lorentzian width is determined by a constant scattering rate $1/\tau_D$. This derivation assumes that the elementary excitations are well defined, implying that the (energy) width of the wave packet representing the electronic excitation is small compared to the energy of the packet. For the approximations leading to Eq. (2) to be valid, a spectral function of electronic excitations, defined as

$$A(\mathbf{k},\omega)=-\frac{1}{\pi}|\mathrm{Im}\,G(\mathbf{k},\omega)| =\frac{1}{\pi}\frac{\mathrm{Im}\,\Sigma(\omega)}{[\omega-\epsilon_k-\mathrm{Re}\,\Sigma(\omega)]^2+[\mathrm{Im}\,\Sigma(\omega)]^2}, \tag{3}$$

must be a narrow peak centered at $\omega=\epsilon_k+\mathrm{Re}\,\Sigma(\omega)$. Here $G(\mathbf{k},\omega)$ is a Green's function of the electronic excitation and $\Sigma(\omega)$ is the self-energy part of the Green's function. The narrowness of the peak means that the excitation energy must be much larger than the damping term $\gamma(\omega)=-2\,\mathrm{Im}\,\Sigma(\omega)$. This is certainly true in the case of standard Fermi-liquid theory, where $\mathrm{Re}\,\Sigma(\omega)\sim\omega$ and $\mathrm{Im}\,\Sigma(\omega)\sim\omega^2$ so that the electronic excitations (quasiparticles) are well defined at zero temperature and at energies close to the Fermi energy E_F (Abrikosov *et al.*, 1975). A weak electron-phonon coupling does not drastically change the transport properties at low temperatures, since in this case the number of electronic states where the quasiparticle description is violated is small (Shulga *et al.*, 1991).

Linear response theory allows one to obtain an expression for the real part of the conductivity in terms of the Fourier transform of the current operator $j(\mathbf{q},t)$ (Kubo formula):

$$\sigma_1(\mathbf{q},\omega)=\frac{1}{\hbar\omega}\int_0^\infty dt e^{i\omega t}\langle\psi|[j^\dagger(\mathbf{q},t),j(\mathbf{q},0)]|\psi\rangle. \tag{4}$$

The wave function $|\psi\rangle$ is the ground state of the many-body Hamiltonian H containing all possible interactions in the solid except the interaction with the vector potential. The right-hand side describes the fluctuations of the current in the ground state. Equation (4) is extensively used in condensed-matter physics. Assuming that the current-current correlation function is exponentially decaying in time (the relaxation time approximation), the

Kubo formula in the limit of $q \to 0$ evolves into the Drude expression (see, for example, Dressel and Grüner, 2002). For the states obeying Fermi statistics, linear response theory allows one to express the real part of the conductivity in terms of the dipole matrix element $p_{s's}$ between states s and s' and the joint density of states $D_{s,s'}(\omega)$:

$$\sigma_1(\omega) = \frac{\pi e^2}{m^2 \omega} |p_{s',s}(\omega)|^2 D_{s's}(\omega). \tag{5}$$

This equation is often referred to as the Kubo-Greenwood formula. The most common use of Eq. (5) is to describe electronic transitions between different energy bands.

B. The complex memory function

The optical conductivity can be extended beyond the simple Drude form by making the damping term in the Drude formula complex and frequency dependent: $1/\tau = M(\omega) = M'(\omega) + iM''(\omega)$, where $M(\omega)$ is called a memory function (Allen and Mickelsen, 1976; Götze, 1981). This so-called *extended Drude model* has been employed to analyze the infrared conductivity of metals with a strong electron-phonon interaction in the limit of $T \to 0$ by Allen (1971) and at finite T by Shulga *et al.* (1991). The formalism has been extensively applied to elemental metals (van der Eb *et al.*, 2001; Basov *et al.*, 2002), transition-metal compounds (Allen and Mikkelsen, 1976), heavy-fermion systems (Webb *et al.*, 1986; Bonn *et al.*, 1988; Dolgov and Shulga, 1995; Degiorgi, 1999), and the high-T_c cuprates (Thomas *et al.*, 1988; Collins *et al.*, 1990; Rieck *et al.*, 1995; Puchkov, Basov, and Timusk, 1996). The complex conductivity $\sigma(\omega)$ can be expressed in terms of a complex memory function, $M(\omega, T) = 1/\tau(\omega, T) - i\omega\lambda(\omega, T)$, as (Mori, 1965; Timusk and Tanner, 1989):

$$\sigma(\omega, T) = \frac{1}{4\pi} \frac{\omega_p^2}{M(\omega, T) - i\omega} \tag{6}$$

$$= \frac{1}{4\pi} \frac{\omega_p^2}{1/\tau(\omega, T) - i\omega[1 + \lambda(\omega, T)]}. \tag{7}$$

It is believed that the theory is valid in the case of coupling of a Fermi liquid to any bosonic spectrum. Adopting the Boltzmann-type terminology, the quantities $1/\tau(\omega, T)$ and $1 + \lambda(\omega, T)$ describe the frequency-dependent scattering rate and mass enhancement of electronic excitations due to many-body interactions.

Equation (6) can be reduced to the familiar Drude formula by introducing the so-called renormalized scattering rate $1/\tau^*(\omega, T) = 1/\tau(\omega, T)[1 + \lambda(\omega, T)]$ and the effective plasma frequency $\omega_p^{*2}(\omega, T) = \omega_p^2/[1 + \lambda(\omega, T)]$:

$$\sigma(\omega, T) = \frac{1}{4\pi} \frac{\omega_p^{*2}(\omega, T)}{1/\tau^*(\omega, T) - i\omega}. \tag{8}$$

This form suggests the optical conductivity is now composed of an infinite set of Drude peaks, each describing $\sigma(\omega)$ in the vicinity of a particular frequency ω with a set of parameters $1/\tau^*(\omega)$ and $\lambda(\omega)$. The term $1/\tau^*(\omega)$ has a phenomenological meaning of a width of the Drude peak local to a frequency ω, while $\lambda(\omega)$ represents the interaction-induced velocity renormalization. The renormalized scattering rate $1/\tau^*(\omega)$ is not causal and, other than the local Drude width, does not have a real physical sense as it includes both the velocity renormalization and the lifetime effects. In contrast, the unrenormalized scattering rate, $1/\tau(\omega)$, is, up to a constant, the real part of $1/\sigma(\omega)$:

$$1/\tau(\omega) = \frac{\omega_p^2}{4\pi} \mathrm{Re}\left(\frac{1}{\sigma(\omega)} \right), \tag{9}$$

that is, a real part of a physical response function. The mass enhancement factor $\lambda(\omega)$ is given as the imaginary part of $1/\sigma(\omega)$:

$$1 + \lambda(\omega) = -\frac{\omega_p^2}{4\pi} \frac{1}{\omega} \mathrm{Im}\left(\frac{1}{\sigma(\omega)} \right). \tag{10}$$

The total plasma frequency ω_p^2 in Eqs. (9) and (10) can be found from the sum rule $\int_0^\infty \sigma_1(\omega) d\omega = \omega_p^2/8$. Since $\sigma(\omega)$ is causal, $\lambda(\omega)$ and $1/\tau(\omega)$ are not independent and are related by the KK relation. An experimental validation for the interpretation of the results of the extended Drude formalism in terms of mass enhancement is provided by heavy-fermion systems. The quasiparticle effective masses extracted through this procedure are in reasonable agreement with the data inferred from specific-heat measurements or direct studies of the Fermi surface with quantum oscillation techniques (Degiorgi, 1999; Dordevic, Basov, *et al.*, 2001).

Another useful quantity that can be derived from the extended Drude model is the imaginary part of the optical scattering rate γ_2 defined in

$$4\pi\sigma(\omega) = \omega_p^2/[\gamma(\omega) - i\omega], \tag{11}$$

where $\gamma(\omega) = \gamma_1(\omega) + i\gamma_2(\omega)$. Here $\gamma_1(\omega)$ is the optical scattering rate and $\gamma_2(\omega)$ its imaginary part which is closely related to the real part of the self-energy of the quasiparticles, $\gamma(\omega) \approx -2i\Sigma(2\omega)$ (Littlewood and Varma, 1991). We shall give an example of this in Sec. VII.

The connection between the conductivity and the quasiparticle self-energy is given by the general expression

$$\sigma(\omega, T) = -i\frac{\omega_p^2}{8\pi\omega} \int dy \left[\tanh\frac{\beta(y+\omega)}{2} - \tanh\frac{\beta y}{2} \right] \times \left[\frac{1}{\Sigma^R(y+\omega) - \Sigma^A(y) - \omega} \right], \tag{12}$$

where Σ^R and Σ^A are the retarded and advanced self-energies, respectively. For the marginal Fermi-liquid model these are (Littlewood and Varma, 1991; Abrahams and Varma, 2003) $\Sigma^R(\omega) = \lambda\omega \ln(x/\omega_c) - i(\pi\lambda/2)x$, $\Sigma^A(\omega) = \Sigma^R(\omega)^*$; $x = \max(|\omega|, \pi T)$, ω_c is the cutoff frequency, and $\beta \equiv 1/k_B T$, λ is a coupling constant, ω_c is a cutoff frequency of the marginal Fermi-liquid fluctuations, and T is the absolute temperature.

We see that the complex memory function $M(\omega)$ is a physical response function and experimental data can be presented in terms of $M(\omega,T)$ or the complex optical conductivity $\sigma(\omega,T)$ equally well. In certain cases the memory function is easier to calculate analytically, thus making it easier to analyze the physics behind the system behavior when using experimental results for $M(\omega)$.

We would like to stress that, although Eq. (6) is very general, the interpretation of experimental results for $M(\omega,T)$ in terms of scattering rate and mass enhancement only makes sense when a (generalized) Boltzmann equation can be used. For example, if the optical response is determined by two distinct charge-carrier systems (two-component), such that the optical conductivity takes the form $\sigma(\omega)=\sigma^{\mathrm{I}}(\omega)+\sigma^{\mathrm{II}}(\omega)$, the interpretation of $M'(\omega)$ and $M''(\omega)$ as a scattering rate and a mass enhancement is meaningless. This is the case if an interband transition is present in the same frequency region where there is an intraband response. Another example is the superconducting state at $T=0$, when for a conventional superconductor $\sigma_1(\omega)$ is zero at all nonzero energies below 2Δ, where Δ is the superconducting gap. According to Eq. (9), $M'(\omega)$ is zero in the same energy range. However, this effect cannot be meaningfully interpreted as a result of an infinite quasiparticle lifetime since there are no quasiparticles in this energy range. This is a purely density-of-states effect that has its origin in the redistribution of the one-particle density of states at $T<T_c$. Since in the superconducting state $\sigma_1(\omega)$ is suppressed, the low-frequency optical conductivity is dominated by the imaginary term $\sigma_2(\omega)=\omega_{ps}^2/4\pi\omega$. In this case, the low-frequency mass enhancement factor gives a ratio of the total plasma frequency ω_p^2 to the plasma frequency of the superconducting carriers ω_{ps}^2: $1+\lambda(\omega)=\omega_p^2/\omega_{ps}^2$. This example shows that density of states may greatly influence the memory function, and while changes in effective mass reflect the underlying density of states, it does serve as a reminder that the interpretation of $M(\omega)$ results purely in terms of the scattering rate and effective mass enhancement should be approached with extreme care.

C. Electron-boson scattering and strong-coupling effects

Electron-phonon scattering is an instructive example of the successful use of the memory-function analysis to elucidate the behavior of optical constants in infrared (Allen, 1971; Allen and Mikkelsen, 1976; Millis *et al.*, 1988; Shulga *et al.*, 1991). Shulga *et al.* (1991) have been able to obtain the following expression for the frequency and temperature dependence of the transport scattering rate $1/\tau(\omega,T)$ based on the Kubo formula for the conductivity:

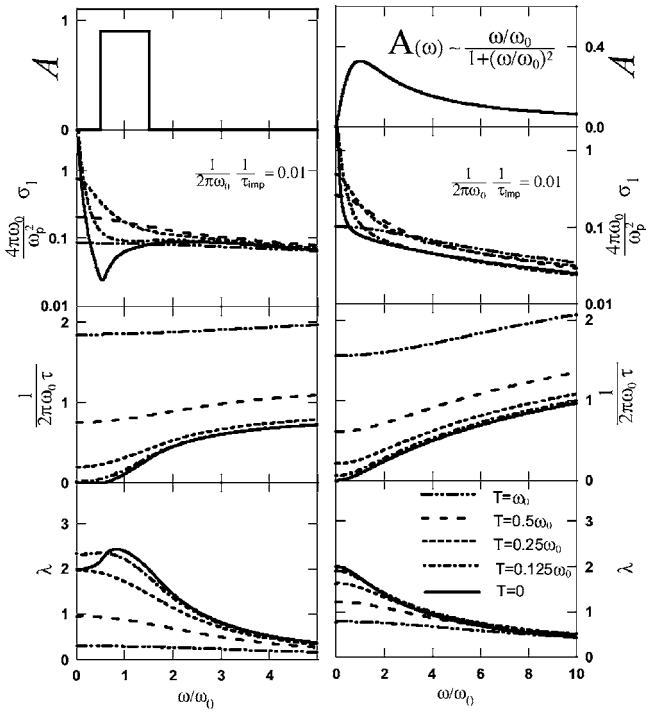

FIG. 7. Model calculations of the optical conductivity, scattering rate, and mass enhancement λ. Two bosonic spectral functions are used: a "square" spectrum (left panels) and a form capturing key features of the spin fluctuations spectrum (right panels). The coupling constant is equal to 1. From Puchkov, Basov, and Timusk, 1996.

$$\frac{1}{\tau}(\omega,T)=\frac{\pi}{\omega}\int_0^\infty d\Omega\,\alpha_{\mathrm{tr}}^2(\Omega)F(\Omega)\left[2\omega\coth\left(\frac{\Omega}{2T}\right)-(\omega+\Omega)\coth\left(\frac{\omega+\Omega}{2T}\right)+(\omega-\Omega)\coth\left(\frac{\omega-\Omega}{2T}\right)\right]+\frac{1}{\tau_{\mathrm{imp}}}. \tag{13}$$

Their results allow one to express the scattering rate in terms of the phonon density of states weighted by the amplitude for large-angle scattering on the Fermi surface $\alpha_{\mathrm{tr}}^2(\Omega)F(\Omega)$. Impurity scattering is represented by the $1/\tau_{\mathrm{imp}}$ term which produces a frequency-independent background. At $T\to 0$ Eq. (13) evolves to the form originally discussed by Allen (1971). This formalism was generalized by replacing the Eliashberg function $\alpha_{\mathrm{tr}}^2(\Omega)F(\Omega)$ in Eq. (13) with the corresponding spectral density $\mathcal{A}_{\mathrm{tr}}(\Omega)$. As an example we show in Fig. 7 a calculation of Puchkov, Basov, and Timusk (1996) for two particular shapes of $\mathcal{A}_{\mathrm{tr}}(\Omega)$: a "square" spectrum and $\mathcal{A}_{\mathrm{tr}}(\Omega)=\Gamma\Omega/(\Gamma^2+\Omega^2)$. The latter spectrum is believed to be appropriate for the scattering of electrons by spin fluctuations (Millis *et al.*, 1990).

Inspecting the left panel in Fig. 7 one notices that $1/\tau(\omega,T)$ saturates at frequencies that are higher than the cutoff in $\mathcal{A}_{\mathrm{tr}}(\Omega)$. The value of $1/\tau(\omega,T)$ in the saturation regime is strongly temperature dependent and is linear in T at high enough temperatures. However, if

there is no cutoff in $\mathcal{A}_{tr}(\Omega)$, as in the case of the magnetic spectrum (right panels in Fig. 7) there is no obvious high-frequency saturation of $1/\tau(\omega,T)$. Both forms of the $\mathcal{A}_{tr}(\Omega)$ spectrum produce significant enhancement of the effective mass at low frequencies. This effect can be interpreted in terms of the boson "cloud" dragged by the charge carriers. A $\lambda(\omega)$ spectrum seen in the data for a rectangular $\mathcal{A}_{tr}(\Omega)$ is nonmonotonic and shows a peak at ω near the onset of the spectral function. In the case of the magnetic $\mathcal{A}_{tr}(\Omega)$, such a peak feature is not observed, since bosons can be emitted by a carrier with arbitrarily small energy. At high temperatures λ asymptotically approaches zero. The onset of absorption at $\omega=\omega_0$ at low temperature is usually referred to as the *Holstein band*. This onset is associated with the opening of an additional absorption channel due to the emission of a boson of frequency ω_0. A similar absorption onset is difficult to identify in the right panels of Fig. 7. As the temperature is increased, all sharp features in σ_1 are smeared out and at very high temperatures the conductivity can be described by a single Lorentzian of Eq. (2).

D. Electrodynamics in the superconducting state

Superconductivity is a macroscopic quantum state in which some of the electrons condense into a quantum state extending over macroscopic dimensions. The density of condensed electrons n_s determines the penetration depth of the magnetic field,

$$\lambda_L = \sqrt{m^* c^2/4\pi n_s e^2}. \tag{14}$$

The London penetration depth characterizes the length scale over which the supercurrent in a superconductor screens out an applied field. The complex conductivity of a London superconductor has a fairly simple form: $\sigma_1(\omega)=(n_s e^2/m^*)(\pi/2)\delta(0)$ and $\sigma_2(\omega)=n_s e^2/m^*\omega$. The former equation is simply a delta function with an area proportional to the density of superconducting electrons. The superfluid density is $\rho_s=4\pi n_s e^2/m^*=c^2/\lambda^2$. The two equations are connected with KK relations. The picture of exponential decay of the electromagnetic field in a superconductor was refined by Pippard (1953) to include nonlocal effects. These effects become important if the coherence length ξ characterizing the correlated nature of supercurrents becomes comparable to the penetration depth. In the local limit $\xi \ll \lambda_L$ the London theory is adequate.

The form of the London equations for the complex conductivity implies that all electrons contributing to the Drude conductivity at $T>T_c$ have condensed since the dissipative term $\sigma_1(\omega)=0$ for all finite frequencies. To remedy this unrealistic assumption, the complex conductivity is often analyzed in a "two-fluid" form yielding the following expression for $\sigma(\omega)$:

$$\sigma_1(\omega) = \sigma^{\text{reg}} + \frac{\pi}{2}(n_s e^2/m^*)\delta(0). \tag{15}$$

Here the first term, the so-called regular component, accounts for all contributions to the conductivity other than the superfluid contribution described by the second term. This expression is particularly useful in modeling the low-energy response of thermally excited quasiparticles in a superconductor at finite temperature. Assuming the latter is consistent with the Drude model, one arrives at the following equation:

$$\sigma_1(\omega,T) = \frac{\pi}{2}\frac{ne^2}{m^*}\left[x_n(T)\frac{\tau}{1+\omega^2\tau^2} + x_s(T)\delta(0)\right]. \tag{16}$$

This equation suggests that the two conductivity terms share the oscillator strength, which is divided between the normal fluid and the superfluid such that $x_n(T)+x_s(T)=1$ at all temperatures.

Both London electrodynamics and the two-fluid electrodynamics fail to explicitly account for the energy gap 2Δ which is a hallmark of the density of states of a BCS superconductor. At $T \ll T_c$ the quasiparticle excitations are frozen out. Since no absorption is possible for $\omega < 2\Delta$, the dissipative part of the complex conductivity $\sigma_1(\omega)$ vanishes at all frequencies below the gap but is expected to rise steeply as soon as ω exceeds the gap. Tinkham reminisces: "Although in hindsight this is very straightforward, the situation was quite different in the pre-BCS days of 1956 when Glover and I were making first crude far infrared experiments in an attempt to see whether there was an energy gap of the order of kT_c as had been speculated by various earlier authors" (Tinkham, 1974): These experiments have indeed uncovered the presence of the energy gap having a magnitude consistent with the BCS result (Glover and Tinkham, 1956). The frequency dependence of the optical constants of a superconductor was first considered by Mattis and Bardeen (1958).

Several features of the BCS electrodynamics are particularly worthy of attention since they will be later compared and contrasted with the response of high-T_c materials. Although the density of states in a BCS superconductor diverges at Δ, the experimental data show no such divergence in accord with the Mattis-Bardeen description. The smooth increase of the conductivity approximately follows the $\sigma_1(\omega)/\sigma_n \propto 1-(\hbar\omega/kT_c)^{-1.65}$ behavior prescribed by the model. The real part of the conductivity in the superconducting state at $T \ll T_c$ does not cross the normal-state curve at any energies in the so-called dirty limit where $1/\tau_D > 2\Delta$. A crossing between $\sigma_1(\omega, T \ll T_c)$ and $\sigma_1(\omega, T > T_c)$ is possible in the clean limit where $1/\tau \ll 2\Delta$. A theoretical description in different regimes of the scattering rate has been carried out by Leplae (1983) and by Zimmermann *et al.* (1991). Evidently, the spectral weight in the superconducting-state conductivity $\int_{0+}^{\infty} d\omega\sigma(\omega)$ is reduced compared to the normal-state value. As we shall discuss in the next subsection, this result is fully consistent with the global conservation of the spectral weight, since the "missing area" in the conductivity data,

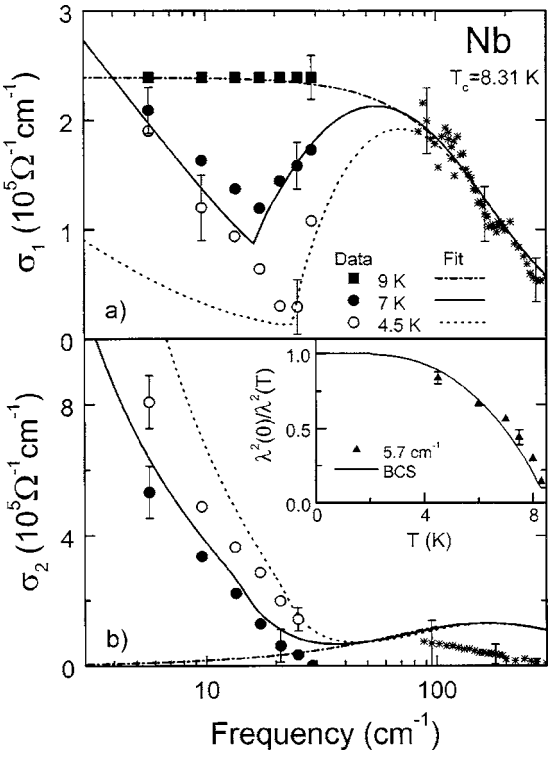

FIG. 8. Frequency dependence of the (a) real and (b) imaginary parts of the conductivity at 4.5 and 7 K compared to the predictions of the BCS weak-coupling limit using the formulas of Mattis and Bardeen with a finite scattering time $\tau=3\times10^7$ s. Also shown is the normal-state behavior at $T=9$ K fitted by the Drude model. The far-infrared data (stars) show no temperature dependence below 10 K. In this spectral range, the imaginary part of the conductivity $\sigma_2(\omega)$ has large error bars. The inset shows the temperature dependence of the penetration depth $\lambda(T)$ compared with the predicted behavior. From Pronin *et al.*, 1998.

$$A=\rho_s=\int_{0+}^{\infty}d\omega[\sigma_1(\omega,T>T_c)-\sigma_1(\omega,T<T_c)], \quad (17)$$

is accounted for by the weight under the superconducting delta peak at $\omega=0$. Finally, we note that in the limit of $\omega\to0$ and $T\to0$, the BCS equations for the optical conductivity evolve into the London expressions.

An inspection of Fig. 8 shows that key parameters of the superconducting state such as the energy gap $2\Delta(T)$ and the density of the superconducting condensate can be inferred from the analysis of the optical constants of a superconductor. The magnitude of $2\Delta(T)$ is given by a sharp onset in the $\sigma_1(\omega,T<T_c)$ spectra. The superfluid density $\rho_s=c^2/\lambda^2$ can be extracted from the complex conductivity data using several different approaches. The most commonly used techniques include (a) the sum-rule analysis [Eq. (17)] since $A=\rho_s$; and (b) an examination of the imaginary part of the conductivity:

$$\rho_s=4\pi\omega\sigma_2(\omega). \quad (18)$$

The latter approach is afforded by KK transformation, implying that the $\delta(0)$ peak in the real part of the conductivity corresponds to $4\pi\sigma_2(\omega)=\rho_s/\omega$. Therefore the magnitude of ρ_s can be estimated from $\omega\sigma_2(\omega)$ in the limit of $\omega\to0$. This method (b) is useful but is prone to systematic errors. Indeed, the relation $\sigma_2(\omega)=\rho_s/\omega$ is valid only if $\sigma_1^{\rm reg}(\omega)=0$. Typically, this is not the case in high-T_c superconductors, which all show residual absorption in the far-IR conductivity. Naturally, a finite regular contribution to $\sigma_1(\omega,T<T_c)$ implies a finite contribution to $\sigma_2(\omega,T<T_c)$. Various forms of corrections for this latter contribution are discussed by Dordevic, Singley, *et al.* (2002).

E. Sum rules

The optical constants of solids obey a variety of sum rules (Smith, 1998). The origins of the sum rules can be traced back to fundamental conservation laws and are intimately connected to the causality of the electromagnetic response. Analysis of the sum rules is a powerful tool that can be used to study the distribution of the spectral weight in correlated electron systems. Of special practical importance is the *global oscillator strength sum rule* relating the integral of the dissipative part of the optical conductivity to the density of particles participating in optical absorption and their bare mass:

$$8\int_0^{\infty}\sigma_1(\omega)d\omega=\frac{4\pi ne^2}{m_e}. \quad (19)$$

The optical conductivity of a metal is dominated by the electronic response and therefore an integration of the data using Eq. (19) can be compared to the total number of electrons, including both core and valence electrons. When applied to the data for Al this procedure yields an accurate electron count (Smith and Shiles, 1978).

The integration to infinite frequency in Eq. (19) can rarely be exercised because of experimental constraints. Therefore sum rules with integration confined to the limited range within the electronic band width W are commonly used. A sum rule

$$8\int_0^{W}\sigma_1(\omega)d\omega=\frac{4\pi ne^2}{m_b} \quad (20)$$

is often referred to as a *partial sum rule*, where m_b is different from the free-electron mass. Within the tight-binding approximation m_b can be interpreted as the band mass. The tight-binding model also allows one to express the electronic kinetic energy K_r along the direction r in terms of the integral of the conductivity probed in the polarization r:

$$\int_0^{W}d\omega\sigma_{1,r}(\omega)=-\frac{\pi e^2a_r^2}{2\hbar^2}K_r, \quad (21)$$

where a_r is the lattice spacing in the direction **r**. This equation offers an interpretation of such a well-defined experimental parameter as the effective spectral weight,

$$N_{\rm eff}(\omega) = \int_0^{\omega} d\omega' \sigma_1(\omega'), \tag{22}$$

in terms of the electronic kinetic energy. While both the band mass and the kinetic-energy interpretations of the partial sum rule are often instructive, it is important to keep in mind that these latter expressions are model dependent in contrast to Eq. (19).

Several sum rules become particularly useful for data analysis when they are written in terms of differences between the optical constants. The most extensively used *difference sum rule* is the so-called Ferrell-Glover-Tinkham sum rule, which is the direct consequence of Eq. (19). Indeed, expression (19) demands that the total spectral weight at $T<T_c$ confined under the δ function and under the regular contribution of the conductivity $\int_0^{\infty} d\omega \rho_s \delta(0) + \int_{0+}^{\infty} d\omega \sigma_1^{\rm reg}(\omega)$ be the same as $\int_0^{\infty} d\omega \sigma_1(\omega, T>T_c)$. This equality imposed by charge conservation implies the Ferrell-Glover-Tinkham form Eq. (17). In most superconductors the spectral weight of the superfluid is accumulated from energies of the order of 2Δ. It is therefore sufficient to carry out integration to a relatively narrow frequency range $\ll W$. Any substantial contribution to the condensate density originating from an energy range significantly exceeding the magnitude of W can be regarded as anomalous and can be explicitly stated in the following differential sum rule (Hirsch, 1992):

$$\rho_{s,r} = \int_{0+}^{W} d\omega [\sigma_{1,r}^N(\omega) - \sigma_{1,r}^{SC}(\omega)] + \frac{\pi e^2 a_r^2}{2\hbar^2} \Delta K_r. \tag{23}$$

The second term in Eq. (23) stands for the high-energy contribution to the superfluid density and within a number of models can be interpreted in terms of the kinetic-energy change at $T<T_c$ (Hirsch, 1992; Anderson, 1998; Chakravarty, 1998). When searching for the high-energy contribution to the superconducting delta function it is useful to define the normalized spectral weight in a superconductor (Basov *et al.*, 1999):

$$N'(\omega) = [N^N(\omega) - N^{SC}(\omega)]/\rho_s, \tag{24}$$

where $N^N(\omega) = (120/\pi) \int_{0+}^{\omega} d\omega' \sigma_1^N(\omega)$ and $N^{SC}(\omega) = (120/\pi) \int_{0+}^{\omega} d\omega' \sigma_1^{SC}(\omega)$. In conventional superconductors $N'(\omega)$ saturates at $\omega \approx (10-15) kT_c$ reaching the level of $N' \simeq 1$. However, deviation of $N'(\omega)$ from unity in the saturated region can be interpreted in terms of kinetic-energy change. Experimental uncertainties connected with the application of Eqs. (23) and (24) to the analysis of actual data were discussed by Basov *et al.* (2001) and Santander-Syro *et al.* (2004).

Basov *et al.* (2002) introduced an approximate sum rule for the difference between energy-dependent scattering rates:

$$\int_0^{\omega_c} d\omega \left(\frac{1}{\tau^A(\omega)} - \frac{1}{\tau^B(\omega)} \right) \simeq 0, \tag{25}$$

where indexes A and B refer to different states of the system under study (e.g., normal, pseudogap, superconducting). Their argument is based on the exact value of the imaginary part of the loss function (Pines and Nozières, 1996). Indeed at $\omega < \omega_p$ the scattering rate can be expressed as $1/\tau(\omega) \approx \omega_p^{-1} \, {\rm Im}(1/\varepsilon)$ and therefore the sum rule may be expected. Abanov and Chubukov (2002) have expressed the integral of the scattering rate in terms of the current-current correlator $\Pi(\omega)$ as $\int d\omega \tau^{-1}(\omega) = (\pi/2)\{{\rm Re}[\omega^2/\Pi(\omega)_{\omega \to 0}] + C\}$. The sum rule of Eq. (25) is therefore obeyed provided $\omega^2[1/\Pi^A(\omega) - 1/\Pi^B(\omega)]$ vanishes. This appears to be the case at least in both clean and dirty BCS superconductors (Chubukov, Abanov, and Basov, 2003). For a discussion of Eq. (25) in connection to the interlayer conductivity of cuprates, see Shah and Millis (2001).

V. INSULATING AND WEAKLY DOPED PHASES

The dominant feature in the in-plane ($E \| ab$) response of undoped cuprates is a sharp onset at $\omega = 1-2$ eV in $\sigma_1(\omega)$, which originates from a charge-transfer gap (Fujimori *et al.*, 1987; Tokura *et al.*, 1990). The difference in the magnitude of the charge-transfer gap between various cuprates was ascribed primarily to distinctions in the coordination of the oxygen sites surrounding the Cu site. The magnitude of the gap increases with the number of apical oxygen sites. Interestingly, the *c*-axis response with $E \| c$ shows no sharp structure in the charge-transfer region. This anisotropic character of the charge-transfer excitations suggests that they are mainly associated with the transitions from O $2p$ to Cu $3d_{x^2-y^2}$ states. In all compounds the absorption edge appears to be broadened. The detailed investigations of the temperature dependence of the 2-eV threshold in La_2CuO_4 by Falck *et al.* (1992) also accompanied by photoconductivity experiments in the same energy range suggest that the broadening could be attributed to coupling of the charge-transfer excitations to optical phonons.

Charge-transfer excitations are clearly visible in the data for doped crystals, as well (Fig. 9). Both the undoped insulating cuprates and the weakly doped nonsuperconducting phases reveal a rich variety of absorption structures below the charge-transfer excitation. Thomas *et al.* (1988) have identified several distinct mid-IR peaks common to the response of several insulating compounds including $YBa_2Cu_3O_{6+x}$, La_2CuO_{4+y}, and Nd_2CuO_{4-y}. They analyzed the position of these peaks and compared them with other related energy scales in these materials. As pointed out by many authors, special care has to be taken in assigning the mid-IR structure to intrinsic properties of insulating phases. In La_2CuO_{4+y} and Nd_2CuO_{4-y} phases, small amounts of excess or deficient oxygen are known to produce effects similar to Sr or Ce doping (Uchida *et al.*, 1991; Quijada *et al.*, 1995). The same problem originates from unintentional oxygen doping in $YBa_2Cu_3O_{6+x}$. Grüninger *et al.* (2000a, 2000b) have addressed this issue by annealing "undoped" single crystals of Y-123 in high-purity argon. This has resulted in a depression of the absolute value of $\sigma_1(\omega)$ in the mid-IR to the level of $1-2\ \Omega^{-1}\ {\rm cm}^{-1}$. Typically, much

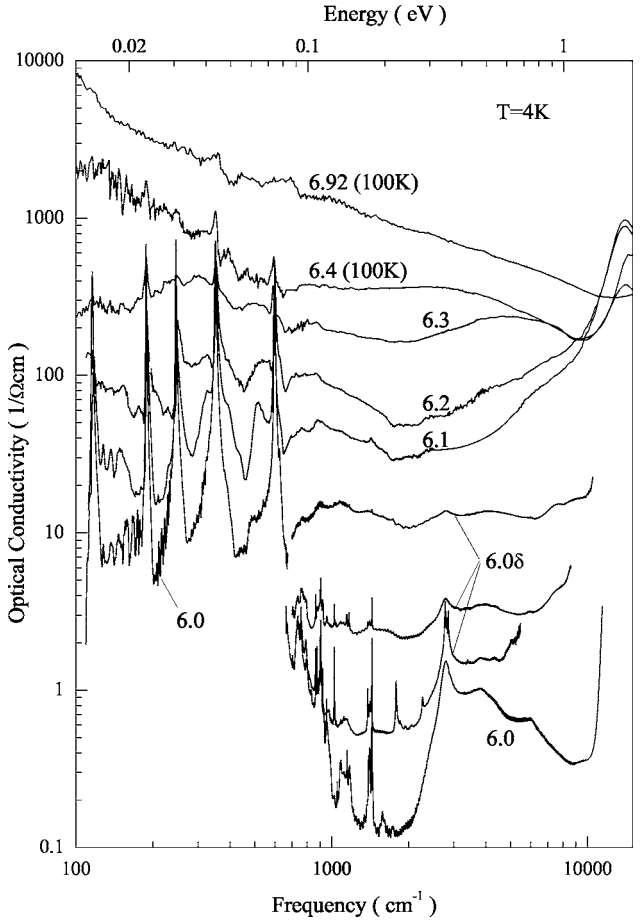

FIG. 9. Doping dependence of $YBa_2Cu_3O_x$ at 4 K (100 K for the superconducting samples with $x=6.4$ and 6.92). From Gruninger, 1999.

stronger absorption is observed in La_2CuO_{4+y} phases.

An interpretation of the structure in the mid-infrared in terms of polarons has been advanced by several groups (Dewing and Salije, 1992; Alexandrov *et al.*, 1993). As pointed out by Falck *et al.* (1992), a polaron absorption model quantitatively describes the broadening of the charge-transfer excitation peak. Calvani *et al.* (1996) have argued that the polaronic features persist in superconducting samples of $Nd_{2-y}Ce_yO_{4-\delta}$. These and many other experiments have led to the suggestion that the electron-phonon interaction is an important factor in the electromagnetic response of cuprates and may be responsible for some of the peculiar features seen in the conductivity spectra such as the anomalous coupling of the in-plane charge carriers to the *c*-axis longitudinal modes, first observed by Reedyk and Timusk (1992). However, recent work suggests that this effect is sample dependent and may result from structural defects (Tajima *et al.*, 2003).

Perkins *et al.* (1993) have observed a feature at 0.35 eV in the absorption of the undoped materials La_2CuO_4, $Sr_2CuO_2Cl_2$, Nd_2CuO_4, and Pr_2CuO_4. This weak absorption was also found in $YBa_2Cu_3O_6$ (Grüninger *et al.*, 1996; Tanner *et al.*, 1996). According to Lorenzana and Sawatsky (1995), this peak originates from the creation of a two-magnon quasibound state which is coupled to an optical phonon. Magnons are not expected to give rise to infrared absorption in materials with inversion symmetry such as La_2CuO_4 and other systems studied by Perkins *et al.* (1993). However, in a process involving a phonon and two magnons the symmetry of the lattice is effectively lower, and this absorption becomes allowed. The theory predicts a very different line shape for structurally similar La_2NiO_4, in which Ni having spin 1 replaces copper (spin 1/2). The experimental data obtained by Perkins *et al.* (1995) for the Ni-based compound indeed reveal a different line shape for the mid-infrared absorption. The detailed analysis of the bimagnon structure and magnetoelastic polarons in the Y-123 system has been reported by Gruninger and coworkers (Grüninger, 1999; Grüninger *et al.*, 2000a, 2000b). This analysis shows in a convincing way that in low-doped cuprates interactions of the doped carriers with both spin and lattice degrees of freedom play a role.

However, there is very little evidence to support the idea that interaction with the lattice modes in any form is the dominant mechanism of superconductivity at high critical temperatures. Allen (1992) and Emery and Kivelson (1995a) have pointed out a paradoxical situation with the electron-phonon interaction in cuprates and other doped insulators. In models based on the polaronic interpretation of the optical conductivity, or in models explaining the temperature dependence of the phonon frequencies, the electron-phonon interaction would be quite strong. However, there are no signatures of strong electron-phonon coupling in transport properties. The in-plane resistivity of many cuprates varies linearly with T from T_c up to 1000 K with a nearly zero intercept on the temperature axis. This is inconsistent with scattering of charge carriers by phonons, where an intercept on the temperature axis of the order of Debye temperature is expected. Several reviews of the role of phonons are available, including one on vibrational spectroscopy by Litvinchuk *et al.* (1994) and one on Raman spectroscopy by Thomsen and Cardona (1989).

VI. EMERGENCE OF CONDUCTING STATE IN DOPED CUPRATES

A. Evolution of the spectral weight with doping

A typical variation of the in-plane optical conductivity $\sigma_1^{ab}(\omega)$ with doping is shown in Fig. 10 for Y-123 (Cooper, Reznik, *et al.*, 1993). Similar results were previously obtained for La-214 materials by Uchida *et al.* (1991). The principal result is that in doped materials the energy region below the charge-transfer gap is filled with states at the expense of the spectral weight associated with the charge-transfer excitation in the undoped counterpart. Another characteristic of doped samples is that a feature due to the charge-transfer gap persists in the spectra up to a level of doping when the system is well into the metallic regime. With increasing oxygen or strontium concentration, the low-frequency spectral weight builds

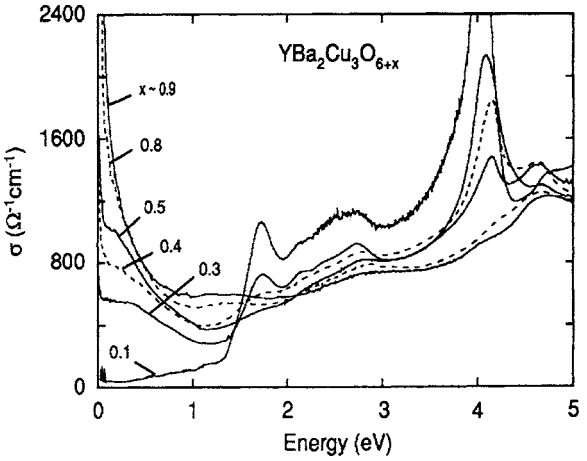

FIG. 10. In-plane ($E \perp c$) optical conductivity $\sigma(\omega)$ obtained from a Kramers-Kronig analysis of the reflectivity data for various compositions of $YBa_2Cu_3O_{6+x}$. Adapted from Cooper, Reznik, *et al.*, 1993.

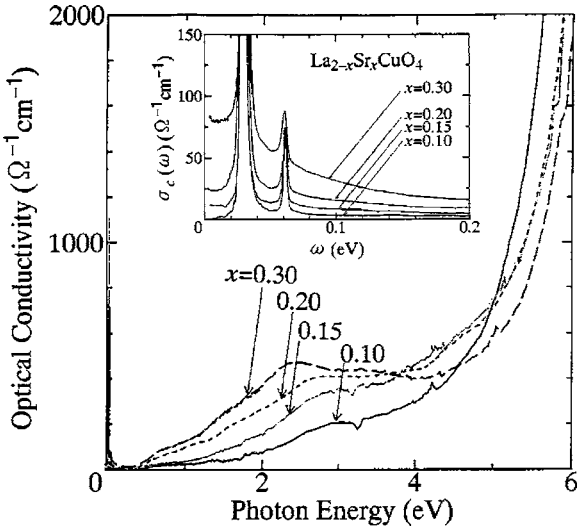

FIG. 11. Evolution of the *c*-axis optical conductivity spectra below 6 eV for $La_{2-x}Sr_xCuO_4$. The inset displays infrared region in more detail. From Uchida *et al.*, 1996.

up rapidly and varies nearly linear with doping. It follows from Fig. 10 that doping affects electronic excitations located below 3 eV. Puchkov, Fournier, *et al.* (1996) have analyzed the variation of the spectral weight with doping in a variety of high-T_c materials. Their conclusion is that the effective spectral weight N_{eff} either saturates or even decreases above optimal doping, which was defined as the carrier density that corresponds to the maximum critical temperature. This effect has also been seen in LDA calculations (Ambrosch-Draxl *et al.*, 2003). To summarize:

(i) the charge-transfer gap is filled with states at the expense of $\sigma_1^{ab}(\omega)$ depression at $\omega > E_g$;

(ii) total spectral weight in $\sigma_1^{ab}(\omega)$ integrated up to 3 eV is unchanged at small or moderate dopings and is suppressed in the overdoped regime;

(iii) the low-frequency N_{eff} ($\omega < 1.5$ eV) increases faster than y in underdoped samples and is suppressed in the overdoped regime.

Points (i)–(iii) should be contrasted with the behavior of a Fermi liquid with a large Fermi surface. Doping with holes reduces the size of the Fermi surface and one expects to see a decrease of spectral weight with doping x as $1-x$ rather than the observed increase proportional to x. On the other hand, these features seem to be generic for a broad variety of Mott insulators, including cuprates. A comprehensive discussion of the optical conductivity data for a variety of doped MH insulators is given by Imada *et al.* (1998). The Mott-Hubbard picture, which accounts for the antiferromagnetic insulator state of undoped compounds, also helps us to understand the changes in the redistribution of the spectral weight with doping (Dagotto, 1994; Jarrell *et al.*, 1995; Georges *et al.*, 1996; Kajueter *et al.*, 1996). The authors obtained spectra of $\sigma_1^{ab}(\omega)$ that reproduce the principal trends of the experimental data for cuprates.

The doping dependence of the interplane *c*-axis conductivity has been systematically studied for La-214 (Uchida *et al.*, 1996) and Y-123 (Cooper, Reznik, *et al.*, 1993; Homes, Timusk, *et al.*, 1995a, 1995b; Tajima *et al.*, 1997). Figure 11 reveals an important difference between the in-plane and interplane properties of cuprates. Indeed, the charge-transfer gap at 1.5 eV is not seen in the interplane conductivity of undoped compounds. The electronic contribution to $\sigma_c(\omega)$ is strongly suppressed at $\omega < 5$ eV (Fig. 11). One can recognize a clear threshold at $\simeq 5$ eV in the conductivity for $La_{2-x}Sr_xCuO_4$, whereas the increase of $\sigma_1^c(\omega)$ for $YBa_2Cu_3O_{6+y}$ is more gradual. In $La_{2-x}Sr_xCuO_4$ upon doping a certain portion of the spectral weight in the 5–6-eV region is transferred to low frequencies. Experimental results for $YBa_2Cu_3O_{6+y}$ do not clearly show this spectral weight transfer. In both systems the overall magnitude of the interplane conductivity in infrared frequencies is reduced by at least an order of magnitude compared to the in-plane data.

We conclude this subsection by noting that Nd_2CuO_{4-z}, La_2CuO_{4+z}, and some other materials could be doped not only by substitution of Nd or La with Ce or Sr but also by partial removal or addition of oxygen. Quijada *et al.* (1995) have studied the conductivity of oxygen-doped $La_2CuO_{4.12}$–Sr-free material with T_c as high as 40 K. Their results for the in-plane conductivity are in agreement with the data of Uchida *et al.* (1991) for the Sr-doped crystal near optimal doping. This suggests that there is an equivalence between the different approaches that introduce carriers into the CuO_2 planes. Finally, Y-123 systems can be doped not only by oxygen on the chain site but also by replacing Y with Pr. Praseodymium is the only rare-earth element known to reduce the T_c of the Y-123 system. Both the in-plane (Liu *et al.*, 1999; Lobo *et al.*, 2002) and interplane (Bernhard *et al.*, 1998) conductivity of $Y_{1-z}Pr_zCu_3O_7$ are

analogous to the data obtained for oxygen-deficient samples with depressed values of T_c.

B. One-component versus multicomponent description of the in-plane conductivity

As the doping level increases, the sharp features seen in the mid-infrared response of cuprates acquire an increasing amount of oscillator strength (Fig. 10). It is also more difficult to resolve these features in the superconducting phases as they blend into the broad Drude peak centered at zero frequency and a featureless background extending throughout the whole mid-infrared range. Most cuprates at metallic and superconducting doping levels show a smooth mid-infrared conductivity without any characteristic absorption bands. At frequencies below 500–800 cm^{-1} this behavior evolves into a Drude-like feature. The falloff of $\sigma_1(\omega)$ in Y-123 and all other cuprates is significantly slower than is prescribed by the Drude formula. As discussed in detail by Orenstein, Thomas, *et al.* (1990), it is impossible to fit the conductivity of the optimally doped cuprates with a simple Drude equation. If the scattering rate in the Drude equation is set at a low value to reproduce the shape of the low-frequency peak in $\sigma_1(\omega)$, then the fit is completely wrong at higher frequencies. If the width of the Drude peak is chosen to be anomalously broad in accord with the behavior of the conductivity at $\omega > 600$ cm^{-1}, then the model yields the wrong magnitude of low ω behavior and reveals strong disagreement with the dc conductivity. The smooth mid-infrared continuum that follows the peak at $\omega=0$ is found not only in doped cuprates but in other classes of doped MH insulators (Bozovic *et al.*, 1994; Imada *et al.*, 1998).

Two principal approaches are commonly used to describe the deviations of the conductivity in mid-infrared frequencies from the Drude formula: *multicomponent* and *one-component models*. Within the latter approach it is assumed that the sole cause of the frequency dependence of $\sigma(\omega)$ is the response of itinerant carriers, which acquire frequency-dependent scattering rate $1/\tau(\omega)$ and frequency-dependent mass $m^*(\omega)$ as the result of strong interactions. Several models including the "marginal Fermi-liquid" (Varma *et al.*, 1989; Littlewood and Varma, 1991), the "nested Fermi-liquid" (Virosztek and Ruvalds, 1990), the "Luttinger-liquid" (Anderson, 1997), the antiferromagnetic Fermi-liquid (Monthoux and Pines, 1994a), and the spin-fermion model (Chubukov, Pines, and Schmalian, 2003) use this approach. Generally, the frequency-dependent scattering rate is expected to be found in systems close to a quantum ($T=0$) phase transition. In the vicinity of such a transition the response of a system to external stimuli is anticipated to follow universal trends defined by the quantum-mechanical nature of fluctuations (Sondhi *et al.*, 1997). Whether or not such universal quantum critical behavior is indeed experimentally observed in cuprate high-T_c superconductors remains a subject of debate (Ioffe and Millis, 1998; Jaklic and Prelovsek, 2000; van der Marel *et al.*, 2003).

The multicomponent approach [Eq. (2)] describes the complicated functional form of the conductivity spectra with a free-carrier Drude term and a set of Lorentzian oscillators (Tanner and Timusk, 1992) assigned, for example, to two-magnon excitations, interband transitions, polarons, and impurity states. Mid-IR bands are expected within models describing hole motion in a quantum antiferromagnet (Trungman, 1988; Kane *et al.*, 1989; Sachdev, 1989) and also predicted with the electronic phase separation scenario (Emery and Kivelson, 1993). The strongest argument in favor of the multicomponent scenario Eq. (2) is that the spectra obtained for lightly doped materials reveal distinct and well-separated absorption resonances, which evolve into a smooth background that blends in with the Drude band as one proceeds with doping.

Both the single-component and the multicomponent approaches have advantages and important shortcomings. The former picture offers a better treatment of the response at low frequencies but its applicability at energies of the order of 1 eV is meaningless, since at these high energies there are additional (interband) contributions to $\sigma(\omega)$. The effective mass $m^*(\omega)$ becomes negative at frequencies above 7000 cm^{-1}, which clearly supports the view that the high-energy part of the spectrum is influenced by additional excitations (Puchkov, Basov, and Timusk, 1996a). Generally, it is not easy to separate contributions to the conductivity arising from "free" and "bound" carriers because there are no experimentally detectable signatures of the crossover from one behavior to the other.

In an attempt to come up with a more rigorous procedure to separate the free carrier response from the mid-infrared term, Romero *et al.* (1992) have analyzed the superconducting-state response of $Bi_2Sr_2CaCu_2O_8$ single crystals (Fig. 12). They assumed that at $T \ll T_c$ all free carriers condense and their spectrum consists simply of a delta function at $\omega=0$. This is a reasonable picture, since various experiments suggest that the in-plane response of high-T_c superconductors is in the clean limit (Bonn *et al.*, 1992). The clean-limit condition is that the residual elastic scattering rate due to impurities is much smaller than the magnitude of the superconducting gap. Thus the remaining contribution to $\sigma(\omega)$ may be assigned to the mid-infrared term. Following this logic, the difference between the spectra in the normal state and in the superconducting state, $\sigma_1^{\mathrm{I}}(\omega,T)=\sigma_1(\omega,T>T_c)-\sigma_1(\omega,T\ll T_c)$, yields the free-carrier contribution to the normal-state conductivity.

C. Infrared signatures of spin/charge self-organization

Neutron and x-ray studies of cuprates reveal the formation of stripes: unidirectional charge-rich regions separating antiferromagnetically ordered spin domains (Kivelson *et al.*, 2003). Tajima *et al.* (1999) used IR spec-

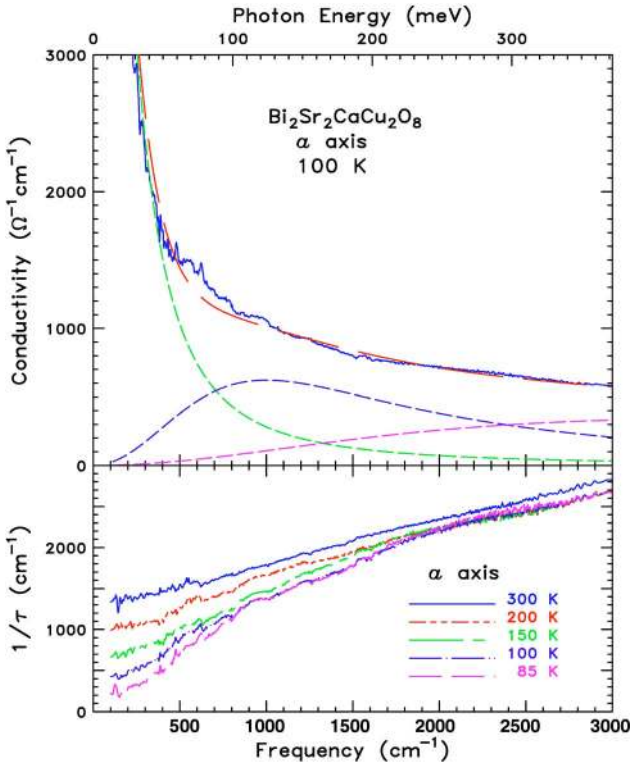

FIG. 12. (Color in online edition) Infrared response of $Bi_2Sr_2Ca_2CuO_8$ single crystal: Top panel, the in-plane conductivity of optimally doped Bi-2212 untwinned single crystals probed with the polarization of incident light along the *a* axis. The dashed lines show separately each of the contributions within the multicomponent picture of the electromagnetic response [Eq. (2)]. Bottom panel, the results of the analysis of the data in the top panel within the one-component model, implying a frequency-dependent scattering rate $1/\tau(\omega)$ (components are given by the dashed lines). From Quijada *et al.*, 1999.

troscopy to examine stripe order in Nd-doped $La_{2-y}Sr_yCuO_4$. The primary role of Nd doping is to stabilize stripes by slowing their fluctuations without directly affecting the doping. On theoretical grounds static stripe ordering can be expected to induce a charge-density-wave gap in the excitation spectrum. However, such a gap is not evident either in the original data or in the later experiments (Dumm *et al.*, 2002). The relative insensitivity of the in-plane conductivity to the stripe order has to be contrasted with photoemission results where it has been claimed that the static ordering of stripes promoted by Nd doping leads to a strong depletion of the nodal quasiparticles (Zhou *et al.*, 1999). Because the in-plane electromagnetic response is primarily formed by the nodal quasiparticles the latter claim is not supported by the optical data. The overall character of the conductivity data for Nd-doped samples is typical of that of disordered cuprates (Tajima *et al.*, 1999; Dumm *et al.*, 2002). Specifically, the $\sigma_1(\omega)$ spectra of the Nd-doped compounds are characterized by a shift of the spectral weight associated with the Drude-like carriers to finite energy. This behavior is characteristic of carrier localization produced by a charge-ordering instability (Caprara *et al.*, 2002). According to the analysis carried out by Benfatto and Smith (2003), this structure is characteristic of the pinning of stripes. Another prominent impact of stripe ordering is the depression of superconductivity. Tajima *et al.* (1999) have found that in samples where stripe order and superconductivity coexist the superfluid density is significantly suppressed. Waku *et al.* (2004) investigated the optical conductivity of $Ca_{2-x}Na_xCuO_2Cl_2$: a system revealing charge ordering in a form of a four CuO_2-unit cell square "checkerboard" (Hanaguri *et al.*, 2004). The direct impact of this peculiar ordered state on the optical properties is not readily apparent. Both temperature and doping trends in the optical conductivity are consistent with the results for La-214.

Recently Homes, Tranquada, *et al.* (2003) analyzed the electromagnetic response of a closely related $La_2NiO_{4.133}$ system that is known to form stripe order within the NiO_2 planes. They argued that mid-IR absorption common for both cuprates and nickelates may be related to stripe ordering. A rich structure in the mid-IR range attributable to stripe ordering in cuprates is expected based on the calculations carried out within the framework of the Gutzwiller approximation (Lorenzana and Siebold, 2003) as well as within the dynamical mean-field theory (Fleck *et al.*, 1999).

The formation of unidirectional order within the 2D CuO_2 planes is expected to trigger strong anisotropy of both transport and optical properties. This expectation is supported by a theoretical analysis of the problem within the *t-J* model (Shibata, 2001). The net result of this work is the complete disappearance of the Drude conductivity in the polarization across the stripes with the transfer of the electronic spectral weight to energies of the order of *t*. Spectroscopic investigation of stripe-related anisotropy within the CuO_2 planes is difficult because in most relevant materials stripe patterns in the neighboring CuO_2 planes are rotated by 90° (Tranquada *et al.*, 1996). However, weakly doped La-214 crystals with $x<0.05$ can be prepared in single-domain form, thus enabling a spectroscopic search for stripe-induced anisotropy using reflectance measurements with polarized light. Such experiments have been reported by Dumm *et al.* (2003). In $La_{2-x}Sr_xCuO_4$ crystals with $x<0.05$, stripes run along the *b* axis of the orthorhombic lattice. The anisotropic response with the enhancement of the conductivity along the stripe direction is evident in the data presented in Fig. 13. Nevertheless, the anisotropy is too weak (<2) to provide direct support to a hypothetical picture of "metallic stripes" rigidly embedded in an antiferromagnetic background. Marked distinction of the anisotropic response of La-214 from that of 1D conductors (Jacobsen *et al.*, 1981) is indicative of novel electronic degrees of freedom relevant to dynamic characteristics of the stripe-ordered state that are not present in conventional 1D systems (Castellani *et al.*, 1997; Kivelson *et al.*, 1998; White and Scalapino, 1998; Chernyshev *et al.*, 2000; Zhou *et al.*, 2001).

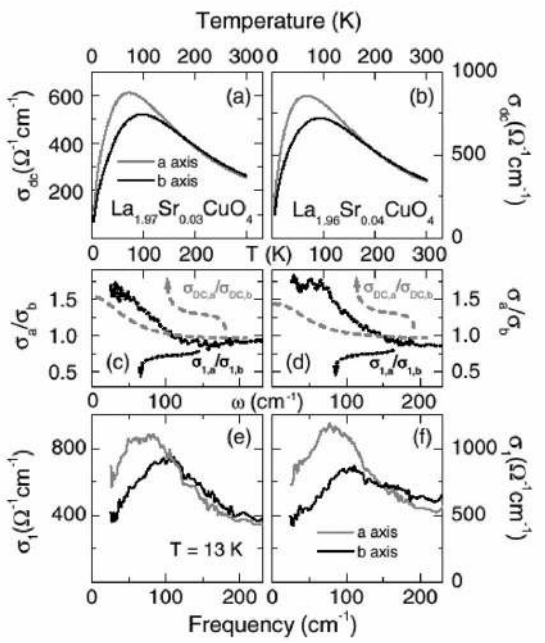

FIG. 13. Anisotropic conductivity of $La_{1.97}Sr_{0.03}CuO_4$ (left panels) and $La_{1.96}Sr_{0.04}CuO_4$ (right panels). Panels (a), (b), (e), and (f) show temperature and frequency dependence of the conductivity. The *a* axis corresponds to the direction of spin stripes; the *b* axis is across the direction of spin stripes. The lattice contribution has been subtracted from $\sigma_1(\omega)$ in (e) and (f) by fitting the phonon peaks to Lorentzian oscillators. Panels (c) and (d) display the anisotropy of both ac and dc conductivities. Dashed line, $\sigma_{dc,a}(\omega)/\sigma_{dc,b}(\omega)$; dotted line, $\sigma_{1,a}(\omega)/\sigma_{1,b}(\omega)$ at 13 K. From Dumm *et al.*, 2003.

VII. ELECTRODYNAMICS IN THE NORMAL STATE

It was clear from the beginnings of high-temperature superconductivity that the normal state of the new superconductors was highly anomalous (Anderson, 1987). The transport properties are superficially metallic with a linear temperature dependence of the resistivity and a Drude-like metallic infrared reflectance but these properties differ in very important ways from those of ordinary metals. The extrapolation of the linear resistivity to $T=0$ does not cut the temperature axis at a temperature that in ordinary metals is a fraction of the Debye temperature—a signature of electron phonon interaction (Allen, 1992). Instead, the resistivity extrapolates to a nearly zero value at $T\rightarrow 0$ in good samples at optimal doping. Also, there was no sign of resistivity saturation expected when the mean free path approached the unit cell size (Gurvitch and Fiory, 1987).

The *c*-axis optical conductivity is also highly anomalous. There is no Drude mode, and apart from obvious peaks due to transverse phonons, the conductivity is nearly frequency independent. In Fig. 16 we show data generated for a variety of high-T_c systems in different experimental groups reproduced from Dordevic, Singley, *et al.* (2004). The unusual nature of the electronic conductivity becomes more obvious if the phonons are modeled as Lorentzian functions and subtracted from the $\sigma(\omega)$ spectra (Fig. 15). This analysis when applied to underdoped Y-123 uncovers a flat spectrum at high temperature that develops a gaplike depressions as the temperature is lowered (Homes, Timusk, *et al.*, 1993).

A. Survey of experimental results

1. In-plane conductivity

The first systematic study of the in-plane conductivity throughout the phase diagram of the cuprates was by Orenstein, Thomas, *et al.* (1990). This work used twinned single crystals of Y-123. Although the data represent a mixture of the genuine response of CuO_2 planes and Cu-O chains, the authors were able to identify many important trends. Specifically, the conductivity spectra of underdoped samples showed the formation of a gaplike feature already at $T>T_c$. The authors proposed that the origin of this gap may be related to the spin gap seen in the NMR experiments since both effects occur approximately in the same temperature range. An experimental study of untwinned crystals reported by Rotter *et al.* (1991) shows a similar depression of $\sigma_a(\omega)$ in 500-cm^{-1} region measured in the polarization normal to the Cu-O chains accompanied by a narrowing of the Drude peak (Fig. 14). A detailed discussion of the charge dynamics in cuprates from underdoped to overdoped regimes was reported by Puchkov, Basov, and Timusk (1996) and also discussed by Basov and Timusk (2001). Since it is difficult to access all doping regimes using one family of cuprates, they used Y-123, Y-124, Bi-2212, and Tl-2201 materials which in combination allow one to follow trends in the evolution of the electromagnetic response throughout the entire phase diagram. As the doping progresses from underdoped to overdoped one witnesses a continuous increase of the strength of the low-energy (Drude-like) contribution to the conductivity relative to the conductivity in the mid-IR plateau. The minimum in the $\sigma(\omega)$ spectra near 500 cm^{-1} weakens in optimally doped samples and disappears on the overdoped side. These trends are common for double-layered cuprates such as Y-123 and Bi-2212 as well as for single-layered materials such as Tl-2201 (Puchkov, Fournier, *et al.*, 1996) and La-214 (Takenaka *et al.*, 2003). We shall revisit these issues in the following subsections.

2. Interplane conductivity

Systematic studies of the interplane response across the phase diagram of cuprates were reported by Homes, Timusk, *et al.* (1995a, 1995b) for the Y-123 system and by Uchida *et al.* (1996) for La-214. The electronic background in the *c*-axis conductivity is strongly depressed and the spectra are dominated by phonons (Fig. 15). At high doping levels the $\sigma_c(\omega)$ data may be compared to those of a dirty metal: the spectral dependence at least remotely resembles a broad Lorentzian with $1/\tau$ narrowing at low T (Schützmann *et al.*, 1994). In most materials the mean free path along the *c* direction is of the order of the interlayer spacing (Schützmann *et al.*, 1994) making the conductivity almost completely incoherent. Fur-

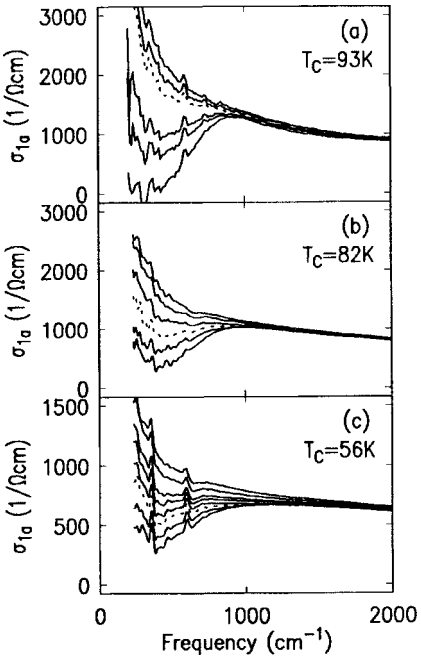

FIG. 14. CuO_2 plane conductivity $\sigma_a(\omega)$ for various temperatures in both the normal and superconducting states of Y-123. Panel (a): nearly optimally doped crystal with $T_c=93$ K from top to bottom, $T=120,100,90$ (dashed), 70, and 20 K; panel (b): underdoped crystal with $T_c=82$ K at $T=150$, 120, 90, 80 (dashed), 70, and 20 K; panel (c): underdoped crystal with $T_c=56$ K at $T=200$, 150, 120, 100, 80, 60 (dashed), 50, and 20 K. Note the persistence of the 500-cm^{-1} threshold above T_c (above dashed curves). From Rotter *et al.*, 1991.

ther in the underdoped regime both the ω and the T dependence of the interlayer conductivity are definitely nonmetallic: $\sigma_c(\omega)$ is suppressed at low T with a transfer of spectral weight to higher energy. Crystals of Y-123, with oxygen concentrations below $y=6.7$, reveal the pseudogap discovered by Homes, Timusk, *et al.* (1993) which will be analyzed in more detail in the following subsections.

3. Response of Cu-O chains

In addition to the copper-oxygen planes, $YBa_2Cu_3O_x$ and $YBa_2Cu_4O_8$ materials have one-dimensional Cu-O chains extending along the b axis of the crystals. Polarized light measurements of untwinned Y-123 and Y-124 crystals show a remarkable anisotropy with enhanced b-axis reflectance (Bozovic *et al.*, 1988; Schlesinger *et al.*, 1990; Pham *et al.*, 1991; Bucher *et al.*, 1992; Cooper *et al.*, 1992; Schützmann *et al.*, 1992; Tanner, Gao, *et al.*, 1992; Basov, Liang, *et al.*, 1995; Wang *et al.*, 1998; Homes, Bonn, *et al.*, 1999; Takenaka *et al.*, 2000; Lee *et al.*, 2005a). The position of the plasma minimum in reflectance is about 1.2 eV for $E\|a$ and about 2.5 eV for $E\|b$. The conductivity obtained through Kramers-Kronig analysis shows a significant enhancement of the b-axis spectral weight, which can be interpreted in terms of an additional conductivity channel associated with the chains.

This anisotropy is also observed in the dc conductivity with enhancement of σ_{dc} along the b direction (Friedmann *et al.*, 1990; Welp *et al.*, 1990; Rice *et al.*, 1991). While there was considerable scatter in the data for the anisotropy in the samples studied in 1988–1992, later results seem to indicate that the σ_b/σ_a is the same as $\omega_{pb}^2/\omega_{pa}^2$ (Zhang *et al.*, 1994; Basov, Liang, *et al.*, 1995). Applying the simple Drude formula to these results $4\pi\sigma_{dc}=\omega_p^2/\tau$ suggests that the scattering rate is the same for the carriers in the CuO_2 planes as in the chains. In strongly underdoped Y-123 crystals chain segments appear to imprint charge modulation in the CuO_2 planes leading to a strongly anisotropic scattering rate (Lee *et al.*, 2004).

Takenaka *et al.* (2000) and Lee *et al.* (2005a) reported on a power-law scaling at mid-IR frequencies consistent with predictions for Tomonaga-Luttinger liquid (Giamarchi, 1997; Schwartz *et al.*, 1998), thus supporting the notion of one-dimensional transport in the chains. The analysis carried out by Lee *et al.* (2005a) indicates that the chain segment length has to exceed a minimum value of 15–20 Å to trigger the universal power law in $\sigma(\omega)$. Once the chain fragment length exceeds the critical value and the separation between these fragments is reduced, the conductivity associated with chains reveals Drude-like behavior, which would be impossible in a system of isolated disordered chains. Therefore these experiments support the idea of strong coupling between the chain segments that is likely to be mediated by proximity to CuO_2 planes.

B. Interplane conductivity and the pseudogap

The interplane conductivity of cuprates is not only much smaller than σ_{ab} but also varies widely from a maximum of about 400 Ω^{-1} cm^{-1} in the most isotropic compound $YBa_2Cu_3O_7$ down to 0.01 Ω^{-1} cm^{-1} in one of the most anisotropic $Bi_2Sr_2Ca_2CuO_8$. As Fig. 15 shows, the spectra are dominated by sharp peaks due to direct absorption from optical phonons which are superimposed on an almost completely frequency-independent electronic background. The phonon modes observed at room temperature, where the electronic effects are not anomalous; they are what one would expect from lattice dynamics models based on neutron scattering (Timusk *et al.*, 1995). The only exception is the mode at 560 cm^{-1} that involves the apical oxygen atom, which appears to be anomalously strong. The electronic background is essentially featureless above the pseudogap temperature at T^*. In the strange-metal region of the phase diagram, this conductivity is both temperature and frequency independent. In the highly overdoped region, conductivity begins to show slight evidence of emerging coherence (Schützmann *et al.*, 1994).

The pseudogap produces a strong gaplike depression in the c-axis conductivity (Homes, Timusk, *et al.*, 1993, 1995a, 1995b; Basov, Timusk, *et al.*, 1994; Schützmann *et al.*, 1994; Bernhard *et al.*, 1998, 1999). Figure 15 shows this effect where below 300 K a gaplike depression oc-

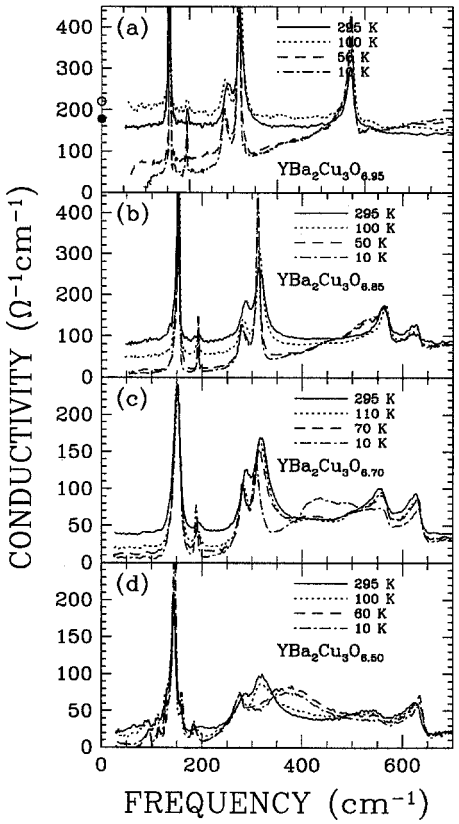

FIG. 15. The optical conductivity for the Y-123 system for radiation polarized along the c axis for four different oxygen dopings. In the highly doped material below $T_c=93.5$ K a gaplike depression opens up below 500 cm^{-1} but at 10 K the conductivity is nonzero down to at least 100 cm^{-1}. In the $x=0.85$ material, the conductivity is clearly nonmetallic in nature, a trend that resolves itself into a pseudogap for $x<0.70$. Adapted from Homes, Timusk, *et al.*, 1995a.

curs in the optical conductivity for underdoped crystals. At $T>T^*$ the electronic contribution to the conductivity is nearly frequency independent signaling incoherent c-axis response. Several aspects are notable about the pseudogap: (i) The frequency of the gap does not go to zero as the temperature is raised, i.e., the gap does not close. Unlike collective gaps, such as the superconducting gap, which gradually close as pair-breaking excitations build up, the pseudogap appears at full width at high temperature. (ii) The pseudogap has a rather flat bottom and its magnitude and depth do not change much when the superconducting state is reached. [It should be noted here that striking changes take place in the imaginary part of the optical conductivity as superconductivity sets in, leading to a sharp plasma edge in raw reflectance (Fig. 5).] A very similar structure to what is seen in the superconducting cuprates is also observed in the nonsuperconducting ladder cuprate $Sr_{14-x}Ca_xCu_{24}O_{41}$ (Osafune *et al.*, 1999).

As pointed out by Homes, Timusk, *et al.* (1993), the formation of a gap in c-axis conductivity explains the change in slope of the dc resistivity $\rho_{dc}=1/\sigma_{dc}$ which changes from metallic ($d\rho/dT>0$) in the optimally doped and overdoped samples to semiconducting ($d\rho/dT<0$) in underdoped compounds (Ito *et al.*, 1993; Nakamura and Uchida, 1993).

Bernhard *et al.* used infrared ellipsometry to analyze c-axis optical conductivity in a series of Ca-doped Y-123 crystals (Bernhard *et al.*, 1998, 1999). Ca^{2+} substitution for Y^{3+} adds holes to the copper-oxygen plane in addition to those that are transferred from the copper-oxygen chains. These authors were able to observe the same pseudogap effects with Ca doping that were seen with oxygen doping, showing that the pseudogap was a property of the copper-oxygen plane and not a special feature associated with the chains. They were also able to reach the overdoped region and show that the nature of the gap changed—it became more conventional. It was not present in the normal state but appeared only below T_c, the superconducting transition. Also, unlike the pseudogap, the superconducting gap closes at T_c.

The close correlation between depressed c-axis conductivity and the pseudogap found by Homes, Timusk, *et al.* (1993) supplies us with a tool for studying the pseudogap with simple transport measurements. An example of this kind of data is the work of Shibauchi *et al.* (2001), who studied the influence of high magnetic fields on the pseudogap as a function of doping in Bi-2212. They found that the pseudogap onset temperature drops uniformly with field. According to this work the pseudogap can still be observed in Bi-2212 up to a doping level of $p=0.22$. A pseudogap in overdoped Bi-2212 has also been reported by Suzuki and Watanabe (2000) and by Krasnov *et al.* (2000).

A number of mechanisms have been proposed that would result in an incoherent conductivity spectrum (Kumar *et al.*, 1990; Ioffe *et al.*, 1993; Rojo and Levin, 1993; Nyhus *et al.*, 1994; Clarke *et al.*, 1995; Graf *et al.*, 1995; Alexandrov *et al.*, 1996; Ioffe and Millis, 1999). The underlying physics of this incoherence is clear. In the strange-metal region the electronic states of the carriers in the copper-oxygen planes are very short lived, as shown by the very large ab-plane scattering rates, which are of the order of 100 meV and higher. On the other hand, the interplane transfer matrix elements are much smaller, according to band-structure calculations, with a maximum of around 30 meV for the most conducting systems (Cooper and Gray, 1994). There simply is not enough time to set up a coherent wave in the c direction before it becomes disrupted by frequent in-plane collisions.

C. Transverse plasmon in c-axis conductivity and bilayer effects

An inspection of Fig. 16 reveals an important distinction between the interlayer response of high-T_c cuprates with just one CuO_2 plane per unit cell (left panels) and those that have bilayers of CuO_2 (right panels). In the latter class of materials the spectra measured in the su-

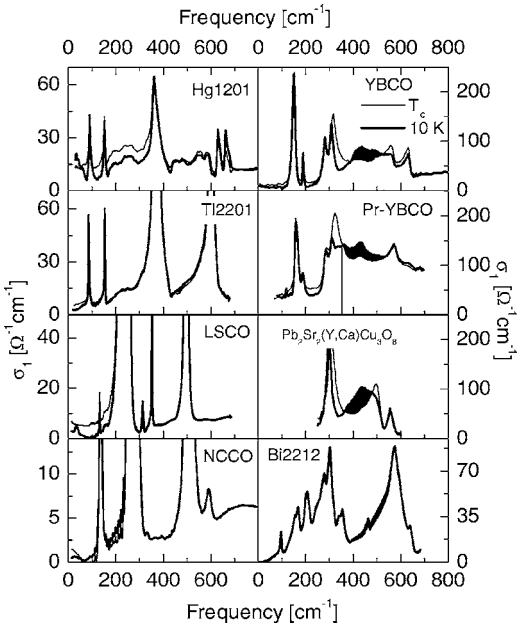

FIG. 16. Interlayer conductivity $\sigma_1(\omega)$ of single-layer (left panels) and double-layer cuprates (right panels) at T_c and $T \ll T_c$. Experimental data: $HgBa_2CuO_4$ (Hg-1201; Singley *et al.*, 2001); $Tl_2Ba_2CuO_{6+x}$ (Tl-2201; Basov, Woods, *et al.*, 1999; Katz *et al.*, 2000), $La_{2-x}Sr_xCuO_4$ (Dordevic, Singley, *et al.*, 2002), $Nd_{2-x}Ce_xCuO_4$ (NCCO; Singley *et al.*, 2001), $YBa_2Cu_3O_{6.6}$ (YBCO; Homes, Timusk, *et al.*, 1995a, 1995b), $Pr_yY_{1-y}Ba_2Cu_3O_{7-\delta}$ (Dordevic, Singley, *et al.*, 2004), $Pb_2Sr_2(Y/Ca)Cu_3O_8$ (Reedyk *et al.*, 1994), $Bi_2Sr_2CaCu_2O_z$ (Bi-2212; Dordevic, Singley, *et al.*, 2004). In single-layered systems the $\sigma_1(\omega, T \ll T_c)$ spectra are suppressed compared to $\sigma_1(\omega, T_c)$ data, in accord with type-II coherence factors relevant to the response of superconductors in the dirty limit. In contrast crossing between normal and superconducting data (shaded areas) is apparent in the conductivity spectra for several different classes of double-layered materials. Adapted from Dordevic, Singley, *et al.*, 2004.

perconducting state reveal excess conductivity at $\omega \simeq 400-500$ cm^{-1}. Such a resonance is not found in any of the single-layered compounds. This latter behavior is incompatible with type-II coherence factors in an extreme dirty superconductor, relevant to the *c*-axis conductivity of cuprates (Grüninger *et al.*, 2000a, 2000b). A similar feature in the response of an underdoped Bi-2212 crystal was reported by Zelezny *et al.* (2001). Recent data for a triple-layered $Bi_2Sr_2Ca_2Cu_3O_{10}$ also show a similar crossing effect (Boris *et al.*, 2002), suggesting that this behavior is likely to be a common property of all multilayered cuprates.

An interesting model for the 400-cm^{-1} resonance feature in the *c*-axis conductivity of multilayered cuprates was advanced by van der Marel and co-workers. Assuming that a double-layered cuprate can be viewed as a stack of geometrically separated metallic layers, the dielectric function (van der Marel and Tsvetkov, 1996; Grüninger *et al.*, 2000a, 2000b) acquires the following form:

$$\epsilon(\omega) = \frac{(\omega^2 - \omega_{p,A}^2)(\omega^2 - \omega_{p,B}^2)}{\omega^2(\omega^2 - \omega_0^2)}. \tag{26}$$

In Eq. (26) $\omega_{p,A}$ and $\omega_{p,B}$ are the plasma frequencies of the two layers. Equation (26) implies that in addition to the usual bulk plasma mode at $\omega=0$ with the strength $\rho_s=(\omega_{p,A}\omega_{p,B}/\omega_0)^2$, a new transverse mode at the frequency $\omega_0=\sqrt{x_B\omega_{p,A}^2+x_A\omega_{p,B}^2}$ develops in the conductivity spectrum. The oscillator strength ρ_0 of this latter mode is given by

$$\rho_0 = \frac{(\omega_{p,B}^2 - \omega_{p,A}^2)^2}{\frac{\omega_{p,A}^2}{x_A} + \frac{\omega_{p,B}^2}{x_B}}, \tag{27}$$

where x_A and x_B are the relative volume fractions of the two subcells in a crystal ($x_A+x_B=1$). This formalism therefore describes a *transverse* plasma resonance occurring in situations when two or more plasmas are geometrically separated. Two longitudinal Josephson plasma resonances were reported for $SmLa_{1-x}Sr_xCuO_{4-d}$ (Shibata and Yamada, 1998). This cuprate has a single CuO_2 plane separated by alternating Sm_2O_2 and $(La,Sr)_2O_{2-d}$ blocking layers. When the material becomes superconducting, two resonances are seen. Both appear at T_c and follow mean-field temperature dependencies, although the two curves are not identical. The authors attribute the resonances to the two different series of Josephson junctions in the two different blocking layers. A transverse plasma resonance in this material has also been seen (Dulic *et al.*, 2001; Kakeshita *et al.*, 2001; Shibata 2001). van der Marel (2004) reviewed enigmatic plasmon phenomena in cuprates.

Grüninger *et al.* (2000a, 2000b) employed the framework of the transverse Josephson mode to interpret an anomalous *c*-axis resonance in the conductivity of double-layered cuprates shown in Figs. 16 and 17. Moreover, this model has been extremely successful in self-consistently explaining "phonon anomalies" in the *c*-axis spectra (Munzar *et al.*, 1999b). The important new feature of the analysis of Munzar *et al.* (1999a, 1999b) is a proper account of the local electric fields acting on the ions participating in the phonon modes. In particular, the dramatic loss of intensity of the bond-bending mode of the planar oxygen atoms at 320 cm^{-1} was well accounted for. Accurate fits of complex phonon behavior at all temperatures (Fig. 18) uncover both the significance of the local fields and the ability of the multilayered model to elucidate this behavior.

The microscopic origin of the transverse resonance is being debated. The original interpretation assigns these modes to Josephson currents in bilayer systems. However, the analysis of the temperature dependence of interlayer conductivity suggests that this feature develops near 150 K, well above the T_c of underdoped crystals (Homes, Timusk, *et al.*, 1995a, 1995b; Bernhard *et al.*, 2000). To explain the appearance of the peak at temperatures above T_c Grüninger *et al.* (2000a, 2000b) had to invoke the idea of preformed pairs, i.e., supercon-

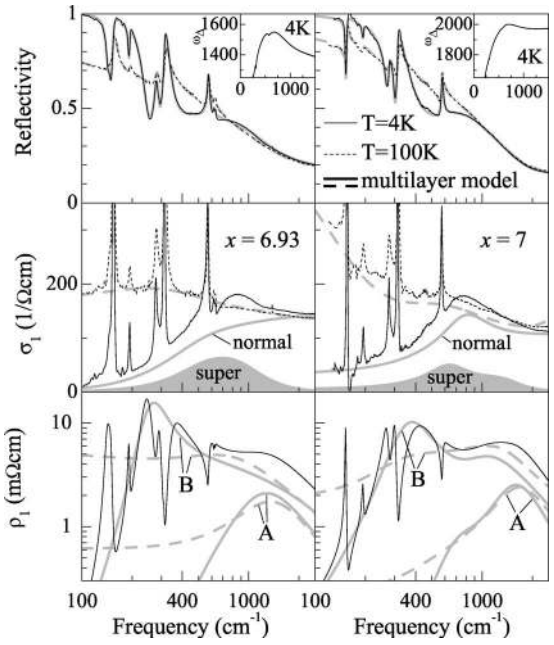

FIG. 17. The c-axis reflectivity R, real part of the conductivity $\sigma_1(\omega)$, and real part of the complex impedance $\rho_1(\omega)$ above (dashed lines) and below T_c (solid lines): left panels, $YBa_2Cu_3O_{6.93}$; right panels, $YBa_2Cu_3O_7$. The thick gray lines depict fits of reflectance and of the conductivity using the multilayer model. The shaded areas show the electronic contribution due to superconducting carriers. In order to demonstrate that the total Re $\rho(\omega)$ is a linear superposition of the subcell contributions, also displayed are the electronic contributions Re ρ_A and Re ρ_B along with the total dynamical resistivity, including the phonons, as obtained from the fit in the upper panel. The "superconducting" contribution to the conductivity is not confined to the δ function at $\omega=0$ but also appears at finite energies in these bilayered materials (shaded regions in the middle panels). From Grüninger *et al.*, 2000a.

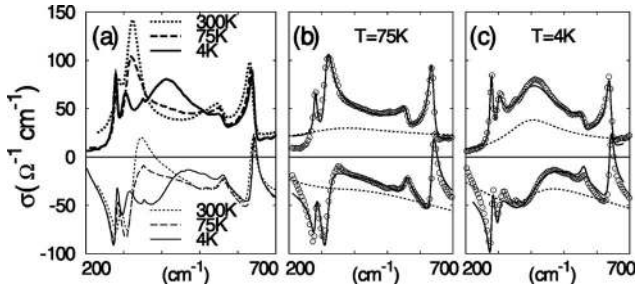

FIG. 18. An account of the local fields associated with the transverse resonance in multilayered crystals, allowing one to accurately describe anomalies in the phonon line shapes and oscillator strengths: (a) Experimental spectra of the c-axis conductivity, $\sigma=\sigma_1+i\sigma_2$, of $YBa_2Cu_3O_{6.55}$ with $T_c=53$ K; top panels, $\sigma_1(\omega)$ spectra; bottom panels, $\sigma_2(\omega)$ spectra, ○, experimental data; solid lines, the fits obtained by using the multilayered model described in the text for (b) $T=75$ K and (c) $T=4$ K; dotted lines in (b) and (c), the electronic contributions. From Munzar *et al.*, 1999a.

ducting fluctuations (without long-range order) at temperatures higher than T_c. Such fluctuations have indeed been observed in the vicinity of T_c in both charge transport (Corson *et al.*, 1999; Xu *et al.*, 2000) and the Nernst effect (Xu *et al.*, 2000; Wang *et al.*, 2001). It was shown by Timusk and Homes (2003) that the intensity of the resonance can be explained, within the transverse plasmon model, by assuming that the resonance is caused by coherent c-direction currents between the bilayers, whose lifetime is set by the in-plane lifetime. This scenario offers an explanation for the close correlation between magnetic resonance and the c-axis spectral features.

A very different point of view has been advocated by Dordevic, Singley, *et al.* (2004), who assigned this mode to a peculiar interband transition. If the degeneracy between the bonding and antibonding bands associated with the two constituents of the CuO_2 bilayer (a so-called bilayer splitting effect) is lifted by interactions, then an interband transition is expected to be observed in the c-axis conductivity. Bilayer splitting has been theoretically predicted by Chakravarty *et al.* (1993) and also inferred from an analysis of the electronic band structure (Massidda *et al.*, 1988; Mazin *et al.*, 1992; Andersen *et al.*, 1995; Eder *et al.*, 1995; Liechtenstein *et al.*, 1996). Bilayer splitting has been experimentally detected in Bi-2212 compounds using ARPES measurements (Chuang *et al.*, 2001; Feng *et al.*, 2001) most recently in underdoped crystals (Borisenko *et al.*, 2004).

D. One-component analysis of the in-plane conductivity

The one-component method for analysis of the optical conductivity (extended Drude model in Secs. IV.B and IV.C), when applied to the cuprates[1] showed that the scattering rate $1/\tau(\omega)$ was frequency dependent. At room temperature $1/\tau(\omega)$ spectra are nearly linear, with ω over a broad range of frequencies extended up to a good fraction of an electron volt. Furthermore, the magnitude of the scattering rate exceeded the frequency, violating the basic assumption of Fermi-liquid theory, which demands that the quasiparticles be coherent: $1/\tau(\omega) < \hbar\omega$.

Fundamental assumptions of the one-component analysis (Sec. VI.B) can be questioned, particularly in underdoped materials, where a separate mid-infrared band can be clearly resolved (Fig. 23). On the other hand, there is ample evidence for the strong scattering processes of the one-component modelnear optimal doping. ARPES dispersions have strong curvatures in the energy range of the mid-infrared (Damascelli *et al.*, 2003), and these can be analyzed to yield scattering rates that agree with those derived from infrared data (Kaminski *et al.*, 2000; Hwang, Timusk, and Gu, 2004). Raman and magnetic neutron scattering show that strong spin fluctuations exist in this spectral region. These may

[1]See, for example, Thomas *et al.*, 1988; Schlesinger *et al.*, 1990; Bucher *et al.*, 1992; Cooper *et al.*, 1992; El Azrak *et al.*, 1994; Basov, Liang, *et al.*, 1996; Quijada *et al.*, 1999; McGuire *et al.*, 2000; Tu *et al.*, 2002; and Hwang, Timusk, and Gu, 2004.

play the role of the phonon in conventional superconductivity (Carbotte *et al.*, 1999; Abanov *et al.*, 2001; Schachinger *et al.*, 2003).

An important result of the one-component analysis of optical conductivity is the presence of gaplike depressions of the scattering rate that develop as the temperature is lowered below ambient temperature (Basov, Liang, *et al.*, 1996). In systems with coherent metallic conductivity, a gap in the scattering rate is suggestive of a gap in the corresponding bosonic spectrum. We shall see below that an analysis of scattering-rate spectra obtained from infrared conductivity can be used to map out these bosonic spectra and compared in detail with the results of other spectroscopies, ARPES, and magnetic neutron scattering, in particular. However, unlike phonons of the conventional metals, which are present at all temperatures, the excitations in high-temperature superconductivity change as one moves around on the temperature-doping phase diagram. We start with a brief summary of our current knowledge of this phase diagram and then discuss the optical properties of each region in detail.

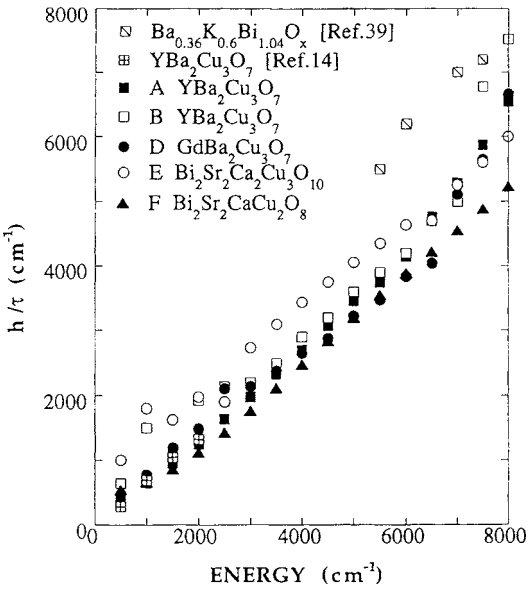

FIG. 19. The frequency-dependent scattering rate for various high-temperature superconductors plotted over a wide frequency range. The quantity plotted is $1/\tau^*$, the renormalized scattering rate. Adapted from El Azrak *et al.*, 1994.

1. The strange-metal region and the quantum critical point

At high temperature in the strange-metal region of the phase diagram, the infrared reflectance of the cuprates is approximately linear as a function of frequency up to nearly 0.5 eV. The slope varies linearly with doping—the curves get steeper as the doping decreases. This fact can be used to calibrate the doping level of crystals in the infrared (Hwang, Timusk, Puchkov, *et al.*, 2004). Kramers-Kronig analysis of the reflectance shows that this behavior is the result of non-Drude behavior of the optical conductivity. Instead of dropping off as ω^{-2} at high frequency, the variation of the conductivity is much flatter, varying approximately as $\omega^{-0.77}$ (El Azrak *et al.*, 1994; van der Marel *et al.*, 2003). This unusual behavior is seen in all cuprate superconductors that have been investigated in the mid-infrared. Within the one-component model, this conductivity leads to a scattering rate that varies approximately linearly with frequency. Figure 19 shows the scattering rate for a series of thin films of different high-temperature superconductors. In this figure, the renormalized scattering rate $1/\tau^* = \omega[\sigma_1(\omega)/\sigma_2(\omega)]$ is plotted. This quantity can be determined without a need to know the plasma frequency ω_p. A procedure for determining the plasma frequency from near-infrared data was introduced by Hwang, Timusk, Puchkov, *et al.* (2004).

van der Marel *et al.* (2003) found that the conductivity of Bi-2212 crystal varies with frequency as $\omega^{-0.65}$. These authors focus on the phase angle of the complex conductivity and find that the conductivity is given by $\sigma(\omega) = C\omega^{\gamma-2}e^{i(\pi/2)(2-\gamma)}$ with $\gamma=1.33$ in the optimally and slightly overdoped region. They argue that this power law for the amplitude and the frequency independence of the phase are evidence of a quantum critical point in the optimally doped region. The idea of a quantum critical point at a doping level that separates the low-doping region dominated by the pseudogap and a high-doping region governed by Fermi-liquid behavior has been suggested by several authors (for an overview see Sachdev, 2003 and Varma *et al.*, 2002). It is expected that at the critical doping level the transport scattering rate would be linear in frequency and temperature down to the lowest temperatures. One problem with this scenario is that the superconducting state interferes by gapping the fluctuations at T_c, and the measurements should be carried out in the normal state. This can be achieved, for example, through the destruction of superconductivity through magnetic fields (Shibauchi *et al.*, 2001).

Power-law behavior of the conductivity has been proposed by several authors. Anderson suggests a conductivity given by $\sigma(\omega)=(-i\omega)^{\gamma-2}$ based on theories of 1D Luttinger liquids. The predicted magnitude of γ is in good agreement with what is seen in the mid-infrared: $\gamma=1.33$ (El Azrak *et al.*, 1994; Baraduc *et al.*, 1996) and $\gamma=1.35$ (van der Marel *et al.*, 2003). Varma *et al.* (1989) have advanced the so-called marginal Fermi-liquid hypothesis, which also yields a power-law conductivity with $\gamma=1.0$. The cold-spot model of Ioffe and Millis (1998) also predicts a power law with $\gamma=1.5$. Fermi-liquid models based on a flat spectrum of spin fluctuations also produce approximate power-law frequency dependences of the optical conductivity (Jaklic and Prelovsek, 2000; Abanov *et al.*, 2001; Schachinger *et al.*, 2003).

Another difference that appears in the overdoped region is the frequency dependence of $1/\tau(\omega)$, which becomes superlinear in the strongly overdoped cuprates and has a reduced magnitude compared to underdoped or optimally doped materials. The effective mass, as calculated from the extended Drude model, is very close to m_e. Fits of the reflectance to marginal Fermi-liquid spec-

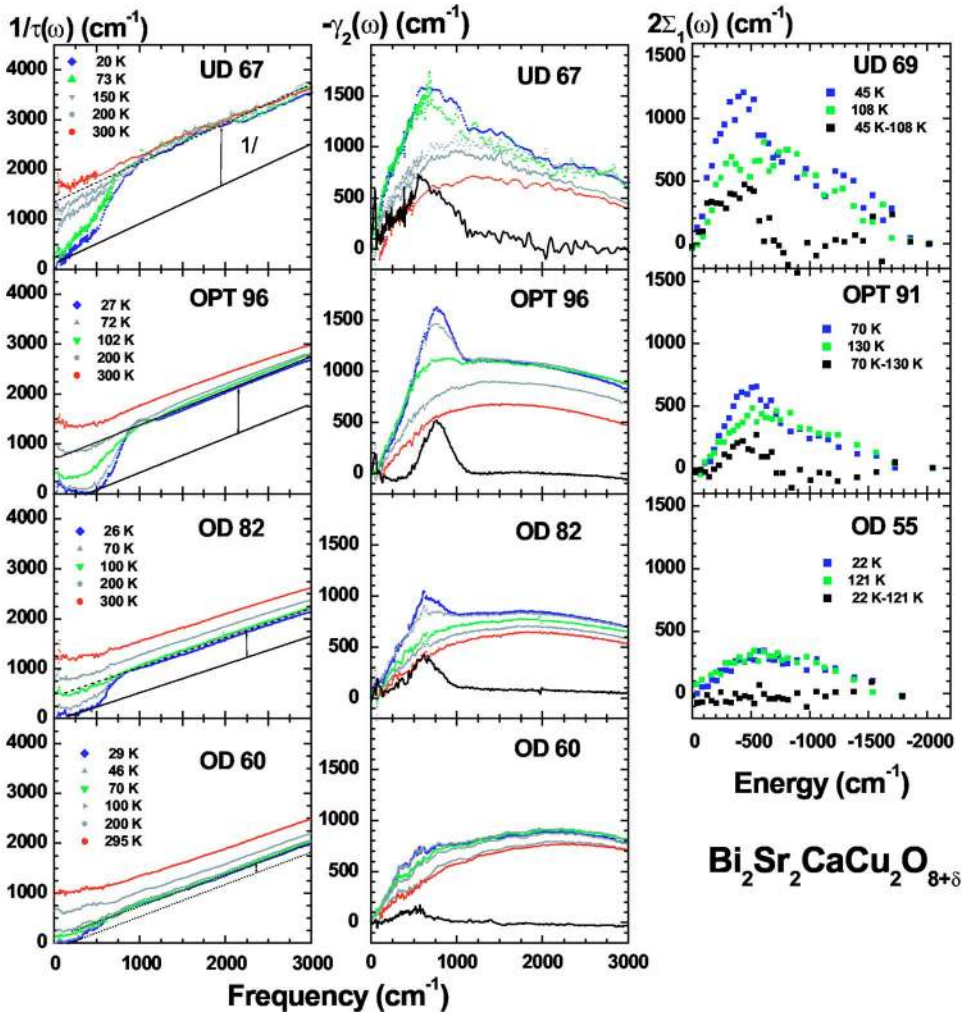

FIG. 20. (Color in online edition) Electronic self-energy-effects probed by means of IR and ARPES spectroscopy: Left panels, real part, and middle panels, imaginary part of the frequency-dependent scattering rate at a series of doping levels for Bi-2212. UD, underdoped regime; OPT, optimally doped regime; OD, overdoped regime. There is a gradual decrease of the steplike onset in scattering as the doping level increases. The middle panels show that the scattering can be separated into two channels: a sharp peak and a broad background. Black lines in the middle panel show the differential spectra between data at $T \approx T_c$ and the lowest temperature. From Hwang, Timusk, and Gu, 2004. Right panel shows the self-energy spectra from ARPES measurements of Johnson *et al.* (2001).

tra of excitations show that the coupling constant to the spectrum λ decreases uniformly with doping (Hwang, Timusk, Puchkov, *et al.*, 2004).

2. The bosonic resonance and the in-plane response

As the temperature is lowered below ≈150 K in underdoped Bi-2212, drastic changes take place in nearly all the properties that affect the charge carriers. The in-plane scattering rate at low frequencies drops dramatically. As shown in Fig. 20, the scattering rate is now smaller than the frequency, and the conductivity becomes coherent. Closely connected with this coherence is the appearance of new features in the infrared spectra. The first of these is a sharp onset of in-plane scattering at 500 cm^{-1}, giving rise to the familiar steplike decrease in infrared reflectance at this frequency. At the temperature and doping level of the onset of coherence, a sharp resonance develops in the magnetic neutron-scattering cross section, the well-known 41-meV peak (its energy in optimally doped Y-123). In the coherent region, the interplane conductivity develops an unusual peak at approximately 400 cm^{-1}, discussed above in Sec. VII.B.

The coherence that emerges at low temperature is restricted to the low-frequency region (Fig. 20). Above 500 cm^{-1} there is a strong steplike onset of scattering. Model calculations show that such a sharp onset of scattering is caused by a bosonic mode in general and the 41-meV neutron resonance in particular since it appears at the same temperatures and doping level as the step in reflectance (Puchkov, Basov, and Timusk, 1996; Norman and Ding, 1998). We shall discuss these calculations below in more detail. Close to optimal doping, the coherence temperature T_s approaches the superconducting transition temperature T_c and it becomes difficult to distinguish between the onset of coherence seen in the spin-gap state and true superconductivity. In optimally

doped samples, the sharp onset in scattering appears just above or at T_c, the superconducting transition temperature.

The spectra in the heavily overdoped region do not show any evidence of the steplike onset of scattering from the boson mode down to the lowest temperatures. As Fig. 20 shows, the curves are smooth at all temperatures and display a simple temperature dependence in which the scattering rate is approximately linear in temperature with a prefactor such that $\hbar/\tau \approx \pi k_B T$. In a recent paper Hwang, Timuks, and Gu (2004) suggested that in the Bi-2212 system the coupling to the bosonic resonance weakens with doping to disappear completely at a doping level of $p=0.24$. This observation is consistent with the data on the Tl-2201 material (Puchkov, Fournier, *et al.*, 1996). Figure 20, adapted from the paper of Hwang, Timusk, Puchkov, *et al.* (2004), shows the gradual weakening of the contribution of the bosonic resonance to the self-energy. The middle panels of Fig. 20 plot the imaginary part of the scattering rate $\gamma(\omega)$. This quantity is closely related to the self-energy of quasiparticles, which can be measured directly with ARPES although there are important differences (Kaminski *et al.*, 2000; Millis and Drew, 2003; Shachinger *et al.*, 2003). The figure shows clearly that as the doping level increases, the contribution of the bosonic resonance to the self-energy decreases and nearly vanishes at the highest doping level observed of $p=0.23$. The frequency position of the resonance extracted from IR data correlates with the transition temperature (Fig. 21), as will be discussed in Sec. VII.H.

In Fig. 20 we compare the approximation to the self-energy measured through the imaginary part of the infrared scattering rate with the corresponding ARPES quantity. The close quantitative agreement between the two sets of data suggests it may be possible to analyze infrared spectra to find directly the bosonic function that describes the interaction between the charge carriers. Such a procedure worked in conventional superconductors, where the Eliashberg function $\alpha F^2(\Omega)$ was extracted from the self-energy structure of tunneling spectra (Carbotte, 1990). In the case of the high-temperature cuprates, in addition to tunneling spectroscopy we have, as the figure shows, potential data from both ARPES and infrared conductivity. In this section we shall describe some initial steps of a program for extracting the free-carrier self-energies from optical spectra and compare these with other spectroscopies, principally ARPES but also tunneling and neutron scattering.

Several approaches have been used. The simplest has been to assume a model for the excitation spectrum and the background electronic density of states and then use standard Fermi-liquid theory to calculate the frequency-dependent scattering rate and the optical conductivity and the infrared reflectance. The model parameters can then be adjusted to bring the model and the experimental data into accord. The work of Orenstein, Thomas, *et al.* (1990), Norman and Ding (1998), Puchkov, Basov, and Timusk (1996), and Munzar *et al.* (1999a) showed that at least at some doping levels and temperatures a

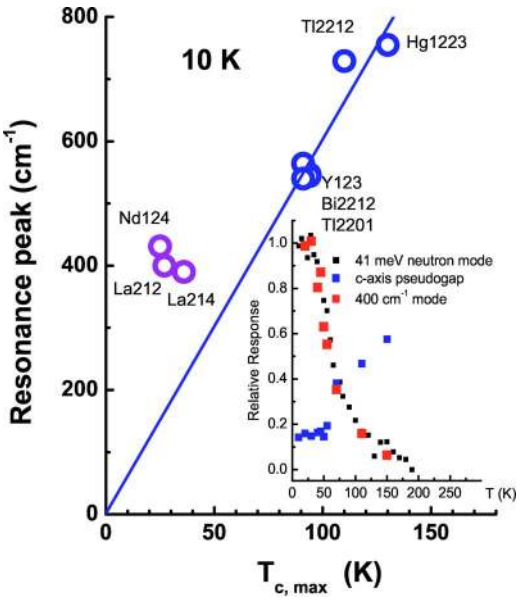

FIG. 21. (Color in online edition) The frequency of the resonance as calculated from the optical scattering rate plotted against maximum T_c for a series of high-temperature superconductors from Timusk (2003). The family of superconductors with a T_c that is over 90 K form a separate group from the low-T_c group. Inset, small squares show the intensity of the 41-meV magnetic resonance, while large squares show the peak c-axis conductivity. Both features appear below 150 K and reach half of their peak values at the superconducting transition temperature. Medium squares show the pseudogap amplitude, which develops already at 300 K. From Timusk, 2003.

reasonably sharp bosonic mode was needed to reproduce the reflectance shoulder that appears at low temperature and just above T_c in the spin-gap region. The other ingredient that was necessary was a broad continuum of excitations that extended to very high frequencies (Varma *et al.*, 1989; Schlesinger *et al.*, 1990; Schachinger *et al.*, 2003).

The second, more general, approach has been to extract the fluctuation spectrum directly from the experimental data without any *a priori* assumptions about the shape of the spectrum. Such procedures had been used in conventional strong-coupling superconductors with good success for both tunneling spectra (Carbotte, 1990) and infrared (Joyce and Richards, 1970; Allen, 1971; Farnworth and Timusk, 1974). The physical principle behind the method is simple: Since the optical conductivity involves multiple integration over densities of final states, for both the excitation and the scattered particles, an inversion of the process involves multiple differentiation. A formula derived by Marsiglio (1998) demonstrates this process:

$$W(\omega) = \frac{1}{2\pi}\frac{d^2}{d\omega^2}\frac{\omega}{\tau(\omega)}. \tag{28}$$

This method has been successfully applied to the scattering rate spectra of ^{60}C by Marsiglio *et al.* (1998), Carbotte *et al.* (1999), and Schachinger and Carbotte (2001) to Y-123. This analysis did not account well for a region

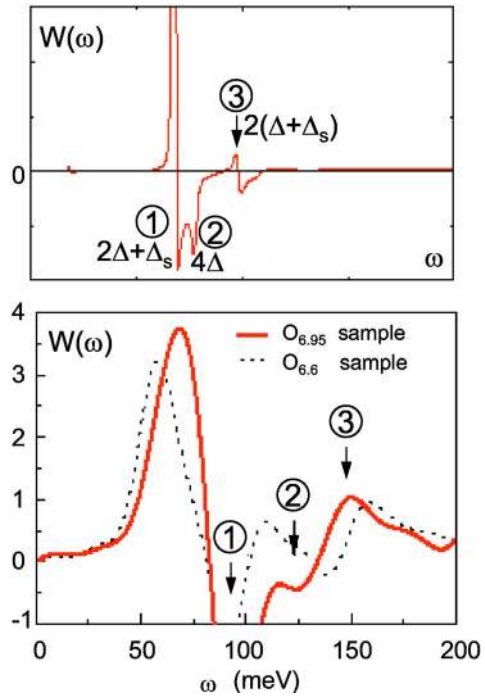

FIG. 22. (Color in online edition) Electron boson spectral function $W(\omega)$ for an Y-123 system near optimal doping: Bottom panel, inverted data from Carbotte *et al.* (1999) of the second derivative of the frequency-dependent scattering rate for YBCO compared with a model calculation in the lower panel showing that the higher-frequency fine structure can be used to extract the superconducting gap from the optical data. From Abanov *et al.*, 2001.

of negative $W(\omega)$ seen above the broad peak in the superconducting state.

Abanov *et al.* (2001) showed that the negative peak could be used to determine the superconducting gap Δ as detailed in the bottom panel of Fig. 22. Using the method of Abanov, Tu *et al.* (2002) analyzed optimally doped Bi-2212 and found a gap value of $\Delta=30\pm4$ meV and a resonance $\omega_s r=40\pm4$ meV (322 cm^{-1}), in excellent agreement with tunneling data at $\Delta=27$ meV and the mode seen in magnetic neutron scattering, $\omega_{sr}=41$ meV. The method has been applied to Tl-2201 by Wang *et al.* (2003). The results have been summarized by Singley *et al.* (2001) and by Timusk (2003). A summary of the frequencies of the resonance as seen in *ab*-plane scattering is shown in Fig. 21, where the resonance frequency has been plotted as a function of maximum T_c for a number of optimally doped cuprates. The resonance frequency scales with maximum T_c for all the high-temperature cuprates but not for single-plane low-temperature ones. It appears as if the low-temperature family suffers from a reduced transition temperature. Dordevic, Homes, *et al.* (2005a) proposed a method to extract the electron-boson spectral function from infrared and photoemission data using the inverse theory. This method allows one to treat on an equal footing the impact of the energy gap and of strong-coupling effects on the optical constants.

Of particular interest here is the three-layer Hg-1223 superconductor. The data come from a paper of McGuire *et al.* (2000), which offers the only analysis of single crystals of this system with a $T_c=140$ K. The authors found that the spectra of $1/\tau(\omega)$ for this system could be scaled with similar spectra of the Bi-2212 system with a scaling factor of 1.4, the ratio of transition temperatures. This suggests that the sum of the energy gap and the boson resonance in this material also scales with the transition temperature. These results are a challenge to models of the resonance that involve optical phonons, since the latter are expected, on the basis of lattice parameters, not to differ in the two materials. The higher energy scale of the mercury compound is, on the other hand, consistent with magnetic measurements, which also point to a substantially higher exchange coupling in the mercury material (Julien *et al.*, 1996). Raman spectroscopy, too, shows a 45% higher pair-breaking peak in this material (Sacuto *et al.*, 1998). Because large crystals of the three-layer mercury material are very difficult to grow, it will be a real challenge to perform magnetic neutron scattering on this system to verify the predicted 40% enhancement of the frequency of the magnetic resonance.

The overall result of these inversion procedures is that the broad onset of absorption seen in all infrared spectra can be accounted for by assuming an underlying bosonic spectrum consisting of a peak followed by a broad continuous spectrum extending to high frequencies.

E. Two-component analysis and the nodal metal state

While the one-component analysis seems to work well near optimal doping levels it is clear that it has to break down as the doping level is lowered (Thomas *et al.*, 1988; Grüninger, 1999). This is shown clearly by a recent study of Lee *et al.* (2005b), who have followed in great detail the doping trends across the phase diagram of the cuprates, with particular focus on the lower doping levels. Representative experimental results are displayed in Fig. 23. In all samples they find evidence for a charge-transfer gap near 10 000 cm^{-1}. The intragap conductivity of all materials also reveals common patterns that become particularly clear in the low-T spectra (thick lines). Indeed the low-T spectra in the heavily underdoped region are composed of two separate absorption features: a coherent mode (at $\omega<600$ cm^{-1}) followed by a mid-IR absorption at 0.5–0.6 eV. The mid-IR structure is virtually T independent, whereas the coherent mode significantly narrows at low T. The mid-IR absorption gradually shifts to lower frequency from $\sim$5000 cm^{-1} in the $y=6.28$ sample down to $\sim$1300 cm^{-1} for $y=6.75$, still distinguished from the well-developed coherent mode. Notably, conventional Drude behavior, a standard characteristic of metallic transport, has been found in an antiferromagnetically ordered crystal with $y=6.35$ (Fig. 23). This result is quite remarkable, since it conflicts with the common reference to weakly doped cuprates as "antiferromagnetic insulators." Signatures of localization

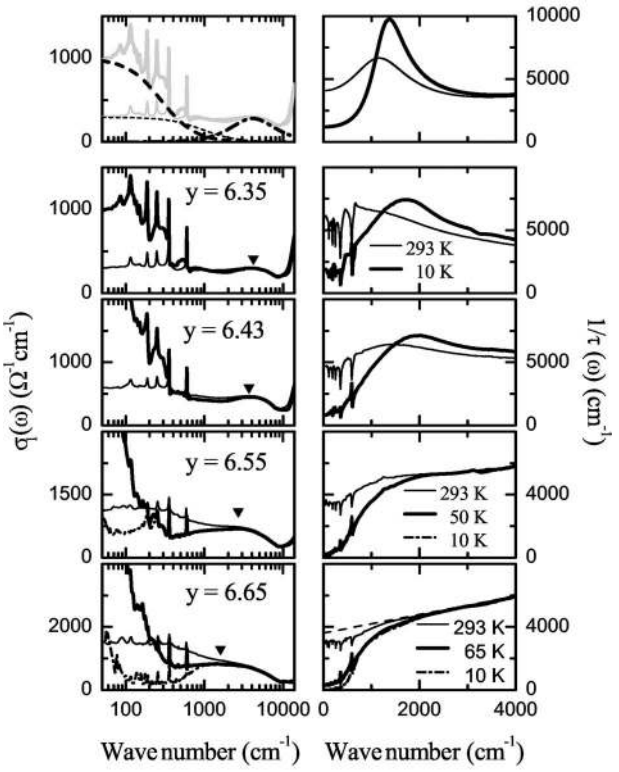

FIG. 23. The extended Drude model: left panels, spectra of the a-axis conductivity $\sigma_1(\omega)$, right panels, the scattering $1/\tau(\omega)$ extracted from the extended Drude model as described in the text for a series of Y-123 single crystals. Thick solid lines show the data at lowest temperature in the normal state: 10 K for a nonsuperconducting crystal with $y=6.35$ and $T\sim T_c$ for superconducting compounds $y=6.44$, 6.55, and 6.65. The solid triangles in the left panels mark the positions of the mid-IR absorption bands. In the right panel for $y=6.65$ the dashed line represents the linear ω dependence. Top panels display the two-component analysis of the conductivity for a $y=6.35$ crystal [Eq. (2)]. Dashed lines in the top left panel show separately the Drude and Lorentzian contributions. Top-right panel displays the model $1/\tau(\omega)$ spectra calculated from the oscillator fit. Clearly, the simple two-component description captures the key features of the experimental data. Adapted from Lee *et al.*, 2005b.

can be identified in the ω dependence of the conductivity measured for samples with $y\leqslant 6.3$. In the latter compounds the coherent contribution to the conductivity reveals a peak at finite far-IR frequencies similar to the behavior of weakly doped La-214 samples (Dumm *et al.*, 2003; Fig. 13). Importantly, the response of all crystals remains gapless down to the lowest ω, as evidenced by a substantial spectral weight in the $\sigma(\omega)$ down to $\omega\rightarrow 0$. Therefore the positive slope of the low-T resistivity in weakly doped cuprates is not due to the opening of the insulating gap. Instead we believe this behavior is associated with a bandlike response even in lightly doped samples that is modified by weak localization.

It is instructive to discuss the evolution of the conductivity spectra with both temperature and doping in the context of the phase diagram of the Y-123 system. At $T>T^*$ the in-plane conductivity shows a broad spectrum extending from $\omega=0$ to the charge-transfer frequency. This response can be characterized as single component, since multiple absorption features cannot be unambiguously singled out. Lee *et al.* (2005b) have found that crossing the T^* boundary in Fig. 1 vertically (by changing temperature at constant y) or horizontally (by changing doping at constant T) yields similar results for the form of the $\sigma(\omega)$ spectrum. Indeed, either route resulted in the observation of two distinct absorption structures to the left of the T^* boundary of the phase diagram. These structures include a Drude mode at the lowest frequencies and mid-IR band. Similarities are especially clear when the low-T data are compared. The main distinction in the latter spectra taken for nonsuperconducting crystals with $y<6.35$ and superconducting ones is in the frequency position of the mid-IR band. The softening of this feature with increasing doping is continuous, as can be clearly seen in Fig. 23.

A debate on both the merits and pitfalls of the single- and muiltiple-component scenarios [Eqs. (2) and (6)] goes back to the early days of high-T_c superconductivity (Timusk and Tanner, 1989). Here we shall focus on the behavior of $1/\tau(\omega)=(\omega_p^2/4\pi)\mathrm{Re}[1/\tilde{\sigma}(\omega)]$ pertaining to the problem of the pseudogap and coupling to a bosonic mode. The right panels of Fig. 23 reveal the evolution of $1/\tau(\omega)$ with temperature and doping. The panel presenting the $1/\tau(\omega)$ data for the $y=6.65$ crystal are in good agreement with the earlier results (Basov, Liang, *et al.*, 1996). The scattering rate is nearly linear in ω at room temperature but shows a characteristic threshold structure near 500 cm^{-1} at $T<T^*$. It is this depression that is usually associated with the pseudogap state. It is also commonly asserted that this form of $1/\tau(\omega)$ spectrum is indicative of coupling of a quasiparticle to a (bosonic) mode occurring in the vicinity of the threshold structure, as detailed in the previous subsection.

New and unexpected features of the in-plane electrodynamics are uncovered by the data for heavily underdoped materials. In these materials the $1/\tau(\omega)$ spectra at room temperature show a broad peak around 1000 cm^{-1}. With T decreasing, the scattering rate in the far-IR is significantly suppressed, while the peak intensity is enhanced and the peak position shifts to higher frequencies. The nonmonotonic form of the $1/\tau(\omega)$ observed in all crystals with $y<6.5$ is suggestive of the formation of an energy gap in the excitation spectrum (Basov, Singley, and Dordevic, 2002). As the doping increases, the peak structures in the $1/\tau(\omega)$ spectra are suppressed and shift to higher frequencies. At doping $y\geqslant 6.5$ the peaks disappear from $1/\tau(\omega)$ making the slope in the $1/\tau(\omega)$ positive at all frequencies. A suppression in the far-IR $1/\tau(\omega)$ at lower T is observed at all the dopings and merely reflects the narrowing of the coherent component in the conductivity data. The separation between the coherent Drude contribution to the conductivity and mid-IR band is most evident in the low-T response at very low dopings. This aspect of elec-

trodynamics is not specific to Y-123 but is also common in the La-214 system (Uchida *et al.*, 1991; Padilla *et al.*, 2005b) and Bi-2212 compounds (Quijada *et al.*, 1999) as well as for electron-doped systems (next subsection). We therefore conclude that the doping-dependent evolution of optical spectra appears to reflect a generic property of cuprates.

Experiments by Lee *et al.* (2005b) unequivocally show that at the pseudogap gap boundary in the phase diagram charge dynamics of the CuO_2 plane endures a crossover from a single-component strange metal to the two-component response of a *nodal metal*. Moreover, at $T<T^*$ both transport and spectroscopic properties are consistent with the Fermi-liquid theory of Ando *et al.* (2004). This conjecture is supported by the Drude frequency dependence of the optical conductivity as well as by the T^2 form of the resistivity. Attributes of the Fermi-liquid dynamics of a nodal metal are most vivid in the temperature-doping parameter space where the coherent contribution is energetically separated from the incoherent mid-IR band. Photoemission experiments for the La-214 system conclusively show that this regime is realized when most of the Fermi surface is gapped and the only remaining portion is the arc formed around the nodal points (Yoshida *et al.*, 2003). However, the indicators of a Fermi liquid can no longer be identified when the two-component behavior is terminated at the pseudogap boundary and the large ungapped Fermi surface is recovered. A corresponding feature of the optical data is the merger between Drude and mid-IR contributions. Hall measurements for La-214 show a dramatic enhancement in the effective number of carriers participating in transport at the same boundary. A quantitative consistency between IR and Hall data was established by Padilla *et al.* (2004). This discussion above shows that the mid-IR band universally found in all high-T_c superconductors is intimately involved in the pseudogap phenomenology and specifically in transport properties at high temperatures.

A combination of transport and IR experiments has allowed Lee *et al.* (2005b) to identify several hallmarks of the nodal metal state, a region of the phase diagram where the electronic properties are governed by quasiparticles residing in the nodes of the Fermi surface. Interestingly, this regime is characterized by high electronic mobility (Ando *et al.*, 2001), relatively low effective mass independent of doping (Padilla *et al.*, 2004), and constant Fermi velocity (Zhou *et al.*, 2003). Signatures of the nodal metal are observed over a broad range of the phase diagram and extend to antiferromagnetic ordered phases. This latter finding clearly shows that the transition from a nodal metal to a Mott insulator is of "vanishing carrier number" (Imada *et al.*, 1998). It appears that transport in nodal metals is governed by excitations topologically compatible with an antiferromagnetic background. One conjecture reconciling anomalous trends seen in weakly doped cuprates is that the local environment of mobile charges in these systems remains unaltered with doping, and it is only the phase space occupied by hole-rich regions that is progressively increasing. Many of the doping trends reported for both Y-123 and La-214 systems are consistent with the projected wave-functions approach developed by Paramekanti *et al.* (2004).

F. Electron-doped materials

Experiments performed on electron-doped cuprates of $A_{2-x}Ce_x\,CuO_4$ materials ($A=La,Nd,Pr,Sm,Eu$) have revealed many features held in common with their hole-doped counterparts (Cooper *et al.*, 1990; Abel' *et al.*, 1991; Lupi *et al.*, 1992; Onose *et al.*, 2001; Singley *et al.*, 2001; Wang *et al.*, 2004). Substitutional doping of Ce on an A site led to a progressive development of a "metal-like" response with a transfer of the electronic spectral weight to low energies from the charge-transfer gap region. An important aspect of the crystal growing procedures is that the as-grown samples have to be annealed to remove additional oxygen from apical sites. Oxygen-reduced samples reveal a stronger free-carrier contribution than do antiferromagnetic, as-grown samples, which do not show metallic or superconducting behavior.

The first systematic study of the electron dynamics across the phase diagram was by Onose *et al.* (2001). These authors discovered that the intragap conductivity of Nd-214 crystals is comprised of two distinct absorption features: Drude-like contributions and mid-IR resonances over a broad range of doping. The mid-IR band softened systematically with increasing concentration of Ce (Fig. 24) but could still be recognized in an optimally doped $x=0.15$ crystal. This behavior is similar to that of hole-doped systems, as shown in Fig. 23. Measurements at elevated temperatures reported by Onose *et al.* (2001) for the $x=0.05$ sample indicate that the mid-IR structure merges with a Drude-like feature at T near 400 K. In an optimally doped sample a similar effect occurs already at 290 K. Zimmers *et al.* (2004) have carried out detailed studies of this structure in a series of $Pr_{2-x}Ce_xCuO_4$ films over an extended region of the phase diagram. They found that a model combining a spin-density-wave gap and a frequency- and temperature-dependent self-energy accounts for the key features in the data. The magnitude of the pseudogap extrapolates to zero for $x\approx0.17$ (Fig. 1), indicating the coexistence of magnetism and superconductivity in this material and the existence of a quantum critical point at this Ce concentration.

G. Optical conductivity and "bad-metal" behavior

A remarkable and unconventional transport property of cuprates is the so-called "bad-metal" behavior: their in-plane resistivity shows metallic (increasing) temperature dependence even though the mean free path of quasiparticles would be less than its de Broglie wavelength $\lambda_F=2\pi/k_F$ (Emery and Kivelson, 1995a, 1995b), thus violating the Mott-Ioffe-Regel limit for metallic transport. This should be contrasted with the phenomenon of resistivity saturation commonly observed in more conventional metals in the regime where the qua-

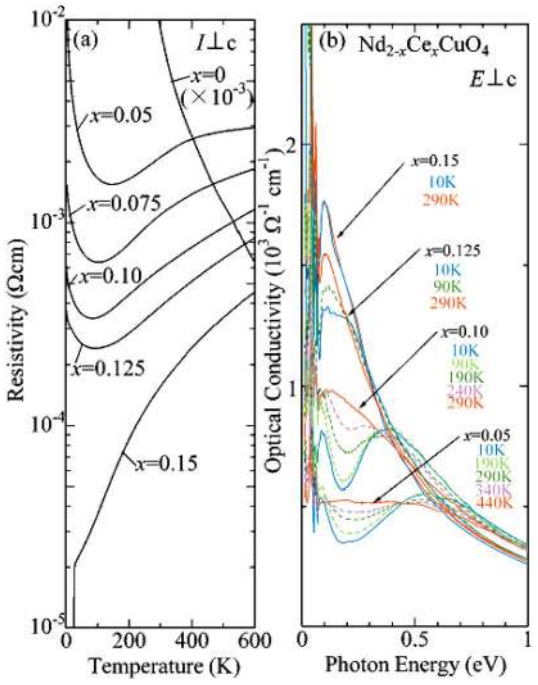

FIG. 24. (Color in online edition) The T dependence of in-plane resistivity (a) and the optical conductivity spectra for oxygen-reduced crystals of Nd-214. Adapted from Onose *et al.*, 2001.

siparticle mean free path approaches interatomic distances (Gunnarsson *et al.*, 2003). Resistivity in the cuprates reveals a crossover to slower increase at high temperatures reminiscent of saturation in ordinary metals. However, this effect occurs at anomalously high absolute values of the resistivity (Fig. 25) where the applicability of the quasiparticle concept is questionable.

Gunnarsson *et al.* (2003), Takenaka *et al.* (2003), and Hussey *et al.* (2004) have pointed out that the bad-metal behavior of cuprates is intimately connected with the flat incoherent background in the optical conductivity of these systems (Fig. 25). Conductivity data by Takenaka *et al.* (2003) show that the Drude-like feature in the $\sigma(\omega)$ data disappears at elevated temperatures, evolving into an incoherent plateau. Evidently, the changes in the optical conductivity involve a broad energy range extending at least up to the charge-transfer gap. The data appear to be consistent with the parallel resistance formula (Wiesmann *et al.*, 1977) used to describe saturation in ordinary metals: $\sigma(\omega)=\sigma_{\mathrm{Drude}}+\sigma_{\mathrm{sat}}$, where the "saturated" value σ_{sat} corresponds to the high-temperature limit of the dc conductivity. Gunnarsson *et al.* (2003) analyzed the restriction on the saturated value of the resistivity ρ_{sat} imposed by the oscillator-strength sum rule and came up with the following expression: $\rho_{\mathrm{sat}} \approx 0.4/x(1-x)$ mΩ cm, where x is doping. They concluded that this upper limit is not exceeded by the experimental data and therefore the issue of high resistivity may be less exotic than it appears on the surface. Ando *et al.* (2001) proposed that high resistivities of cuprates may be related to phase segregation on a mesoscopic scale, which reduces the effective volume relevant to charge transport. An alternative description of the optical data has been proposed by Hussey *et al.* (2004), who argue that the high-T regime of the conductivity can be adequately described by adopting an effective relaxation time of the following form: $\tau(T,\omega) = \tau_{\mathrm{ideal}}(T,\omega)+\tau_{\mathrm{min}}$. When inserted in the effective Drude formula [Eq. 6], this form for the relaxation time reproduces the gross features of the data in Fig. 25.

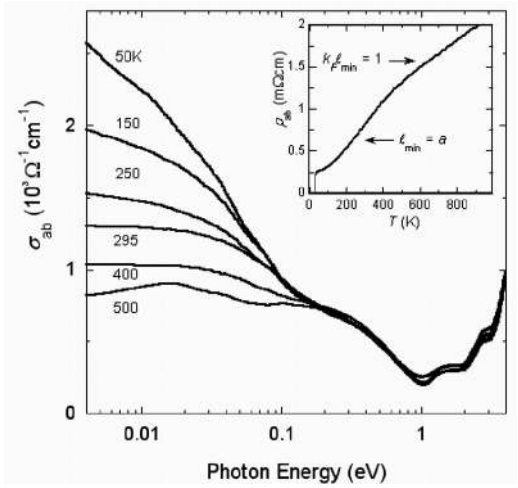

FIG. 25. $La_{1.9}Sr_{0.1}CuO_4$ at specified temperatures. The inset shows the in-plane resistivity data for $La_{1.9}Sr_{0.1}CuO_4$ up to 1000 K. From Hussey *et al.*, 2004.

H. Comparison of the optical data with transport measurements and other spectroscopies

In this subsection we compare the optical data with the results from other techniques. We first focus on transport measurements, which give us the low-frequency limit of the optical conductivity. It is generally found that the *ab*-plane optical conductivity extrapolates to the measured dc conductivity at low frequencies. The same conclusion applies in the *c* direction (Homes, Timusk, *et al.*, 1995a, 1995b) and there is no evidence of hidden low-frequency collective modes in the difficult spectral region between the far-infrared and microwave region as is the case in quasi-one-dimensional organic conductors (Cao *et al.*, 1996; Vescoli *et al.*, 1998).

It is clear that the linear frequency dependence of the CuO_2 in-plane scattering rate is related to the linear temperature dependence of the *ab*-plane dc resistivity $\rho_{\mathrm{dc}}=m/ne^2\tau$. However, the linear law in $1/\tau(\omega)$ and in $d\rho/dT$ is only valid near optimal doping, and deviations from the linear law are observed below a temperature T^* in underdoped materials both in the resistivity (Nakamura and Uchida, 1993; Takenaka *et al.*, 1994) and in the frequency-dependent *ab*-plane scattering rate (Basov, Liang, *et al.*, 1996). There are deviations from the linear law in the overdoped region, as well, where the resistivity and scattering rate curves acquire a positive curvature. This behavior has been attributed to a more Fermi-liquid-like behavior in the overdoped state, since

electron-electron scattering is expected to yield a quadratic frequency dependence of the scattering rate. In real metals this effect is only seen at very low temperatures, since at higher temperatures electron-phonon scattering dominates. Electron-phonon scattering, on the other hand, cannot be responsible for the linear transport behavior at optimal doping, since it would give rise to an intercept at zero temperature on the temperature axis, and in the optimally doped high-T_c cuprates this intercept is zero to a high degree of accuracy. This singular behavior is only possible from an interaction with a continuous spectrum of fluctuations such as the one proposed by Varma *et al.* (1989) or the alternative model of the nearly antiferromagnetic Fermi liquid of Pines and co-workers (Monthoux and Pines, 1993, 1994a, 1994b), which is based on the continuous Millis-Monien-Pines spectrum spin fluctuations (Millis *et al.*, 1990).

The pseudogap seen in the *c*-axis conductivity has also been seen by angle-resolved photoemission spectroscopy. In Bi-2212 it was found that the momentum dependence of the normal-state gap has the same $d_{x^2-y^2}$ symmetry as the gap observed in the superconducting state (Ding *et al.*, 1996, 1997; Loeser *et al.*, 1996; Marshall *et al.*, 1996). From the overall temperature dependence of the gap seen in ARPES, it appears to be related to the gap seen in the Knight shift and *c*-axis optical conductivity, i.e., it appears to be the higher temperature T^* gap. The identification of the gap seen at the antinodes for $(\pi,0)$ states with the *c*-axis pseudogap is plausible but indirect, since most of the infrared data are for the Y-123 system while the ARPES data are for the Bi-2212 material.

A better comparison can be made between *ab*-plane optical scattering rates and quasiparticle lifetimes derived from nodal quasiparticles (Fig. 26). Kaminski *et al.* (2000) compared the scattering rate derived from linewidths in momentum distribution curves seen by ARPES and the optical data for $1/\tau(\omega)$ from a one-component analysis of Bi-2212. They found that not only are the overall scattering rates similar but the detailed onset of scattering associated with the magnetic resonance can be seen in both sets of spectra. This conclusion also holds for electron-doped materials: the scattering rate analysis of the IR data by Singley *et al.* (2001) and the analysis of ARPES spectral functions by Armitage *et al.* (2003) reveal close consistency between the two data sets. Another example is shown in Fig. 20 from a recent paper of Hwang, Timuks, and Gu (2004). The quantity plotted for ARPES is the real part of the self-energy obtained from an analysis of the dispersion curves for quasiparticles near the nodes at (π,π) from the work of Johnson *et al.* (2001), while the left panels show the imaginary part of the optical scattering rate obtained from a one-component analysis of the optical conductivity. Three different doping levels are shown. While the overall magnitudes differ, as expected, there is considerable similarity in the two sets of spectra. One can, for example, identify a low-energy peak that is closely correlated with the appearance of the magnetic resonance in both temperature and doping level. The broad background is present at all temperatures and doping levels.

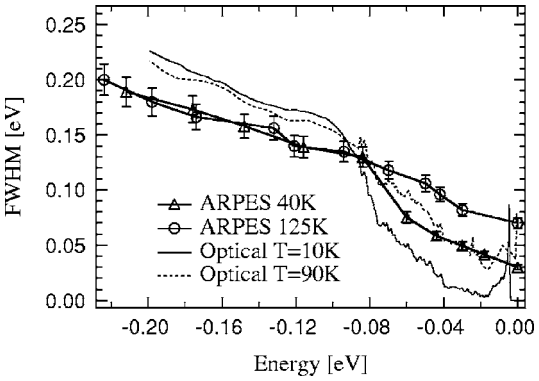

FIG. 26. Self-energy effects in IR and ARPES spectra. Triangles and circles show the full width at half maximum of the spectral peaks vs the binding energy of the spectral peak in ARPES, and the carrier scattering rate vs energy for Bi-2212 (90 K) obtained from infrared reflectivity measurements (solid and dashed lines) after Puchkov, Basov, and Timusk (1996). Adapted from Kaminski *et al.*, 2000.

One does not expect the real self-energies from ARPES to be identical to the imaginary part of the infrared scattering rate. This has been pointed out by several authors (Kaminski *et al.*, 2000; Millis and Drew, 2003; Schachinger *et al.*, 2003). The imaginary part of the optical scattering rate is not a true self-energy but is an average over the Fermi surface, weighted in favor of large-angle scattering. In view of these problems it is surprising that the curves in Fig. 20 agree as well as they do.

The normal-state gap in underdoped cuprates has also been seen by tunneling spectroscopy (Tao *et al.*, 1997; Renner *et al.*, 1998; Pan *et al.*, 2001). Renner *et al.* (1998) showed that the pseudogap in Bi-2212 had a width that was temperature independent and that its width scaled with the superconducting gap. The maximum gap, assuming a *d*-wave gap, at optimal doping in Bi-2212, $\Delta_0 = 41.5$ meV, is consistent with other spectroscopies. The gap ranges from 44 meV for an underdoped sample with $T_c = 83$ K, 41.5 meV at optimal doping, down to 21 meV in an overdoped sample with $T_c = 56$ K. Renner *et al.* also find that even in an overdoped sample with $T_c = 74.3$ K there is a weak pseudogap in the normal state. The phase diagram shown in Fig. 2, where the pseudogap temperature T^* is based on *c*-axis transport measurements, is consistent with these observations.

The low-frequency Raman scattering can be related to the carrier lifetime $\Gamma(\Omega)$, where in the simple Drude picture the Raman cross section is proportional to ω/Γ with Γ the scattering rate (Blumberg and Klein, 1999; Opel *et al.*, 2000; Devereaux, 2003). Nemetschek *et al.* (1997) do find a depression in the Raman scattering of both Bi-2212 and Y-123 in the normal state below 700 cm^{-1} and 200 K, in agreement with the *ab*-plane optical scattering rate data. It is possible to reconcile these results within

the two-gap scenario if the gap in the scattering rate observed by Naeini *et al.* (1998) is related to the *ab*-plane lifetime and has a characteristic temperature substantially lower than the density-of-states gap.

VIII. INFRARED SIGNATURES OF SUPERCONDUCTIVITY IN HIGH-T_c CUPRATES

A. Searching for the superconducting energy gap in the response of the CuO_2 planes

Because the energy gap in the excitation spectrum is a definitive property of a BCS superconductor (Bardeen, Cooper, and Schrieffer, 1957), significant research effort has been dedicated to the search for the gap in high-T_c cuprates. The basics of an infrared probe of the energy gap are discussed in Sec. IV.D. A clear threshold in the dissipative part of the conductivity spectra at $\omega=2\Delta$ due to the onset of absorption is found only in dirty superconductors, where $1/\tau<2\Delta$. In clean superconductors, where $1/\tau\ll 2\Delta$, there is little change in the overall optical properties at the gap frequency. However, in this case an absorption structure can be expected at $\omega\approx 4\Delta$ (Orenstein, 1990; Nicol *et al.*, 1991). Early experimental work on the search for the energy gap in cuprates (Reedyk *et al.*, 1988; Collins *et al.*, 1989; Kamaras *et al.*, 1990; Orenstein, Thomas, *et al.*, 1990; Mandras *et al.*, 1993) and by many other groups is reviewed in an article by Timusk and Tanner (1989), Tanner and Timusk (1999). Unlike conventional low-T_c superconductors, the high-T_c cuprates do not show a well-defined conductivity gap. A residual absorption is universally found in high-T_c materials. Possible microscopic origins of this absorption pertinent to *d*-wave symmetry of the order parameter as well as to disorder will be discussed below.

1. *ab*-plane response at $T\ll T_c$

In order to isolate the essential features of the superconducting-state response we begin with the *ab*-plane conductivity of optimally doped $YBa_2Cu_3O_{6.95}$ crystal (Fig. 27), which is to date the best studied high-T_c material. Data for other systems with $T_{c,\max}\approx 90$ K including Bi-2212 (Tu *et al.*, 2002) and $TlBaCuO_{6+\alpha}$ (Puchkov, Timusk, *et al.*, 1995) do not substantially differ from $YBa_2Cu_3O_{6.95}$ spectra. In the superconducting state the conductivity is suppressed compared to the spectrum measured at $T\simeq T_c$ over an energy range up to 800 cm^{-1}. The conductivity shows a minimum at $\omega\simeq 350$ cm^{-1}, which was often confused with the energy gap in the early literature. However, $\sigma_1(\omega)$ remains finite down to lowest frequencies in infrared and microwave frequency regions (Pham *et al.*, 1991). The minimum of the conductivity is often observed already in the normal state (Reedyk *et al.*, 1988; Orenstein, Thomas, *et al.*, 1990) and its frequency position does not scale with T_c. Work with better experimental techniques and higher quality crystals has confirmed these early results (Basov, Liang, *et al.*, 1995; Puchkov, Timusk, *et al.*, 1995; Barowski *et al.*, 1996; Homes, Clayman, *et al.*, 1997; Wang *et al.*, 1998; Bernhard *et al.*, 2001). Residual absorption has also been detected in many series of both hole- and electron-doped cuprates (Reedyk, 1992; Gorshunov *et al.*, 1998; Pimenov *et al.*, 2003).

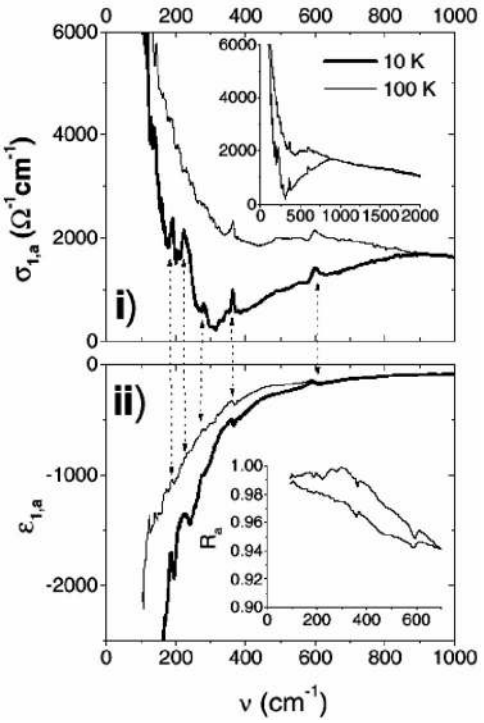

FIG. 27. Ellipsometric data for the *a*-axis component of the real part of the (i) conductivity and (ii) dielectric function of $YBa_2Cu_3O_{6.95}$ ($T_c=91.5$ K) at 100 K (thin solid lines) and at 10 K (thick solid lines). The inset in the top panel shows the conductivity data over an extended frequency region. The inset in the bottom panel displays the reflectance spectra calculated from ellipsometry data (Bernhard *et al.*, 2001). Ellipsometric results for the optical constants of $YBa_2Cu_3O_{6.95}$ are in excellent agreement with the data inferred from the Kramers-Kronig analysis of the reflectance spectra and reveal the same characteristic features, including a threshold near 500 cm^{-1} as well as residual absorption at lower energies.

There have been several attempts to explain the residual absorption in the superconducting state by assuming *d*-wave symmetry. In a *d*-wave superconductor the density of states is finite at all finite energies. This is the necessary condition to account for the nonvanishing absorption. However, detailed calculations for a *d*-wave superconductor show that the experimentally observed residual conductivity in the low-frequency region is still too large for any realistic choice of the scattering rate (Carbotte *et al.*, 1995; Quinlan *et al.*, 1996). Indeed, free-carrier absorption at finite ω is prohibited in a clean system by momentum conservation. Absorption is possible if impurities are introduced, but impurities are detrimental for the transition temperature of a *d*-wave superconductor (Radtke *et al.*, 1993; Rojo and Levin, 1993). Also, it is known that even minor concentrations of impurities lead to changes in the temperature dependence of the penetration depth from linear in clean crystals to quadratic in disordered materials (Bonn *et al.*,

1993). In this context it is important to emphasize that the residual absorption is found in the samples with the highest T_c of the Y-123 series that demonstrate a linear law of penetration depth (Zhang *et al.*, 1994; Basov, Liang, *et al.*, 1995). An important result pertinent to residual absorption in a *d*-wave superconductor is the so-called "universal" conductivity predicted by Lee (1993). One consequence of linear dispersion near the node of the order parameter is that the conductivity is expected to become independent of the relaxation time at low T because quasiparticles are both generated and scattered by impurities. While measurements of the thermal conductivity are consistent with the universal value (Taillefer *et al.*, 1997) both infrared and microwave measurements of the residual $\sigma(\omega)$ yield substantially larger values. In summary, the simple *d*-wave picture is capable of accounting for many important trends in the *ab*-plane response, but not for the residual conductivity in the low-frequency region. We shall return to the issue of the residual absorption in Secs. VIII.B and VIII.D.

2. *c*-axis response

The charge dynamics along the *c* axis are incoherent in most cuprates. In principal this should simplify the search for the superconducting gap. In Fig. 16 we show data generated for a variety of high-T_c systems by different experimental groups, reproduced from Dordevic, Singley, *et al.* (2004). In all materials the conductivity spectra are dominated by sharp phonon peaks as discussed in Sec. VII.A. All materials show small depression of the far-IR conductivity in the superconducting state. Nevertheless, the conductivity remains finite down to lowest frequencies, even at $T \ll T_c$, and there is no evidence for the superconducting energy gap. Thus, the *c*-axis experiments (Figs. 15 and 16) reinforce the conclusion of the gapless response inferred from the in-plane studies discussed in the previous section. Gapless *c*-axis conductivity has been attributed to anisotropy of the order parameter (Graf *et al.*, 1995). However, this scenario cannot account for the conductivity in the underdoped Y-123 samples where the spectra of $\sigma_1(\omega)$ are dominated by the normal-state pseudogap (Fig. 15).

3. Josephson plasma resonance

A salient feature of the *c*-axis response in the superconducting state is the development of a "plasma edge" in the far-IR reflectance. The effect is most clearly observed in the La-214 system (Fig. 5). In these strongly anisotropic materials the reflectance spectra taken in the normal state are "insulatorlike": one finds several strong phonon modes at $\omega > 200\ \mathrm{cm}^{-1}$ and a flat, frequency-independent background in the far infrared where $R_c(\omega) \simeq 0.5$ (Tamasaku *et al.*, 1992; Basov, Mook, *et al.*, 1995; Gerrits *et al.*, 1995; van der Marel and Kim, 1995; Birmingham *et al.*, 1996; Tsui *et al.*, 1996; Uchida *et al.*, 1996). There is very little temperature dependence in the spectrum as T decreases from 300 K to $T \simeq T_c$. However, as soon as these samples undergo the superconducting transition, the reflectance immediately changes character: $R_c(\omega)$ nearly reaches unity in the lowest frequencies and then abruptly drops down to $R \simeq 0.2$. At higher energies the reflectance slowly recovers to the magnitude seen in the normal state. This behavior resembles the plasma resonance that occurs in ordinary metals at $\omega \simeq \omega_p$ (Wooten, 1972). This feature is commonly referred to as the Josephson plasma resonance.

As originally pointed out by Bonn *et al.* (1987) the sharp feature in the reflectivity spectra originates from a zero crossing of the real part of the dielectric function, resulting from an interplay between the positive phonon contribution and the large negative contribution of the superconducting condensate. In the normal state the *c*-axis plasmon is overdamped, but at $T < T_c$ damping suddenly drops and the plasma resonance becomes observable (van der Marel and Kim, 1995). Analysis of the doping trends of the *c*-axis plasmon has led to the conclusion that this feature originates from the Josephson coupling between the CuO_2 layers (Tamasaku *et al.*, 1992; Basov, Timusk, *et al.*, 1994). Employing a theory developed in the early 1970s for the electrodynamics of an array of Josephson-coupled junctions (Lawrence and Doniach, 1971; Bulaevskii, 1973), it is possible to reproduce the frequency dependence of the observed reflectance. An obvious difference between cuprates and artificial Josephson contacts is that the "normal" barriers inside the unit cell of the crystal have thicknesses of the order of interatomic distances. This shifts the plasma edge from GHz frequencies, which are typical for artificial junctions of conventional superconductors, to the THz range ($20-200\ \mathrm{cm}^{-1}$) in cuprates.

Another way of observing Josephson plasma resonance effects is through sphere resonances of small particles of superconductor suspended in an insulating matrix. The phenomenon is well known from classical electromagnetic theory, where a metallic sphere displays an absorption peak at a frequency $\omega_s = \omega_p/\sqrt{(3)}$, where ω_p is the longitudinal plasma frequency of the bulk material. Powdered crystals, suspended in an optically transparent matrix, show a resonance absorption at $\omega = \omega_p\sqrt{(3)}$, where ω_p is the Josephson plasma frequency (Noh *et al.*, 1989; Shibata and Yamada, 1998). Shibata and Yamada have reported the presence of two longitudinal Josephson plasma resonance modes in $SmLa_{1-x}Sr_xCuO_{4-\alpha}$ through the observation of sphere resonances. This material has single copper-oxygen planes separated by alternating Sm_2O_2 and $(La,Sr)_2O_{2-\alpha}$ blocking layers. When the material becomes superconducting, two resonances are seen. Both appear at T_c and follow mean-field temperature dependencies. The authors attribute the resonances to the two different series Josephson junctions in the two different blocking layers. The transverse plasma resonance in this material has also been seen (Dulic *et al.*, 2001; Kakeshita *et al.*, 2001; Shibata, 2001). Dordevic, Komiya, *et al.* (2003a) analyzed the line shape of the Josephson plasma resonance to investigate spatial inhomogeneities of superconducting condensates in CuO_2 planes (Sec. VIII.D).

B. Quasiparticle dynamics in the superconducting state

The electromagnetic response of a superconductor provides experimental access to the dynamical properties associated with quasiparticles even at $T<T_c$, where dc transport is shunted by supercurrents. It is evident from Fig. 20 that the quasiparticle dynamics is dramatically modified at $T<T_c$. Specifically, the scattering rate at $\omega<500$ cm^{-1} is significantly depressed. Since the absolute value of $1/\tau(\omega)$ is related to the effective width of the Drude-like structure at a frequency ω, the data in Fig. 20 imply that the width of this feature falls below 30–40 cm^{-1}. While it is difficult to extend infrared measurements below this limit for highly reflective samples, microwave, submillimeter, and THz experiments in the time domain have been used to systematically investigate the quasiparticle response in the relevant energy range.

1. Microwave and submillimeter conductivity at $T<T_c$

The temperature dependence of the conductivity in the microwave and submillimeter regions contains a wealth of information on quasiparticle response in the superconducting state. The temperature dependence of $\sigma_1(T)$ is nonmonotonic and shows a peak at about 40 K, as displayed in Fig. 28 (Nuss *et al.* 1991; Bonn *et al.*, 1993; Bonn and Hardy, 1996). At the peak the magnitude of the conductivity dramatically exceeds the dc conductivity at T_c. This behavior is consistent with the formation of a narrow quasiparticle mode with width $1/\tau \simeq 1-3$ cm^{-1} at low temperatures. Recently, this mode was resolved in the frequency domain using broadband microwave spectroscopy (Turner *et al.*, 2003; Fig. 29).

The width and the spectral weight of the narrow mode in $\sigma_1(\omega)$ are strongly temperature dependent. Competition between the two effects occurring at $T<T_c$, the suppression of the scattering rate and the reduction of the spectral weight of the normal fluid (due to pair formation), is responsible for a peak in the T dependence of $\sigma_1(\omega)$ at $T\simeq 30-40$ K (Fig. 28). The phenomenological two-fluid model [Eq. (16)] appears to account for the gross features of the microwave and submillimeter data. Parametrizing the normal-fluid response at $T\ll T_c$ with a temperature-dependent density and a scattering rate has been partly justified by calculations of the microwave conductivity of a $d_{x^2-y^2}$ superconductor (Hirschfeld *et al.*, 1993). The competition between the scattering rate and the spectral weight is clearly illustrated in the data displaying $\sigma_1(\omega, T\ll T_c)$ obtained using broadband microwave spectroscopy in Fig. 29 (Turner *et al.*, 2003) and also using submillimeter spectroscopy (Pimenov *et al.*, 1999). The exact position of the peak in $\sigma_1(\omega)$ is determined by a combination of the scattering rate and the probing frequency. A dramatic depression of the relaxation rate in the sub-THz region in optimally doped cuprates (Fig. 28) has been observed using THz time-domain spectroscopy (Nuss *et al.*, 1991; Buhleier *et al.*, 1994; Corson *et al.*, 2000) and also using pump-probe measurements (Averitt *et al.*, 2001). This effect is found not only in Y-123 and Bi-2212 systems but also in La-214 compounds (Shibauchi *et al.*, 1996; Gorshunov *et al.*, 1998).

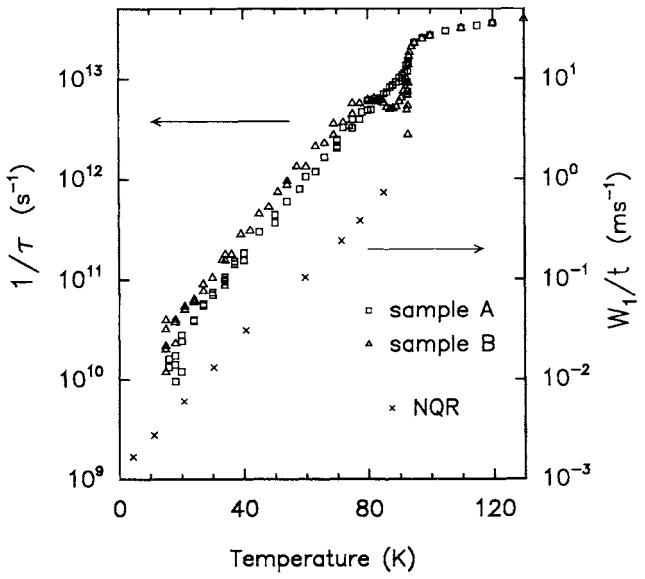

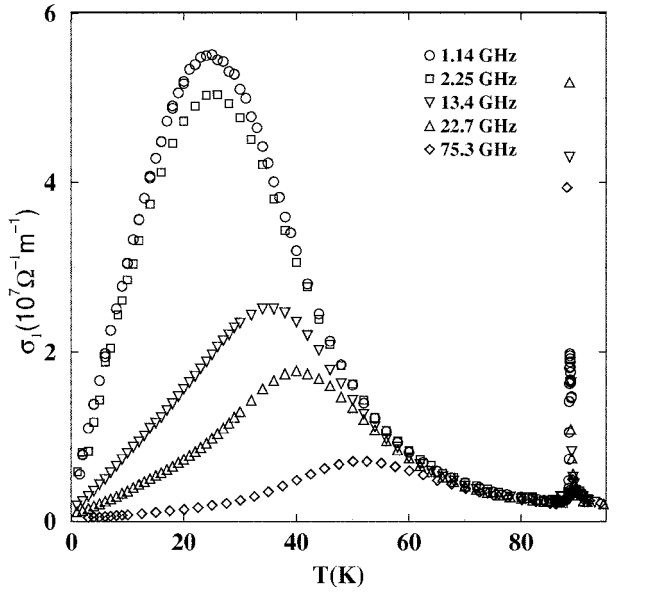

FIG. 28. Microwave response of Y-123 single crystal near optimal doping: Top panel, the temperature-dependent part of the quasiparticle scattering rate obtained from the microwave data. The nearly straight line on a semilogarithmic scale indicates a scattering rate that varies as $\exp(T/T_0)$, a temperature dependence that is also seen in NMR and nuclear quadrupole resonance measurements. From Bonn *et al.*, 1993. Bottom panel, the T dependence of the real part of the conductivity at several different frequencies in the microwave range (Hosseini *et al.*, 1999). From Bonn *et al.*, 1994.

2. Theoretical context and unresolved issues

A rapid temperature dependence of the quasiparticle scattering rate at $T\ll T_c$ is expected if inelastic scattering originates from the excitations developing a gap below the temperature of the superconducting transition. A re-

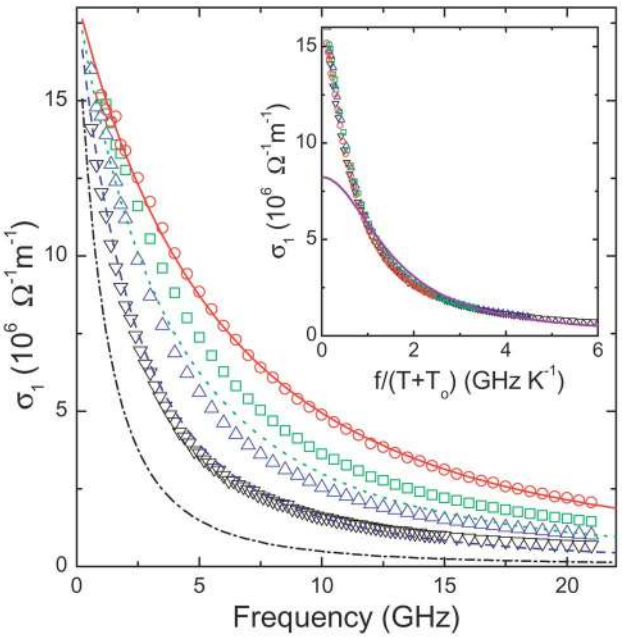

FIG. 29. (Color in online edition) The low-T evolution of the quasiparticle conductivity spectra of an ortho-II $YBa_2Cu_3O_{6.50}$ crystal: black triangles, $T=1.3$ K; lighter triangles, 2.7 K; squares, 4.3 K; dots, 6.7 K. The solid curve is a fit to the 6.7-K data with the Born scattering model described in the text. The dashed curves show that the model fails to capture the observed T dependence. The inset shows that the data obey an unusual frequency-temperature scaling, $\sigma_1(\omega,T)=\sigma_1(\omega/[T+T_0])$, with $T_0=2.0$ K. The Drude fit in the inset illustrates the inadequacy of the Lorentzian line shape. From Turner *et al.*, 2003.

markable parallel between the $1/\tau(T)$ and the temperature dependence seen in NMR and nuclear quadrupole resonance data suggests that the scattering by spin fluctuations may be relevant to the issue (Statt and Griffin, 1992). The d-wave symmetry of the order parameter is essential for a detailed understanding of the low-frequency data. Indeed, the presence of the nodes of the order parameter implies that quasiparticle excitations are relevant even at $T \ll T_c$. Studies of both the T and ω dependence of the scattering rate produced by the spin fluctuations spectrum in a d-wave superconductor capture the essential characteristics of the data (Quinlan *et al.*, 1994, 1996). Nodal quasiparticles also determine the functional form of the temperature dependence of the penetration depth (Sec. VIII.C). Gap anisotropy plays a prominent role in the dynamics of nonequilibrium quasiparticles probed in experiments in the time domain (Segre *et al.*, 2002). Yet another important factor for the accurate description of the fine features of quasiparticle dynamics is related to the Fermi surface of high-T_c cuprates (Walker and Smith, 2000). Examining Fig. 30 one notices the quasiparticle Q_2 is the lowest-energy quasiparticle that can participate in an umklapp scattering of the nodal quasiparticle Q_1. The energy of the quasiparticle Q_2 enters exponentially into the calculations of the T dependence of the scattering rate and allows one to account for the low-T properties of the microwave data shown in the right panel of Fig. 30.

It is worth pointing out that there are several features of the data that are not understood within the two-fluid model of a d-wave superconductor. As emphasized by Turner *et al.* (2003) the ω dependence of the conductivity peak in $YBa_2Cu_3O_{6.50}$ crystals is not consistent with the Lorentzian form predicted by the two-fluid formula [Eq. (16)]. Instead the conductivity shows a cusp form (Fig. 29). Moreover, the conductivity appears to obey an unusual frequency-temperature scaling (inset of Fig. 29). More importantly, it is not obvious that the presence of the strong mode in the conductivity data can be reconciled with the notion of a *clean* d-wave superconductor. As emphasized above, a clean d-wave system is still expected to show vanishingly small conductivity at $\omega \to 0$ at $T \ll T_c$, whereas impurities are expected to trigger "universal" conductivity. Within the d-wave scenario the residual absorption can be accounted for only through a significant concentration of pair-breaking impurities (Carbotte *et al.*, 1995; Quinlan *et al.*, 1996). One possible

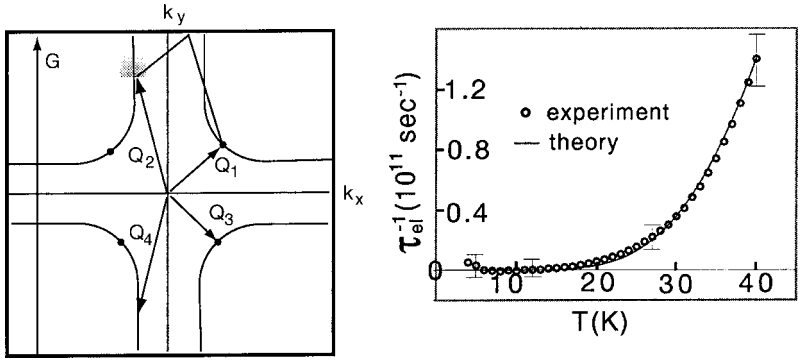

FIG. 30. The role of umklapp processes in the temperature dependence of the scattering rate: Left panel, schematic representation of the Fermi surface associated with a single CuO_2 plane of Y-123. The d-wave superconducting gap varies with momentum along the Fermi surface, going to zero at the nodes indicated by solid circles. The wave vectors Q_i on the Fermi surface are associated with quasiparticles involved in an umklapp processes. G is a reciprocal-lattice vector. Right panel, a comparison of the theoretical curve for the temperature dependence of the quasiparticle scattering rate $t_{el}^{-1}(T)$ calculated by taking account of peculiarities of the umklapp processes in a d-wave superconductor with the data of Hosseini *et al.* (1999). Adapted from Walker and Smith, 2000.

source of residual conductivity with the absolute values of $\sigma(\omega)$ in excess of the universal value of Lee (1993) may be related to the spatial inhomogeneities of superconducting condensate (Corson *et al.*, 2000; Sec. VIII.D). Yet another unresolved issue concerns the assertion that the superconducting transition in cuprates is associated with development of coherence in the quasiparticle transport out of an incoherent response at $T > T_c$. The dramatic depression of $1/\tau$ discussed above corroborates this assertion. Nevertheless, the quasiparticle response even at $T < T_c$ is rather peculiar, since indisputable evidence for coherence is found in the *ab*-plane transport. However, the interplane quasiparticle response still remains incoherent based on the microwave and infrared data for Y-123 (Hosseini *et al.*, 1998; Homes, Dordevic, *et al.*, 2004) but gives some indications of coherence in Bi-2212 (Latyshev *et al.*, 1999). A clear example of coherent interlayer response with a well-defined Drude peak is found in the closely related system Sr_2RuO_4 (Katsufuji *et al.*, 1996; Hildebrand *et al.*, 2001).

C. Anisotropic superfluid response

A hallmark of the electrodynamics of a superconductor at $T < T_c$ is the formation of a delta function in the real part of the conductivity at $\omega = 0$. The spectral weight associated with the δ peak defines the superfluid density of a superconductor ρ_s (Sec. IV.D). In orthorhombic systems (which includes most cuprates) the three diagonal components of the ρ_s tensor will be different. A unique advantage of infrared spectroscopy in studying the superfluid response in cuprates is that all diagonal components of the tensor can be obtained from model-independent analysis. Indeed, the analysis using Eqs. (17) and (18) can be applied to the conductivity probed with polarized light, in which the polarization of E vectors along a, b, or c axes will yield the corresponding plasma frequencies or penetration depth values. The layered crystal structure leads to strong depression of the c-axis superfluid density ρ_c compared to that probed along the direction of the CuO_2 plane. In the Y-123 series there is an additional *ab*-plane anisotropy associated with Cu-O chains. Analysis of the temperature dependence of the superfluid density provides insights into the symmetry of the order parameter in cuprates and also allows one to experimentally address the issue of condensate inhomogeneities.

1. *ab* plane

The form of Eq. (18) suggests that it is instructive to explore the frequency dependence of $\lambda(\omega) = c/\sqrt{\sigma_2(\omega)\omega}$ (Basov, Liang, *et al.*, 1995) in the search for the in-plane anisotropy of the superfluid density. In the limit of $\omega \to 0$, this expression yields the magnitude of the penetration depth, which is proportional to ω_{ps}^{-1}. The results of such an analysis for untwinned Y-123 and Y-124 crystals with the polarizations of the incident radiation along a and b axes are shown in Fig. 31 (Basov, Liang, *et al.*, 1995). Notably, the penetration depth is strongly suppressed when it is probed along the direction of Cu-O chains ($E \| b$). In the double-chained Y-124 crystal the anisotropy is larger. These observations are consistent with the notion that chains are superconducting in Y-123 compounds (Basov, Liang, *et al.*, 1995). In high-quality $YBa_2Cu_3O_{6.95}$ crystals the anisotropy of the penetration depth is approximately the same as that of the dc resistivity or of the normal-state plasma frequency: $\lambda_a^2/\lambda_b^2 \simeq \rho_b/\rho_a \simeq \omega_{pb}^2/\omega_{pa}^2 \simeq 2.3$. Similar experiments carried out for underdoped Y-123 samples also reveal the anisotropy of the penetration depth with strong suppression of the λ_b value (Basov and Timusk, 2001; Lee *et al.*, 2005a). While the absolute values of λ_a and λ_b are different, the temperature dependence of these quantities (Fig. 33) is nearly identical based on microwave measurements (Zhang *et al.*, 1994; Hosseini *et al.*, 1998).

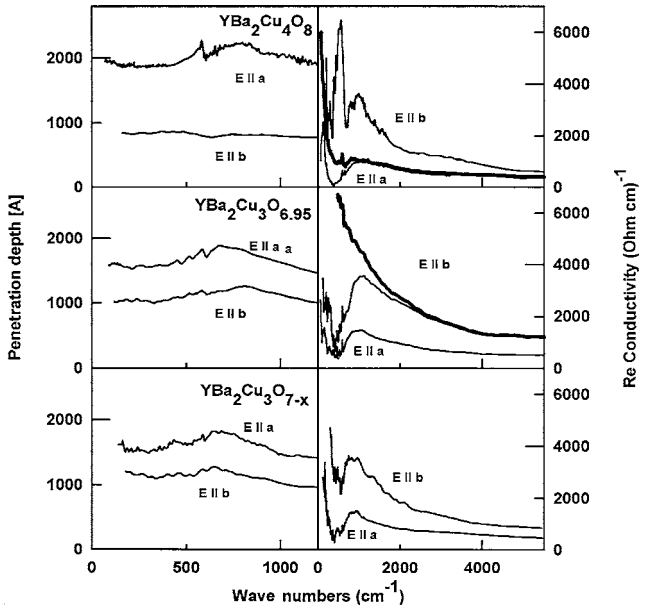

FIG. 31. Infrared response of untwinned YBCO single crystals: Left panels, frequency dependence of $\lambda(\omega) = c/\sqrt{\sigma_2(\omega)\omega}$ for Y-124 sample (upper panel), and two different Y-123 samples (middle and bottom panels). Right panels, the real part of the complex conductivity. All curves shown are at 10 K. Left panels reveal clear anisotropy of the penetration depth, which is stronger for the double-chained Y-124 material. Adapted from Basov, Liang, *et al.*, 1995.

The contribution of the 1D Cu-O chains to the superfluid density, which is directly observed with IR methods (Basov, Liang, *et al.*, 1995), can also be inferred from other techniques (Sun *et al.*, 1995; Tallon, Bernhard, *et al.*, 1995; Pereg-Barnea *et al.*, 2004). Theoretically, the robust condensate density in the Cu-O chains is not well understood. Most models start from the notion that the pairing mechanism is an exclusive property of the CuO_2 planes, whereas other elements of the unit cell are regarded as passive placeholders. Within this approach one attributes the formation of the superconducting condensate in the chains to a proximity effect between "intrinsically superconducting" CuO_2 planes and "intrinsi-

cally normal" Cu-O chains (Kresin and Wolf, 1992; Xiang and Wheatley, 1995; Morr and Balatsky, 2001). The major problem with this interpretation is that proximity-based models cannot account for the identical temperature dependence of λ_a and λ_b found with microwave spectroscopy (Zhang *et al.*, 1994). Indeed, one expects that proximity coupling will induce a gap in the normal layer with the suppressed magnitude (Kresin and Wolf, 1992; Atkinson and Carbotte, 1995). This will inevitably lead to difference in the T dependence of the penetration depth (Atkinson and Carbotte, 1995) and to a difference in the frequency dependence of $\sigma_1(\omega)$ (Atkinson and Carbotte, 1997). Both of these expectations, based on the proximity-coupling model, are inconsistent with experiments. The failure of the proximity-based scenario to account for experimental observations may suggest that the Cu-O chains are also intrinsically superconducting.

Quijada *et al.* (1999) reported on the in-plane anisotropy of the penetration depth in optimally doped Bi-2212 single crystals with mild enhancement of the *b*-axis value: $\lambda_a = 1800$ Å, $\lambda_b = 1960$ Å. This family of cuprates contains no Cu-O chains. However, the *b* axis is the direction of the superstructure in the Bi-O plane. Quijada *et al.* (1999) analyzed the relation between the plasma frequency of the superconducting condensate and that of the Drude component [extracted by the multicomponent approach, Eq. (2)]. From this analysis they concluded that the source of the anisotropy is not related to mass enhancement but is instead due to additional pair-breaking scattering produced by the superlattice in the *b* direction.

2. Systematics of the in-plane superfluid response

The in-plane superfluid response of cuprates was first systematically analyzed by Uemura, who established a scaling between T_c and the superfluid density (Uemura *et al.*, 1989, 1991). Several deviations from the original Uemura universal line are worthy of attention. In Y-123 compounds only the *a*-axis superfluid density correlates with T_c. In disordered materials the linear dependence of the superfluid density on T_c is violated (Nachumi *et al.*, 1996). Also, in electron-doped $Nd_{2-y}Ce_yCuO_4$ (Homes, Clayman, *et al.*, 1997) the superfluid density appears to significantly exceed that of other superconductors with $T_c \simeq 20$ K.

Homes, Dordevic, *et al.* (2004) have shown that many of the above-mentioned deviations from the Uemura plot can be remedied by taking into account differences between the dc conductivities at $T \simeq T_c$. He found that the $\rho_s \propto \sigma_{dc} T_c$ relation is followed remarkably well for a large variety of high-T_c systems. Interestingly, both the in-plane and the *c*-axis superfluid density appear to fall on the same line when plotted against the product of $\sigma_{dc} T_c$. Zaanen (2004) proposed that this scaling relation has roots in the extreme dissipation in cuprates above T_c. Furthermore, Zaanen conjectured that the superconducting transition temperature in cuprates is high because the normal state in these systems is as viscous as is permitted by quantum mechanics. As pointed out in Sec. II.D, the Homes scaling is expected from the Ferrell-Glover-Tinkham sum rule [Eq. (17)]. Homes's scaling is equivalent to the statement that $\hbar/\tau \simeq k_B T_c$, which, as Lee points out (Lee, 2005), follows directly from the fact that $\hbar/\tau \simeq \pi k_B T$ at all temperatures, a fact that has been known from the beginnning of infrared studies of high-temperature superconductivity (Schlesinger *et al.*, 1990).

The BCS theory does not offer an account of any explicit correlation between T_c and the superfluid density at $T=0$. However, $T_c \propto n_s/m^*$ is an essential feature of a Bose-Einstein condensate. Useful inferences in this context were obtained by Uemura (1996), who estimated the number of carriers per area of the coherence length squared ξ_{ab}^2 on the conducting *ab* plane from the superfluid density. Both cuprates and organic superconductors have only several superconducting pairs per ξ^2, which puts these systems close to the limit of Bose-Einstein condensation (one molecule per $1/\xi^2$ as compared to the BCS condensation limit of more than 10 000 carriers/ξ^2). Emery and Kivelson (1995a, 1995b) emphasized that in superconductors with low superfluid density (such as cuprates and organic materials) the role of phase fluctuations is dramatically enhanced. They argued that in the above materials the magnitude of the superfluid density controls the temperature of long-range phase order and thus determines T_c.

The data displayed in Fig. 27 show that only a relatively small fraction of the spectral weight available in the infrared region is involved in the formation of the superconducting condensate at $T < T_c$. To explore the systematic trends of the condensate formation Liu *et al.* (1999) examined the relationship between the number of carriers forming the condensate N_s, the strength of the Drude absorption N_{Drude} [extracted from Eq. (2)], and the total oscillator strength in infrared N_{tot}. The results of their analysis are summarized in Table I. The table shows a correlation between the transition temperature and the total number of carriers in the system. This correlation holds whether one considers the number of carriers in the superfluid N_s or the total number of carriers. Another interesting observation is that the spectral weight of the superconducting condensate is dominated by the Drude weight. However, as much as 20% of the superfluid density can be attributed to condensation of the "incoherent" component of the conductivity.

3. Systematics of the interlayer superfluid response

The magnitude of the *c*-axis penetration depth is strongly enhanced in all high-T_c superconductors compared to λ_{ab} (Fig. 32). Typical values of λ_c range from 100 μm in the one of the most anisotropic Bi-2212 crystals (Cooper *et al.*, 1989) to about 1 μm in the most isotropic $YBa_2Cu_3O_{6.95}$ and Y-124 crystals (Homes, Timusk, *et al.*, 1993; Basov, Timusk, *et al.*, 1994; Schützmann *et al.*, 1994). The magnitude of λ_c shows a systematic correlation with the dc conductivity along the *c*-axis σ_c (Basov, Timusk, *et al.*, 1994; Shibauchi *et al.*,

TABLE I. Effective number of carriers per planar Cu atom. Adapted from Liu *et al.*, 1999.

Material	T_c (K)	N_{tot}	N_{Drude}	N_s	N_s/N_{tot}	N_s/N_{Drude}
$La_2CuO_{4.12}$	40	0.14	0.035	0.028	0.2	0.8
$Bi_2Sr_2CaCu_2O_8$	85	0.38	0.105	0.092	0.24	0.88
Y 0.35	40	0.21	0.04	0.02	0.08	0.5
Pb 0.5, Y 0.2	35	0.23	0.05	0.017	0.07	0.34
$YBa_2Cu_3O_{7-\delta}$	92	0.44	0.093	0.082	0.19	0.89
Pr 0.15	75	0.375	0.073	0.054	0.14	0.74
Pr 0.35	40	0.25	0.045	0.02	0.08	0.44
$Tl_2Ba_2CaCu_2O_8$	110	0.54	0.13	0.115	0.21	0.88
Uncertainties	±2	±0.03	±0.01	±0.01	±0.01	±0.04

1994). As the doping level is reduced the *c*-axis penetration depth is dramatically enhanced, whereas the magnitude of the dc conductivity across the CuO_2 layers is depressed. These effects can be attributed to two different processes. Indeed, both the overall suppression of carrier density in the CuO_2 and the reduction of the hopping amplitude between the layers can, at least in principle, result in both the decline of $\sigma_1(\omega)$ and the enhancement of λ_c. Reduction of the hopping amplitude on the underdoped side may be expected from the increase of the *c*-axis length and may also be due to defects in the reservoir layer. A study of the infrared interlayer response of $Pr_yY_{1-y}Ba_2Cu_3O_{7-\delta}$ (Bernhard *et al.*, 1998; Dordevic, Singley, *et al.*, 2004) discriminates between the two possibilities at least in the case of Y-123 materials. Data obtained by Bernhard *et al.* (1998) and by Dordevic, Singley, *et al.* (2004) show that in the Y-123 system the interlayer transport is determined primarily by the electronic state of the CuO_2 planes.

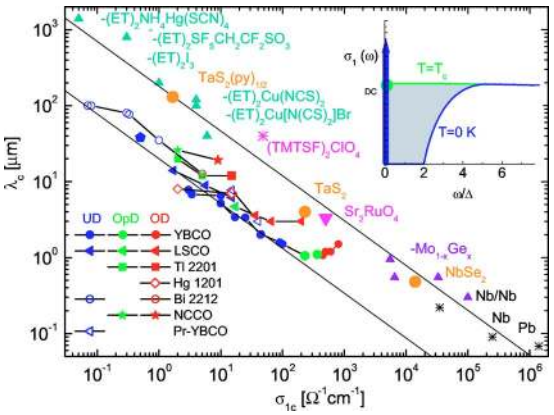

FIG. 32. (Color in online edition) The *c*-axis penetration depth $\lambda_c(T \ll T_c)$ plotted as a function of the *c*-axis dc conductivity σ_{dc} for a variety of layered superconductors. We find two distinct patterns of $\lambda_c - \sigma_{\text{dc}}$ scaling. Cuprate superconductors exhibit much shorter penetration depths than noncuprate materials with the same $\sigma_{\text{dc}}(T)$. This result may be interpreted in terms of a dramatic enhancement of the energy scale from which the condensate is collected as described in the text. See Dordevic, Singley, *et al.* (2002) for a discussion of the raw data points and analysis. Inset: In a conventional dirty-limit superconductor the spectral weight of the superconducting condensate (given by $1/\lambda_c^2$) is collected primarily from the energy-gap region. The total normal weight is preset by the magnitude of σ_{dc} whereas the product of $\lambda_c\sigma_{\text{dc}}$ quantifies the fraction of the weight that condenses.

The proportionality $\lambda_c^{-2} \propto \Delta\sigma_c$ is expected for an array of Josephson junctions (Basov, Timusk, *et al.*, 1994; Shibauchi *et al.*, 1994). Thus Josephson electrodynamics successfully describes the gross features of the *c*-axis penetration depth in a broad variety of cuprates. Other proposed theoretical explanations for the $\lambda_c - \sigma_{\text{dc}}$ correlation have also been discussed in the literature (Hirschfeld *et al.*, 1997; Chakravarty *et al.*, 1999; Kim and Carbotte, 2000; Ohashi, 2000). Furthermore, a correlation between the magnitude of λ_c and the dc conductivity can be anticipated for a dirty superconductor from sum rule arguments. To illustrate this we turn to an expression for the superfluid density in a dirty BCS superconductor (Smith and Ambegaokar, 1992):

$$\frac{n_s}{m^*} = \sigma_{\text{dc}} \frac{\pi}{e^2} \Delta \tanh\left[\frac{1}{2}\beta\Delta\right], \tag{29}$$

establishing a direct connection between the magnitude of $\omega_{ps} = n_s/m^*$ and σ_{dc}. In this expression β is the reciprocal temperature. It is reasonable to expect this particular form of connection where $\omega_{ps} = 1/\lambda$ is proportional to the *product* of the energy gap and σ_{dc}. Indeed, "the missing area" defining the superfluid density is set by the level of the conductivity $\sigma_1(\omega \to 0) = \sigma_{\text{dc}}$ and the energy scale associated with the formation of the condensate. The latter quantity is given by the magnitude of 2Δ in the case of a BCS superconductor. From Eq. (29) one also expects to find the $\lambda_c - \sigma_{\text{dc}}$ scaling with the power law $\alpha = 1/2$, which is close to the $\alpha = 0.59$ seen in Fig. 32. The offset of the scaling along the vertical axis characterizes the energy scale associated with the formation of the superconducting condensate. In this context it is interesting to note that in many underdoped cuprates the λ_c values are depressed by approximately two orders of magnitude compared to the penetration depth in more conventional superconductors having the same σ_{dc} (the upper line in Fig. 32). This can be understood in terms of the dramatic enhancement of the energy scale from

which the superconducting condensate is collected in high-T_c cuprates compared to that of more conventional superconducting materials (Dordevic, Singley, *et al.*, 2002). This effect is intimately related to lowering of the electronic kinetic energy at $T<T_c$ observed in the *c*-axis conductivity of many cuprates (Basov, Woods, *et al.*, 1999).

The anomalous *c*-axis properties of high-T_c superconductors and the strong evidence for Josephson coupling between the CuO_2 layers give experimental support for the interlayer tunneling theory of high-T_c superconductivity (Chakravarty and Anderson, 1994). In this hypothesis the hopping of single electrons between CuO_2 planes is inhibited in the normal state by spin-charge separation. However, tunneling of pairs is allowed at $T<T_c$, which leads to a gain of kinetic energy as Cooper pairs are formed and superconductivity sets in. This energy is the Josephson coupling energy, and it is proportional to the square of the plasma frequency of the condensate probed in the polarization when the E vector is along the *c* axis. Thus if interlayer tunneling of Cooper pairs is the driving force for superconductivity, one would expect to find a correlation between T_c and $1/\lambda_c$ (Anderson, 1995; Leggett, 1996). A brief examination of Fig. 32 suggests that in general such a correlation is not found in cuprates. Moreover, measurements of the *c*-axis penetration depth in $Tl_2Ba_2CuO_{6+\delta}$ and Hg-based cuprates have uncovered a fairly long penetration depth inconsistent with the values of $T_c \simeq 90$ K in these materials (Schützmann *et al.*, 1997; Kirtley *et al.*, 1998; Moler *et al.*, 1998; Tsvetkov *et al.*, 1998; Basov, Woods, *et al.*, 1999). However, it is worth pointing out that the key prediction of this model—the change of the *c*-axis kinetic energy—has been experimentally observed (Basov, Woods, *et al.*, 1999), as will be discussed in Sec. VIII.F.

4. Temperature dependence of the penetration depth and the symmetry of the order parameter

A combination of infrared methods providing the absolute value of $\lambda_a(T\to 0)$, $\lambda_b(T\to 0)$, and $\lambda_c(T\to 0)$ with microwaves giving a detailed and accurate temperature dependence $\Delta\lambda=\lambda(T)-\lambda(0)$ has made possible detailed studies of the penetration depth in high-T_c superconductors. Figure 33 shows the temperature dependence of $\lambda^2(0)/\lambda^2(T)$ for *a*, *b*, and *c* polarizations measured using IR-determined values of $\lambda_a(0)$ and λ_b (Basov, Liang, *et al.*, 1995). Near optimal doping of both the *a*-axis and *b*-axis components of the λ tensor show linear behavior, which was first observed in twinned $YBa_2Cu_3O_{6.95}$ samples (Hardy *et al.*, 1993). On the other hand, the T dependence along the *c* axis is close to quadratic, with a power law of $1/\lambda^2(T)\propto T^{2.1}$ (Hosseini *et al.*, 1998, 2004). For an overview see Bonn and Hardy (1996).

The T-linear or T^2 variation of the penetration depth should be contrasted with an exponential dependence of $1/\lambda^2(T)$ expected for a BCS superconductor with an isotropic gap. While the thin-film specimens studied prior to 1992 tended to show a T^2 law for $1/\lambda^2(T)$ a series of later studies performed for high-quality single crystals show a T-linear law (Jacobs *et al.*, 1995; Ma, 1995). A consensus is emerging in the field that the earlier observations of T^2 dependence were dominated by impurity effects, whereas intrinsic behavior of the penetration depth can be found only in clean samples, and that variation is linear with T. This problem was studied in detail by a group at the University of British Columbia. Starting from a high-purity $YBa_2Cu_3O_{6.95}$ single crystal with $1/\lambda_{ab}^2\propto T$, Bonn *et al.* (1994) deliberately added Zn and Ni ions, which are believed to replace Cu in the CuO_2 planes. They observed a crossover to the $1/\lambda_{ab}^2(T)\propto T^2$ law in the crystal when it contained as little as 0.31% Zn. Thin-film samples also show a linear penetration depth at low temperatures. This behavior was first observed by Gao *et al.* in their microwave experiments conducted at 10 GHz (Gao *et al.*, 1993; Dahne *et al.*, 1995; de Vaulchier *et al.*, 1996). A penetration depth that varies linearly with temperature is expected for a superconductor with *d*-wave symmetry of the order parameter (Prohammer and Carbotte, 1991; Hirschfeld *et al.*, 1994). Therefore *d*-wave symmetry of the order parameter may be regarded as the "minimum model" needed to account for this generic property of cuprates.

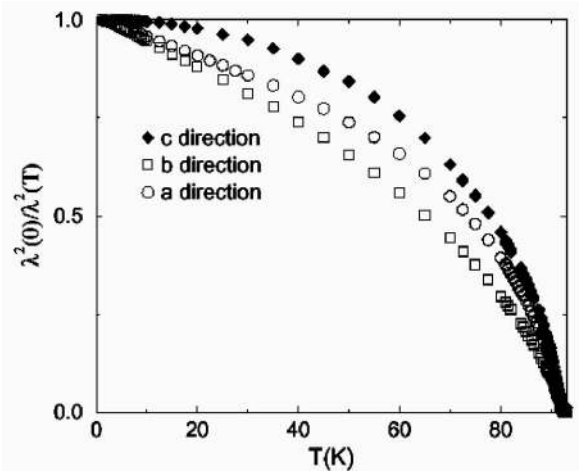

FIG. 33. The temperature dependence of the superfluid fraction probed separately for *a*, *b*, and *c* directions. From Hosseini *et al.*, 1998.

Several groups have reported measurements of the temperature dependence of the *c*-axis penetration depth in Y-123 (Basov, Timusk, *et al.*, 1994; Homes, Timusk, *et al.*, 1995a, 1995b; Mao *et al.*, 1995; Hardy *et al.*, 1996; Lobo *et al.*, 1996; Homes, Clayman, *et al.*, 1997; Tajima *et al.*, 1997), in Bi-2212 (Jacobs *et al.*, 1995), and La-214 (Shibauchi *et al.*, 1994; Basov, Mook, *et al.*, 1995; Henn *et al.*, 1996; Dordevic, Komiya, *et al.*, 2003a), and $HgBa_2CuO_4$ (Panagopoulos *et al.*, 1997). The results of these experiments are rather controversial. Systematic studies of the penetration depth in weakly doped Y-123 crystals ($y\approx 6.35$) have recently been carried out by Hosseini *et al.* (2004). They observed that the T^2 variation of $1/\lambda_c^2(T)$ survives down to very low doping. These experiments imply that the nodes of the *d*-wave energy

gap with no sign of another ordered phase.

The issue of order-parameter symmetry in electron-doped materials remains rather controversial in contrast to the overwhelming acceptance of *d*-wave superconductivity in the hole-doped compounds. Several experimental studies of $\lambda_{ab}(T)$ starting from the work of Wu *et al.* (1993) have uncovered an exponential behavior of the penetration depth inconsistent with the idea of nodes and therefore supportive of *s*-wave symmetry of the order parameter (Alff *et al.*, 1999; Skinta, Kim, *et al.*, 2002; Kim, Skinta, *et al.*, 2003). However, similar studies performed by other groups showed the power-law behavior suggestive of *d*-wave symmetry (Kokales *et al.*, 2000; Prozorov *et al.*, 2000). Systematic investigations of the doping trends in electron-doped materials revealed that the temperature dependence of the penetration depth is exponential near optimal doping but is quadratic in underdoped samples (Skinta, Lemberger, *et al.*, 2002; Pronin *et al.*, 2003). These findings are therefore indicative of a transition from *d* to *s* pairing near optimal doping.

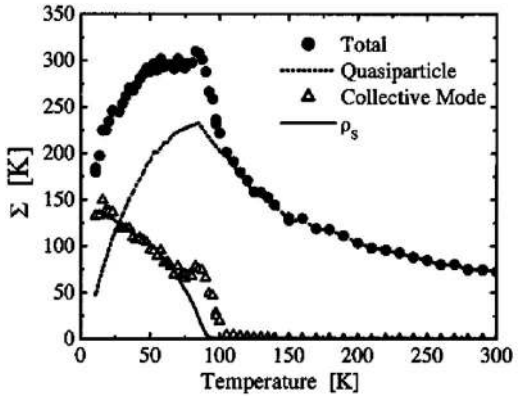

FIG. 34. Temperature dependence of the spectral weight associated with different components of the conductivity in THz region. The spectral weight of the total conductivity from 0.2 to 0.8 THz, $\Sigma(T)$, the quasiparticle Drude conductivity, $\Sigma_{qp}(T)$, and the difference between the two, $\Sigma(T)-\Sigma_{qp}(T)$. The solid line displays the superfluid density ρ_s multiplied by 0.18, showing the proportionality between this and the portion of the spectral weight not due to the quasiparticles. From Corson *et al.*, 2000.

D. Inhomogeneous superconducting condensate

The substantial conductivity at $T \ll T_c$, well documented through both far-IR and microwave experiments in thoroughly characterized samples, is a rather puzzling observation. As pointed out above, in clean *d*-wave superconductors $\sigma_1(\omega \to 0, T \ll T_c)$ is expected to vanish in contrast with the experimental observations. The residual conductivity has been systematically examined in $Bi_2Sr_2CaCu_2O_8$ thin films with THz time-domain spectroscopy (Corson *et al.*, 2000). Careful analysis of the frequency and temperature dependence of the THz conductivity has allowed these authors to identify a *third* component of the conductivity in addition to the Drude-like quasiparticle contribution and superconducting δ function in Eq. (15). This additional collective-mode contribution (Fig. 34) has a T dependence that closely tracks that of the superfluid density. The authors assigned this additional dissipation to phase fluctuations in the presence of (quasi)static variations of the local superfluid density. Their viewpoint is supported by theoretical analyses of the optical constants that have linked the development of finite ac conductivity to quenched disorder in the system (Barabash *et al.*, 2000; Barabash and Stroud, 2003; Orenstein, 2003). It is interesting to note that the appearance of this additional absorption within the quenched disorder model has no connection with unconventional *d*-wave symmetry.

A closely related issue has been theoretically analyzed by Zheng *et al.* (1989). They have been able to demonstrate significant absorption at energies below 2Δ in a two-dimensional composite of a normal metal and *s*-wave superconductor. It is therefore likely that the residual absorption universally found in high-T_c cuprates is at least in part related to intrinsic and/or extrinsic inhomogeneities of these systems. Notably, the length scales associated with quenched disorder are significantly shorter than the wavelengths corresponding to these modes in the conductivity spectra. Nevertheless, these effects can be efficiently probed through measurements in the THz range, thus offering an opportunity to study inhomogeneities of the superconducting condensate.

Dordevic, Komiya, *et al.* (2003a) proposed another method to probe inhomogeneities of the superconducting condensate in CuO_2 planes. Their approach is based on analysis of the Josephson tunneling between the planes and appears to be capable of registering nonuniformity of superfluid density on a length scale of the order of 100 Å. This information is inferred from an examination of asymmetric broadening of the Josephson plasma resonance plasmon (inset in Fig. 35). Random distribution of normal-state regions within the CuO_2 planes is expected to produce such inhomogeneous broadening provided the length scale is comparable to the Josephson wavelength $\lambda_J = \gamma s$ (Koshelev and Bulaevsky, 1999), where γ is the ratio between the in-plane and interplane condensate superfluid plasma frequencies, $\gamma = \omega_{s,ab}/\omega_{s,c}$, and s is the interlayer spacing. The high-energy tail in the loss function spectra is directly related to mixing between local Josephson modes with different momenta and energy produced by in-plane inhomogeneities. Short-range inhomogeneities are averaged out by slowly varying the external field, leading to the narrow Josephson plasma resonances typically observed in most cuprates. However, mode mixing resulting in the asymmetric broadening of the Josephson plasmon gains prominence if the length scale associated with inhomogeneities is comparable to the magnitude of λ_J. Anomalous broadening of the Josephson plasmon in inhomogeneous superconductor has been predicted by van der Marel and Tsvetkov (1996). The asymmetry in the La-214 series can be characterized by examining the width of the mode on the left- and right-hand sides of

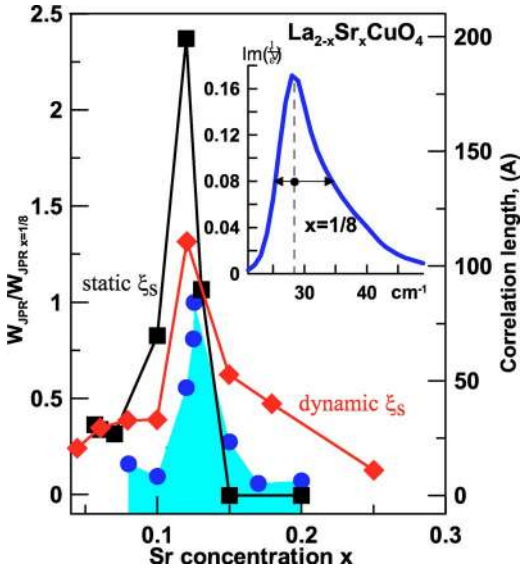

FIG. 35. (Color in online edition) Spin ordering and inhomogeneous superfluid response in an La-214 system: Dots, the doping dependence of the asymmetry of the loss function $W_{\mathrm{JPR}}/W_{\mathrm{JPR},x=0.125B}$. This parameter characterizes the degree of inhomogeneity of the superfluid density within the CuO_2 planes, as discussed in the text. The correlation length ξ_s of both static (squares) and dynamic (rhombs) spin structures is extracted from neutron-scattering experiments (Yamada *et al.*, 1998; Kimura *et al.*, 1999). Adapted from Dordevic, Komiya, *et al.*, 2003a.

the Josephson plasma resonance (W_{JPR} in Fig. 35). This asymmetry is maximized near $x=1/8$ doping, corresponding to commensurate ordering of the stripes. The length scales inferred from the asymmetry of the Josephson plasma resonance feature are suggestive of a formation of fairly large droplets within the CuO_2 planes, where superconductivity is either suppressed or completely depleted. This picture can be readily reconciled with the neutron data assuming that the spin-ordered signal near $x=1/8$ is produced by regions of depressed superconductivity.

E. Impurity effects

Nonmagnetic impurities have little effect on superconductivity in elemental metals (Anderson, 1958). On the other hand, *d*-wave superconductors are expected to be anomalously sensitive to disorder, which can lead to a smearing of the gap anisotropy towards a zero average value. In qualitative agreement with the picture of anisotropic superconductivity, the value of T_c in cuprates is systematically diminished with disorder (Valles *et al.*, 1989; Sun *et al.*, 1994; Toplygo *et al.*, 1996). Another theoretical prediction for *d*-wave superconductors is that impurities cause severe changes in the intragap density of states (Borkowski and Hirschfeld, 1994; Fehrenbacher and Norman, 1994; Preosti *et al.*, 1994a, 1994b; Palumbo and Graf, 1996). Therefore one expects to find dramatic effects of impurities on the temperature dependence of the penetration depth and on the frequency dependence of the complex conductivity, which both probe the low-energy excitations in a superconductor. Indeed, a crossover from the penetration depth varying linearly in T to T^2 behavior has been observed in disordered Y-123 crystals (Bonn *et al.*, 1994). Both of these effects have been systematically explored. Experimental studies of the evolution of the far-IR conductivity in disordered samples are reviewed by Basov and Timusk (2001).

Basov, Dabrowski, and Timusk (1998) reported on the *a*-axis conductivity of Y-124 crystals with Zn substitution for Cu. They showed that Zn leads to the formation of the bound state in the response of the CuO_2 planes at $\omega \simeq 10$ meV. The bound state corresponds to the peak in the real part of the complex conductivity, which develops at the expense of the Drude-like excitation at $\omega=0$. Peaks at finite frequency are often observed in strongly disordered conductors at the borderline of localization (Allen and Mikkalson, 1976; Gold *et al.*, 1982; Ng *et al.*, 1986; Jang *et al.*, 1990). Analysis of the optical conductivity based on solutions of Bogoliubov–de Gennes equations shows that weak localization effects give rise to a finite-frequency peak in the optical conductivity similar to that observed in experiments on disordered cuprates (Atkinson and Hirschfeld, 2002). The results of Basov, Dabrowski, and Timusk (1998) for Zn-substituted $YBa_2Cu_4O_8$ demonstrate that the spectral weight from $\omega < E_c$ does not contribute to a superconducting condensate. This suggests a connection between the metal-insulator transition induced by impurities and the degradation of T_c in disordered superconductors.

Interpretation of the anomalies in the low-frequency in-plane response has to be exercised with extreme caution. Indeed, minor contamination of the $\mathbf{E}\|ab$ data with unwanted *c*-axis polarization can produce significant artifacts in the data (Orenstein and Rapkine, 1988; Pimenov *et al.*, 2002; Tajima *et al.*, 2003). This contamination can originate from (i) miscuts of the sample surfaces, (ii) multiple grains in the bulk of the sample, (iii) surface roughness, and (iv) polarizer leakage. Single crystals synthesized using the flux-growth technique have natural surfaces parallel to principal axes of the crystal and therefore factors (i)–(iv) are usually not relevant. This is also true for Bi-2212 samples prepared in optical furnaces because these crystals easily cleave, revealing pristine surfaces parallel to CuO_2 planes. Special care must be taken while analyzing data for La-214 and Nd-214 systems grown using the optical furnace. An examination of the literature suggests numerous publications of "contaminated" data. We have developed a procedure that allows one to reject samples with strong leakage. Experiments performed on the *ac* phase of a sample permit measurements of both *ab*-plane and *c*-axis reflectance. Leakage of unwanted polarization can lead to a dramatic increase in $R_c(\omega)$ near the minima due to longitudinal optical modes. Near the longitudinal optical frequencies $R_c(\omega) \to 0$ and therefore any increase in reflectivity signals potential problems with a particular sample. In our experience, samples passing this test

reveal properties similar to flux-grown materials in which the impact of leakage is minimized.

F. An infrared probe of the superconducting-state energetics

The Cooper pairing instability in a BCS superconductor leads to an increase in the electronic kinetic energy due to particle-hole mixing. This effect is overpowered by a suppression of the potential energy. The difference between the two energies defines the condensation energy of a superconductor E_c which, at least in principle, can be inferred from specific-heat measurements. Experimental study of the optical conductivity may help to identify different contributions to the condensation energy. This can be accomplished through sum-rule analysis of the optical constants [Eqs. (23) and (24)]. To the best of our knowledge this analysis has not been applied to conventional superconductors. Predictions of the lowering of the kinetic energy at $T<T_c$ by several models of high-T_c superconductivity (Wheatley *et al.*, 1988; Hirsch, 1992; Emery *et al.*, 1997; Chakravarty, 1998) have motivated experimental searches for these enigmatic effects that will be reviewed in this subsection.

Basov *et al.* (1999) examined the formation of the *c*-axis superconducting condensate in a series of high-T_c materials, using an analysis procedure detailed in Fig. 36. They concluded that the spectral weight under the superconducting δ peak in the interlayer conductivity significantly exceeds the weight resulting from the suppression of the normal-state conductivity in the far-IR. According to Eq. (23) this result can be interpreted in terms of lowering of the electronic kinetic energy. Further analysis of the doping dependence of this effect in a series of Y-123 crystals has shown that the sum-rule anomaly is strongest (up to 90%) in underdoped phases and is systematically reduced with doping (Basov, Homes, *et al.*, 2001). This trend is corroborated by $La_{2-x}Sr_2CuO_4$ data (Kuzmenko *et al.*, 2003). The origin of the additional spectral weight has not been identified, in part because it is exceptionally difficult to monitor small changes of the optical conductivity extending over the broad energy range. While the lowering of the *c*-axis kinetic energy is firmly established for many high-T_c cuprates (Basov *et al.*, 1999; Basov and Timusk, 2001; Katz *et al.*, 2001; Munzar *et al.*, 2001, 2003; Boris *et al.*, 2002; Kuzmenko *et al.*, 2003), the actual kinetic-energy saving is insufficient to account for the magnitude of E_c, at least in the case of $Tl_2Ba_2CuO_{6+x}$ and the Hg-1201 compounds (Moler *et al.*, 1998; Tsevtkov *et al.*, 1998).

The spectral weight in the *ab*-plane conductivity dramatically exceeds that of the interplane response, and therefore there is room for much stronger effects (Hirsch, 2002). However, it is universally agreed that the Ferrell-Glover-Tinkham sum rule is satisfied in the case of the *ab*-plane conductivity with $\simeq$10% accuracy (see, for example, recent publications by Tanner *et al.*, 1996, Homes, Tranguada, *et al.*, 2003, and Santander-Syro *et al.*, 2003). In an attempt to probe more subtle effects in the response of the CuO_2 planes, Molegraaf *et al.* (2002) employed spectroscopic ellipsometry (Fig. 37). Careful analysis of the optical constants indicates that about 0.2–0.3 % of the total strength of the superconducting δ function is collected from the energy region beyond 10 000–20 000 cm^{-1}. While the effect is small, it corresponds to a change in the kinetic energy on the order of 1 meV per Cu atom, which is sufficient to account for the condensation energy (Loram *et al.*, 2001; van der Marel, 2003a). In two earlier experiments changes of the optical constants in the visible range were reported (Holcomb *et al.*, 1994; Rubhausen *et al.*, 2001). Ellipsometric studies of the *a*-axis response for optimally doped Y-123 compounds also show superconductivity-induced modifications of the optical constant over an anomalously broad range (Boris *et al.*, 2004). These data agree with the results of Molegraaf *et al.* (2002) in the overlapping frequency region. However, extension of measurements to the far-IR led Boris *et al.* (2004) to the conclusion that the spectral weight relevant to the superfluid density decreases at $T<T_c$. The issues pertaining to

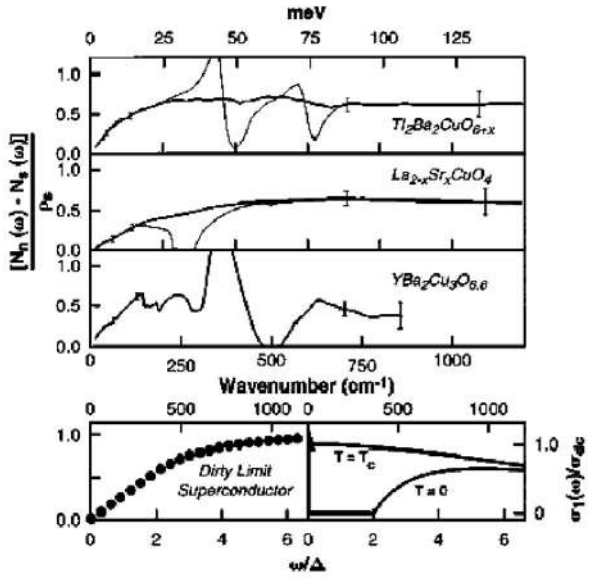

FIG. 36. An infrared probe of the kinetic-energy change associated with the superconducting transition: Top panels, difference between the effective spectral weight in the interplane conductivity of several cuprates at $T\simeq T_c$ and at $T\ll T_c$ normalized by the magnitude of the superfluid density ρ_s extracted from the imaginary part of the conductivity. In these three materials $[N_n(\omega)-N_s(\omega)]/\rho_s$ does not exceed 0.5 at $\omega\simeq 0.1$ eV. In the case of $La_{2-x}Sr_2CuO_4$ and $Tl_2Ba_2CuO_{6+x}$ $[N_n(\omega)-N_s(\omega)]/\rho_s$ spectra are shown without phonon subtraction (thin lines) and with phonons removed (thick lines). Approximate error bars are displayed at selected energies. Left bottom panel, calculations for a conventional dirty-limit superconductor with the scattering rate $\Gamma=20\Delta$, showing that about 90% of the superfluid density is collected from $\omega<4\Delta$. This energy scale corresponds to about 0.1 eV for cuprates where the photoemission result for 2Δ is used. Right-bottom panel, the spectra of $\sigma_1(\omega)$ for a conventional dirty superconductor with $\Gamma=20\Delta$. Adapted from Basov, Woods, *et al.*, 1999.

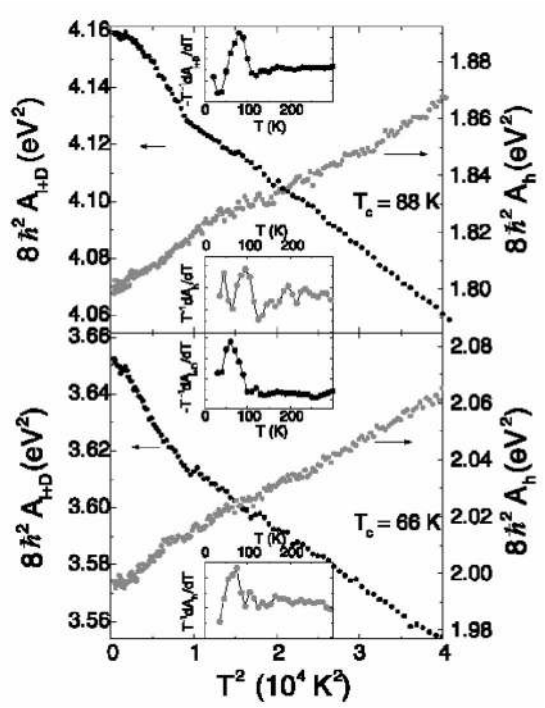

FIG. 37. Temperature dependence of the low-frequency spectral weight $A_{1+D}(T)$ and the high-frequency spectral weight $A_h(T)$, for optimally doped (top) and underdoped (bottom) $Bi_2Sr_2CaCu_2O_{8-d}$. Insets: derivatives $-T^{-1}dA_{1+D}/dT$ and $T^{-1}dA_h/dT$. Adapted from Molegraaf *et al.*, 2002.

these different conclusions inferred from nearly identical data are discussed by Kuzmenko *et al.* (2005).

Changes in the electronic kinetic energy, established by analysis of interplane conductivity (Basov *et al.*, 1999) and also suggested by the in-plane data of Molegraaf *et al.* (2002), highlight the marked departure of superconductivity in high-T_c cuprates from the BCS pairing scheme. In view of the importance of this finding for an understanding of the mechanism of high-T_c superconductivity it is worth restating the underlying assumption of this analysis. The conclusion that the kinetic-energy has changed relies on the single-band sum rule. It is this sum rule that allows one to relate discrepancies in the oscillator strength to the electronic kinetic energy.

The apparent sum rule discrepancy is remarkably different in the *c*-axis and *ab*-plane experiments. This difference may be related to the peculiarities of the infrared probe of the superconducting-state energetics. It was pointed out that the sum-rule anomaly is strongest in underdoped materials in which superconductivity emerges out of a pseudogap state (Basov, Woods, *et al.*, 1999; Basov, Homes, *et al.*, 2001). The latter state can be characterized as "incoherent" because there are no obvious signs of well-defined quasiparticle excitations in this regime. Therefore experiments indicate that the lowering of the electronic kinetic energy is a feature of materials in which global coherence of Cooper pairs is established out of incoherent behavior at $T > T_c$. This hypothesis is supported by the theoretical work of Ioffe and Millis (1999), Kim and Carbotte (2000), Norman *et al.* (2000), Eckl *et al.* (2003), Haslinger and Chubukov (2003), and Iyengar *et al.* (2003). An important point in the context of differences between the *c*-axis and *ab*-plane results on kinetic-energy changes is that these two experiments appear to probe different regions of the Fermi surface. Specifically, the interplane conductivity is primarily determined by the zone-boundary $(\pi,0)$, $(0,\pi)$ regions, where the quasiparticle excitations are overdamped in the pseudogap state. In contrast, the in-plane conductivity is primarily determined by the nodal states residing close to (π,π) yielding a more conventional electromagnetic response. Therefore the contrast between the coherent superconducting state and non-Fermi-liquid state at $T > T_c$ is most vivid in the zone-boundary region. Since it is the zone-boundary region that is explored through the *c*-axis experiments, it is hardly surprising that the relative magnitude of the sum-rule anomalies is strongest in the interlayer response. Norman and Pepin (2000) have been able to explicitly link the magnitude of the kinetic-energy change to incoherence in the system of nodal quasiparticles that can be parametrized with the absolute values of the in-plane scattering rate. The kinetic-energy change in their calculations is systematically diminished as doping level is increased towards the overdoped side, where the absolute values of $1/\tau(\omega)$ are reduced and the Fermi-liquid state is restored.

IX. INFRARED RESPONSE IN A MAGNETIC FIELD

Results of IR measurements in magnetic fields are relatively scarce because these studies are technically demanding. Only in a few special cases have identical experiments been carried out by more than one research group. Nevertheless, IR magneto-optics provides unique insights into the nature of both normal-state transport and superconductivity in cuprates.

A. *ab*-plane conductivity in $H \| c$ field

Several research groups have investigated the in-plane infrared response of cuprates in a geometry with the magnetic field perpendicular to the CuO_2 planes. In this regime one can expect to find changes in the optical properties due to the formation and motion of pancake vortices as well as the suppression of the superconducting condensate. A survey of the literature indicates that there is no universal agreement on the data. This is particularly true for reflectance measurements. For example, Gerrits *et al.* (1994) and Liu *et al.* (1998) reported virtually no changes in superconducting reflectance of $YBa_2Cu_3O_7$ films upon application of a magnetic field. Conversely, Brunel *et al.* (1991) and Eldridge *et al.* (1995) observed a noticeable decrease of $R(\omega)$ in far-IR frequencies.

Thin-film transmission experiments are best suited to probe the influence of static magnetic fields on the *ab*-plane transport. The complex conductivity can be extracted from the power transmission via KK transforma-

tions or directly from THz spectroscopy in the time domain. To obtain the maximum information from the experiments, circularly polarized light is used to measure dichroism (Karrai *et al.*, 1992; Lihn *et al.*, 1996). Alternatively these measurement can be carried out with the sample positioned between crossed polarizers—a geometry that yields the off-diagonal component σ_{xy}, the Hall conductivity (Spielman *et al.*, 1994). The complex transmission $t^{\pm}$ in the far-IR can be converted to the conductivity through $t^{\pm}(H)=[4ne^{i\Phi(\omega)}/(n+1)][1/(Z_0 d\sigma^{\pm}(H)+n+1)]$, where "±" stands for right- and left-hand circularly polarized light, $\Phi(\omega)$ is the frequency-dependent phase shift due to propagation through the substrate, d is the film thickness in cm, $Z_0=377$ is the impedance of free space in ohms (Ω), and n is the index of refraction of the substrate.

Karrai *et al.* (1992) examined transmission through a Y-123 film near optimal doping and observed a strong enhancement of $T(\omega)$ below 80 cm^{-1} in a magnetic field up to 14.5 T. This effect is attributable to the overall reduction of the condensate density due to the presence of vortices. The spectra reveal an edgelike feature in $T(H)/T(H=0)$ spectra, interpreted in terms of the vortex quasiparticle pair excitation resonance. The magneto-optical activity was detected through measurements with circularly polarized light. Transmission of the film in $H=\pm 14.5$ T, measured using a fixed-thickness quartz waveplate, revealed oscillatory behavior with ω when normalized by the transmission at $H=0$. The polarization dependence of magnetoactivity unambiguously pointed to hole conduction. These data are consistent with the notion of the cyclotron resonance with ω_c below the experimental cutoff ($\simeq 25$ cm^{-1}). The latter conclusion is also supported by an analysis of the Faraday effect using THz time-domain spectroscopy (Spielman *et al.*, 1994).

Infrared and THz time-domain experiments have been employed to investigate vortex dynamics in $YB_2Cu_3O_7$ films. Parks *et al.* (1995) compared the results for the off-diagonal components of the conductivity tensor to phenomenological description of vortex motion (Vinokur *et al.*, 1993). These authors found major discrepancies between the values of the vortex parameters predicted by microscopic models and those extracted from the experimental data. Among the factors that may be responsible for the observed discrepancies Parks *et al.* (1995) emphasized the importance of the d-wave symmetry of the order parameter. Because the energy gap vanishes near the nodes, the critical velocity for breaking Cooper pairs is vanishingly small near the nodes. An important consequence in this context is that the superflow around a vortex may lead to depairing at distances much greater than the coherence length. Parks *et al.* (1995) found that the viscosity, Magnus parameter, and pinning constant all could be successfully accounted for by an increase in the number of quasiparticles associated with the vortex in a superconductor with an anisotropic order parameter. The role of nodes in unconventional

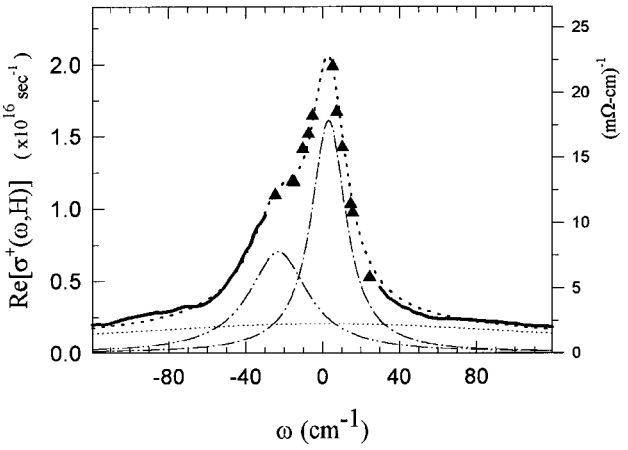

FIG. 38. The magnetoconductivity of $YBa_2Cu_3O_7$ thin film $\mathrm{Re}[\sigma(\omega,H)]$ obtained from a Kramers-Kronig analysis. The change induced by the magnetic field can be described as the sum (dotted line) of a low-frequency oscillator of width $\Gamma_1=10$ cm^{-1}, $\omega_1=+3.15$ cm^{-1} (single dashed line). Adapted from Lihn *et al.*, 1996.

electrodynamics in magnetic fields will be discussed in more detail in Sec. IX.B.

Lihn *et al.* (1996) used a combination of a Michelson interferometer and a monochromatic far-infrared laser source to study the electrodynamics of $YB_2Cu_3O_7$ films in the frequency range 5.25–200 cm^{-1}, which is of primary interest for the analysis of vortex dynamics. In an applied magnetic field, time-reversal symmetry is broken, and it is therefore necessary to determine the optical conductivity $\sigma^{\pm}(\omega,H)$ for both "positive" and "negative" frequencies. Extraction of the conductivity from the KK transformation is nontrivial, since KK dispersion relations are modified in magnetic fields (Smith, 1976). The conductivity spectra displayed in Fig. 38 reveal a reduction of the oscillator strength of the London component, accompanied by the development of two finite-frequency absorption bands at 3.15 and at -24 cm^{-1}. These results, as well as earlier observation of a weaker mode at 65 cm^{-1} (Choi *et al.*, 1994), are consistent with Hsu's theory of vortex dynamics (Hsu, 1993). In order to reconcile these observations with the microwave and GHz probes of the vortex state, Lihn and Drew (1997) have suggested a phenomenological model treating the vortex as a two-component object. The first component, corresponding to overdamped oscillators, is identified with the current vortex outside the vortex core and has properties governed by the equation of motion given by Gittleman and Rosenblum (1966). The other component producing chiral resonances is associated with the vortex core and is described by an equation of motion proposed by Hsu (1993). The two-component model offers a complete description of the magnetoconductivity tensor of $YB_2Cu_3O_7$ films. A theory of the resonant absorption due to vortex-core states has been discussed by Kopnin (1998). Atkinson and MacDonald (1999) have reported on a microscopic evaluation of the electrodynamic response for the vortex lattice states.

One fundamental aspect of the electrodynamics of solids in high magnetic fields is pertinent to the Kohn (1961) theorem. The theorem states that in a uniform magnetic field the only response of an electron system to uniform electromagnetic radiation is the cyclotron resonance at $\omega_c = eH/m_b$, where the band mass m_b is independent of interactions in the system. The validity of the theorem in either two- or three-dimensional electron systems is not in question (Ando *et al.*, 1982). However, one can expect deviations in type-II superconductors due to nonuniformity of the magnetic field at $H > H_{c1}$ and due to the presence of a disordered vortex lattice and/or Meissner currents at the edge of the sample (Drew and Hsu, 1995). This issue has been addressed in a number of theoretical and experimental papers (Karrai *et al.*, 1992; Drew and Hsu, 1995; Lihn *et al.*, 1996). Explicit experimental verification of the Kohn theorem in cuprates is difficult because the cyclotron frequency is low (of the order of few cm^{-1}) and the resonance mode is damped. Additional resonances discussed above are at odds with the theorem. Kopnin and Vinokur (2001) analyzed the electrodynamics of clean type-II superconductors, starting from the Boltzmann kinetic equations. They concluded that the cyclotron resonance in the vortex state generally does not follow the Kohn theorem. The formalism developed by Kopnin and Vinokur permits explicit tests of the theorem through far-IR measurements that are yet to be performed on sufficiently clean samples.

B. Superfluid density in $H \| c$ field: Nonlinear London electrodynamics and pair breaking

The unconventional symmetry of the order parameter in cuprates implies novel effects in the ac response in a high magnetic field, including nonlinear London electrodynamics predicted by Yip and Sauls (1992). These authors pointed out that the equation relating the supercurrent j_s to the velocity v_s remains linear only for $v_s < \Delta/v_F$. The nodes of the order parameter trigger nonlinear corrections, leading to the anisotropy of the superfluid density within the CuO_2 plane as well as reduction of the superfluid density according to the $\sqrt{H}$ law. These predictions have been elaborated on in a number of subsequent publications, showing that studies of the temperature and, particularly, of the magnetic field dependence of the superfluid density may, in fact, enable efficient probe of the nodes of the order parameter (Xu *et al.*, 1995; Zutic and Valls, 1997; Wang and MacDonald, 1999; Amin *et al.*, 2000).

Predictions of the nonlinear London electrodynamics motivated many groups to undertaken systematic studies of the field dependence of the superfluid density. The validity of the early experiments indicating a behavior consistent with the unconventional symmetry of the order parameter (Maeda *et al.*, 1995) has been questioned (Bidinosti *et al.*, 1999). The theoretical analysis of Li *et al.* (1998) suggested that the parameter space where nonlinear London electrodynamics is relevant may be difficult to attain experimentally. Carrington *et al.* (1999) have reported accurate measurements for single-crystal $YB_2Cu_3O_{6.95}$ which supported the power law expected within the Yip-Sauls theory. However, the absolute value of the field-induced suppression of the superfluid density was significantly weaker than that predicted by the theory. Bidinosti *et al.* (1999) reported that both the strength of the superfluid density depression and the power law were consistent with the Yip-Sauls model. However, they failed to detect enhanced pair breaking for the direction between *a* and *b* axes that is expected within the theory. Halterman *et al.* (2001) pointed out that the results on the angular dependence of the $\rho_s(H)$ generated for $YB_2Cu_3O_{6.95}$ have to be analyzed with caution in view of the strong anisotropy of the superfluid density within the *ab* plane, as discussed in Sec. VIII.C. A reexamination of the data with a proper account of this anisotropy (Halterman *et al.*, 2001) has uncovered quantitative agreement between the Yip-Sauls theory and the available experimental data.

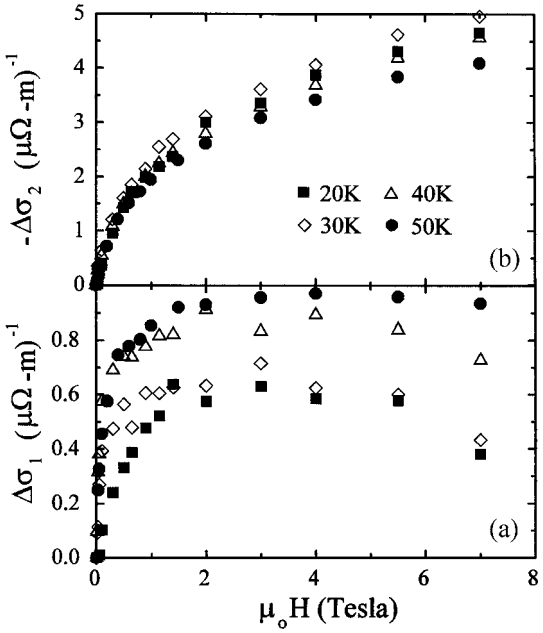

FIG. 39. Evolution of the real and imaginary parts of $\Delta\sigma = \sigma(H) - \sigma(0)$ at 150 GHz for a Bi-2212 thin film. Adapted from Mallozzi *et al.*, 1998.

The Bi-2212 system is nearly isotropic in the *ab* plane and one can therefore expect that experiments in magnetic fields reflect the intrinsic features of the CuO_2 plane response. Orenstein *et al.* (1997) and Mallozzi *et al.* (1998) have carried out extensive studies of the nonlinear electrodynamics in Bi-2212 thin films using THz time-domain spectroscopy. They reported a dramatic depression of the superfluid density: in an 8-T field, the imaginary part of the conductivity at 150 GHz was depressed by 60% of its zero-field value (Fig. 39). Furthermore, they found it is unnecessary to invoke the usual vortex dynamics phenomenology to account for the observed data. Instead, behavior of the complex conductivity is quantitatively described based on the nonlinear London relations of Yip and Sauls. In fact, attempting to

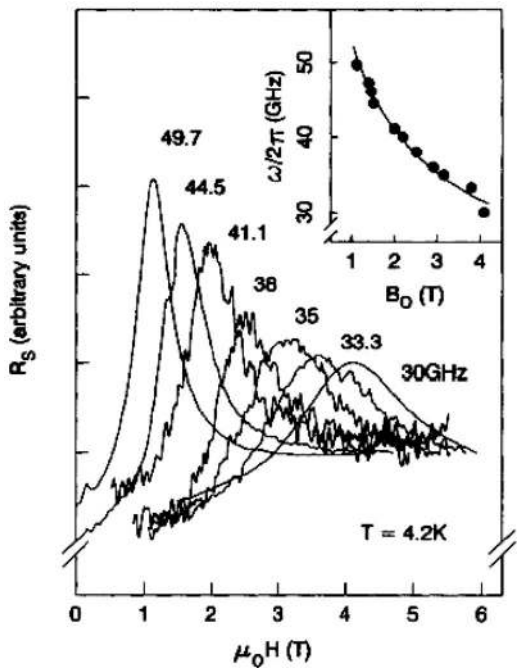

FIG. 40. A series of surface resistance traces vs field for a $Bi_2Sr_2CaCu_2O_{8+\delta}$ crystal for incident microwave frequency between 30 and 50 GHz at 4.2 K. The inset shows the frequency position of the resonance. Adapted from Tsui *et al.*, 1996.

explain these findings in terms of vortex motion leads to nonphysical assumptions for the relevant parameters (Orenstein *et al.*, 1997; Mallozzi *et al.*, 1998).

C. Interlayer response in high magnetic fields

1. Josephson plasmon in the regime of pancake vortices

Investigations of the systematic trends associated with the Josephson plasma resonance in cuprates have provided valuable insights into the nature of interlayer coupling in high-T_c superconductors. The first experimental study of the Josephson plasma resonance mode in magnetic fields was reported by Tsui *et al.* (1996). They explored the *c*-axis surface resistance R_s in the frequency range 30–50 GHz in the Bi-2212 system (Fig. 40). The Josephson plasma resonance mode was detected by sweeping the magnetic field while monitoring the impedance at a constant frequency. The resonance revealed asymmetric broadening at high magnetic fields. Matsuda *et al.* (1995) reproduced these experiments and through systematic analysis of both temperature and field dependence were able to show that the resonance in $R_s(H)$ traces is indeed related to Josephson coupling between the layers.

A comprehensive theoretical analysis of the electrodynamics associated with the field dependence of the Josephson plasma resonance mode has been carried out by Bulaevskii and collaborators (Bulaevskii, Maley, *et al.*, 1996; Bulaevskii, Pokrovsky, and Maley, 1996; Koshelev and Bulaevskii, 1999). Their theory accounts for key features of the data, including the field dependence of the resonance frequency and the asymmetric broadening of the resonance line. Deviations of the pancake vortices from straight lines in equilibrium induce a nonzero phase difference $\phi_{n,n+1}(\mathbf{r})$ between neighboring layers n and $n+1$ at coordinate $\mathbf{r}$. This phase difference suppresses the average interlayer Josephson energy and maximum possible interlayer superconducting current, $J_m = J_0\langle\cos\phi_{n,n+1}(\mathbf{r})\rangle$. Here J_0 is the parameter that characterizes the strength of the Josephson interlayer coupling. For $H=0$ the frequency of the Josephson plasma resonance mode ω_0 is determined by the magnitude of J_0. For a magnetic field this frequency is suppressed as $\omega_1^2(H,T) = \omega_0^2(T)\langle\cos\phi_{n,n+1}(\mathbf{r})\rangle$. This equation shows that no field depression of the Josephson plasma resonance frequency is expected, provided the vortex lattice is perfect. However, misalignment of the pancake vortices along the *c* axis produces a nonzero phase difference and can therefore be detected by monitoring the field dependence of ω_1. Moreover, random spatial variation of the Josephson coupling has been explicitly related to the high-field tail of the resonance when the Josephson plasma resonance mode is resolved in the regime of a sweeping field.

Analogously, the models of disordered vortex lattices can account for the asymmetric broadening of the JPR line at high energies in experiments which resolve the Josephson plasma resonance mode in the frequency domain (Koshelev and Bulaevskii, 1999). This aspect of the model made possible experimental probes of the pancake vortex lattice in CuO_2 planes through an examination of the Josephson plasma resonance. In less anisotropic superconductors such as Y-123, La-214, or Tl-2212 the Josephson plasma resonance mode falls in the THz and infrared range, permitting direct characterization of this feature in the frequency domain. Dulic *et al.* (2001) examined the impact of a weak magnetic field on this resonance in $YBa_2Cu_3O_{6.6}$ and Tl-2201 systems. The field dependence of the Josephson plasma resonance mode in these systems is consistent with the notion of a disordered lattice of pancake vortices. Similar results for Bi-2212 were reported by Shibauchi *et al.* (1999) and by Gaifullin *et al.* (2000a, 2000b) and for $Tl_2Ba_2CaCu_2O_{8+\delta}$ by Thorsmølle *et al.* (2002).

As pointed out in Sec. VII.I, additional plasma resonances were predicted and observed in systems having two different coupling constants between the CuO_2 layers. Naturally, the magnetic-field dependence of these modes is of interest. Pimenov *et al.* (2001) investigated the response of $SmLa_{1-x}Sr_xCuO_{4-d}$ crystals in magnetic fields up to 7 T ($H \| c$), using submillimeter spectroscopy (Fig. 41). Both longitudinal plasmons [$\nu_{1,K}$ resonances in $\mathrm{Im}(1/\epsilon^*)$ spectra] and the transverse plasmon (ν_T peak in σ_1 spectra) are softened in a magnetic field. The full experimental data set was successfully described using the multilayer model of van der Marel and Tsvetkov (2001). The magnetic-field dependence of the plasma frequencies contains the electronic structure of the superconducting CuO_2 layers, that is, their compressibility, which is difficult to obtain otherwise (Helm *et al.*, 2002). This opportunity is afforded because the dispersion of

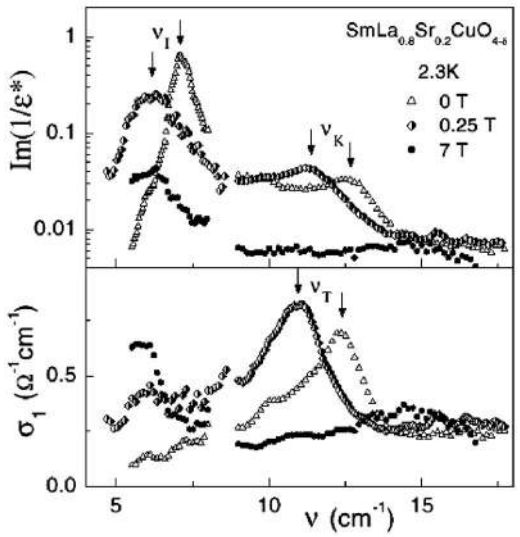

FIG. 41. Real part of the complex conductivity σ_1 and loss function $\mathrm{Im}(1/\epsilon^*)$ $SmLa_{0.8}Sr_{0.2}CuO_{4-\delta}$ along the c axis for different magnetic fields at 2.3 K. The transverse plasmon ν_T shows up as a peak in σ_1 and longitudinal plasmons $\nu_{1,K}$ show up as peaks in $\mathrm{Im}(1/\epsilon^*)$. Adapted from Pimenov *et al.*, 2001.

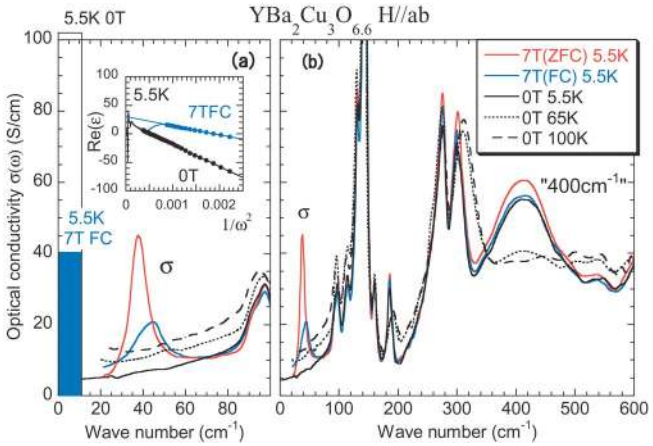

FIG. 42. (Color in online edition) Interlayer response of an underdoped $YBa_2Cu_3O_{6.6}$ crystal in a magnetic field: Panel (a): c-axis optical conductivity under a parallel field H_{ab}. The rectangles indicate the weight of low-energy condensate as derived from fitting by the function $\mathrm{Re}(\epsilon) \simeq \epsilon_\infty - \rho_s/\omega^2$ shown in the inset for 0 and 7 T (field-cooled) at 5.5 K. The solid circles in the inset indicate the data points used for the fitting. Panel (b): optical conductivity on a wider scale. Adapted from Kojima *et al.*, 2002.

the Josephson plasma resonances that is related to the magnitude of the electronic compressibility. Alternatively, the compressibility can be estimated based on the frequency position of the transverse plasmon using the formalism proposed by van der Marel and Tsvetkov (2001). Pimenov *et al.* (2001) and Helm *et al.* (2002) have inferred the values of compressibility $Kn^2 = 0.6 \pm 0.2\ \mathrm{eV}^{-1}$ per Cu atom using the data shown in Fig. 41. This value is close to the compressibility of a 2D noninteracting electron gas and also implies the effective mass $m_{\mathrm{eff}} = 0.95 m_e$.

To the best of our knowledge, there are no reports on experimental studies on the sum-rule anomalies of the c-axis response in magnetic fields at the time of writing. This problem has been addressed theoretically by Kim and Carbotte (2001a, 2001b).

2. Infrared probe of Josephson vortices

The first report of an infrared probe of the Josephson vortex state was that of Gerrits *et al.* (1995), who investigated the interlayer conductivity of single-crystal $La_{1.85}Sr_{0.15}CuO_4$ in magnetic fields up to 17.5 T. In the original publication, the authors reported virtually no dependence of the screened plasma frequency ω_{ps} on magnetic field, whereas the plasma edge had been considerably smeared in high fields. Subsequent reexamination of the data revealed a ~10% shift in the position of the plasma minimum (van Bentum *et al.*, 1995). More recently, the doping dependence of the plasma edge in the La-214 series was investigated (Dordevic *et al.*, 2003b, 2005b). These authors observed a fairly weak field-induced depression of the plasmon throughout most of the phase diagram. These results are consistent with either the TKT or the Bulaevskii models of vortex dynamics (Sec. IV.F). However, the impact of the 17-T field was anomalously strong near $x = 1/8$ doping, where the superconducting condensate has been found to be fragile beyond the predictions of vortex dynamics theories. Dordevic *et al.* (2003b, 2005b) proposed that this anomalous pair breaking may be related to the d-wave symmetry of the order parameter and to the overall suppression of the maximum energy gap near $x = 1/8$. This particular concentration corresponds to quasistatic stripe ordering in the La-214 system.

Entirely novel and unexpected effects in the Josephson vortex state have been discovered by Kojima *et al.* (2002), who studied interlayer electrodynamics of underdoped $YBa_2Cu_3O_{6.6}$ crystals. They found a strong suppression of the superfluid density in a 7-T field, as shown in the shaded area in Fig. 42. Moreover, when experiments were carried out in the field-cooled regime, a new mode centered at 40 cm^{-1} emerges (labeled as the σ mode in Fig. 42). The oscillator strength of the resonance at 400 cm^{-1}, often interpreted in terms of the transverse plasmon in bilayered systems (Sec. VII.I), shows mild enhancement in the magnetic field. The authors interpreted their results in terms of modulation of the interbilayer Josephson coupling strength by parallel magnetic fields. The redistribution of the optical spectral weight between the $\delta(0)$ peak and the σ mode is fully accounted for by such modulation within the framework of a model by van der Marel and Tsvetkov (1996). Interestingly, the 400-cm^{-1} mode fails to display the scaling expected within the multilayer model. Indeed, from Eqs. (26) and (27) one would expect the frequency position of this mode to be depressed when superfluid density in the $\delta(0)$ peak is reduced by external stimuli. Such a depression is not found in the data obtained by Kojima *et al.*

(2002), thus exposing problems inherent to assigning this resonance to the Josephson effect.

Bulaevskii *et al.* (1997) predicted an interesting effect pertinent to the Josephson plasma resonance in a parallel field. They found that the spectral weight in this case is distributed between the ac plasma mode and the dc sliding mode. Notably, the frequency of the plasma resonance increases with increasing field, whereas its oscillator strength is suppressed. This enigmatic effect has important implications for the determination of the critical current using ac probes. To the best of our knowledge, this effect has not been verified by experiments.

We conclude this subsection by pointing out yet another effect specific to the superfluid density depression in a superconductor with anisotropic order parameter. Yang and Sondhi (1998) emphasized the enhanced role of direct pair breaking due to the Zeeman effect in a superconductor with nodes in the gap function. Indeed, superconductivity is expected to be destroyed over parts of the Fermi surface where the Zeeman energy μH exceeds the local gap $\Delta(\mathbf{k})$. Therefore the Zeeman effect should be relevant to the behavior of many observables in high magnetic field, including $H_{c2}(T)$, the superfluid density, and the quasiparticle density. Won *et al.* (2000) have obtained expressions for the H dependence of both in-plane and c-axis superfluid densities. To the best of our knowledge, these predictions for $\mathbf{H}\|c$ have not been tested experimentally. Dordevic *et al.* (2003b, 2005) found that an expression by Won *et al.* (2000) for the superfluid density depression with $\mathbf{H}\perp c$ may account for anomalous effects in La-214 compounds.

D. The ac Hall effect

The normal state-Hall effect in high-T_c superconductors is notoriously difficult to understand. The Drude theory of metals predicts that the resistivity and the cotangent of the Hall angle, $\cot\Theta_H=\sigma_{xx}/\sigma_{xy}$, should reveal the same temperature dependence because both quantities are determined by the scattering rate of the charge carriers. Contrary to this expectation, the normal-state resistance of cuprate superconductors is linear with temperature (at least near optimal doping), whereas the Hall angle has a robust $\cot(\Theta_H)\propto T^2$ behavior (Chien *et al.*, 1991). Anderson (1991) has emphasized that the duality of the relaxation rate is intimately related to a breakdown of the simple quasiparticle picture in cuprates, which can be qualitatively explained within the spin-charge separation hypothesis. Analysis of both the temperature and frequency dependence of $\cot(\Theta_H)$ promises to deliver critical information on the nature of charge dynamics in cuprates.

To investigate magneto-optical activity, Drew and coworkers carried out measurements of far-IR transmission through $YBa_2Cu_3O_7$ films in the Faraday geometry with circular polarization of incident radiation (Kaplan *et al.*, 1996). In order to obtain optical constants, these authors employed KK analysis of transmission (solid circles and solid squares in Fig. 43). These early experiments found that the magneto-optical activity showed an approximately Drude-like behavior but with a smaller scattering rate than in the $H=0$ conductivity. Kaplan *et al.* (1996) described their data using a high-ω extension of the two-excitation model of Anderson (1991). According to this model, σ_{xx} has the ordinary form, $\propto\tau_{\rm tr}$, the decay time for holons scattering from thermally excited spinons. However, σ_{xy} depends on both $\tau_{\rm tr}$ and the scattering time of spinon excitations τ_H: $\sigma_{xy}\propto\tau_{\rm tr}\tau_H$. Furthermore, the decay rate for holons, $1/\tau_{\rm tr}$, depends on the number of thermally excited spinons and is therefore proportional to T, while the scattering rate for spinons, $1/\tau_H$, depends upon magnetic impurity and spinon-spinon scattering and evolves with temperature as $A+BT^2$. The two-excitation model yields the following equation for complex conductivity (Kaplan *et al.*, 1996):

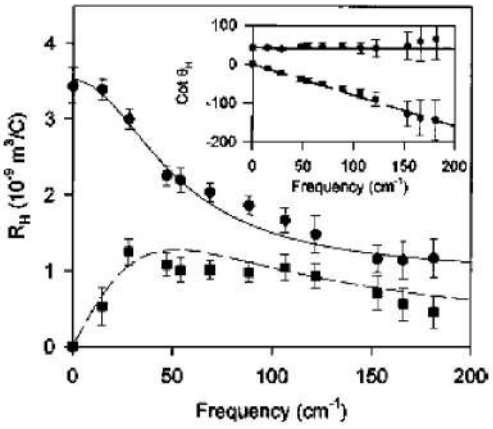

FIG. 43. Hall coefficient R_H vs frequency for thin-film $YBa_2Cu_3O_7$ on a Si substrate sample probed in the Faraday geometry at 95 K: ●, the real part of R_H derived from a Kramers-Kronig analysis of the transmission data in an 8.9-T magnetic field; ■, the imaginary part of the same R_H. The solid and dashed curves show the predicted values from fitting an expression derived by Hsu (1993) to the same data. Inset: Real (circles) and imaginary (squares) parts of cot Θ_H, along with the predictions of the theory by Hsu (1992) (solid and dashed lines). The real part is $1/\omega_c\tau_H$, and the slope of the imaginary part is $-1/\omega_c$. Adapted from Kaplan *et al.*, 1996.

$$\sigma_{\pm}=\frac{n_c e^2\tau_{\rm tr}}{m_{\rm tr}}\frac{1}{1-i\omega\tau_{\rm tr}}\left[1\pm\frac{i\omega_c\tau_H}{1-i\omega\tau_H}\right], \tag{30}$$

where n_c is the carrier density, $m_{\rm tr}$ is the transport mass, and $\omega_c=eH/m_Hc$ is the cyclotron frequency with mass m_H. In the limit of $\omega\to 0$ this expression reduces to Anderson's dc results, and in the case of $\tau_h=\tau_{\rm tr}$ it evolves into a simple Drude model. The form in Eq. (30), however, predicts a non-Drude form of the ac Hall signal, with a rolloff frequency given by $1/\tau_H$, distinct from the decay rate for transport currents. The dashed and solid lines in Fig. 43 were obtained by fitting both raw transmission and conductivity data. Notably, the real part of cot Θ_H (inset) is almost constant within the error bars, and the value of 40 for this quantity agrees well with the dc Hall angle data (Chien *et al.*, 1991). An important

outcome of this analysis is that it suggests the relevance of excitations with two distinct masses and two distinct relaxation times. Specifically, Drew *et al.* reported $m_H = (6 \pm 1) m_e \simeq (2-2.5) m_{\rm tr}$ and $\tau_H^{-1} = 60 \pm 15\ {\rm cm}^{-1} \simeq (0.25 \text{ to } -0.5)\tau_{\rm tr}^{-1}$. The temperature dependence of $1/\tau_H$ is consistent with T^n, $n \geqslant 2$ behavior in the temperature range between 95 and 140 K (Choi *et al.*, 1996; Drew *et al.*, 1996), which is in accord with the transport data. Subsequent work using refined experiments has provided support for these observations and has also yielded additional details of the frequency dependence (Cerne *et al.*, 2000). Specifically, the absolute value of $1/\tau_H$ was found to be independent of frequency between 10 and 100 meV, in contrast to the behavior of $1/\tau_{\rm tr}$.

Evidence for two relaxation times supports the spin-charge separation hypothesis (Anderson, 1991) and is at odds with the Fermi-liquid description of transport properties of cuprates (Abrahams, 1996; Coleman *et al.*, 1996). Alternatively, the effect can be understood within the Fermi-liquid framework if one assumes strong momentum dependence of scattering across the Fermi surface (Carrington *et al.*, 1992), as discussed in detail by Ioffe and Millis (1998) and by Zheleznyak *et al.* (1998). The rationale for this latter interpretation is provided by numerous experimental indications of long-lived nodal quasiparticles and enhanced scattering away from the zone diagonal regions (Stojkovic and Pines, 1996). Marginal Fermi-liquid theory attempts to explain the ac Hall data in terms of the momentum dependence of the self-energy (Abrahams and Varma, 2003).

Although experiments by Kaplan *et al.* (1996) indicate a difference between the transport and relaxation times, the ratio of $\tau_{\rm tr}/\tau_H$ was significantly lower than that estimated by Anderson (1991). Parks *et al.* (1997) revisited the issue through detailed studies of the ac Hall effect in $YBa_2Cu_3O_7$ using THz time-domain spectroscopy. They found that the absolute values of the Hall scattering rate were comparable to the transport scattering rate. This latter conclusion is corroborated by the most recent re-examination of the dynamical Hall effect by Grayson *et al.* (2002). The key outcome of the work of Parks *et al.* (1997) and Grayson *et al.* (2002) is that a single relaxation rate governs transport in the cuprates. Analysis of the temperature dependence of the ac Hall data provides strong support for models of the Hall effect in which the Hall scattering is linear in T. The frequency dependence of Θ_H in these most recent experiments by Grayson *et al.* (2002) is best described in terms of a squared Lorentzian form expected within the marginal Fermi-liquid theory (Varma and Abrahams, 2001; Varma *et al.*, 2002). The first measurements of the ac Hall effect on the underdoped samples reveals a dramatic increase of the Hall frequency ω_H, which is consistent with the idea of partial gapping of the Fermi surface (Rigal *et al.*, 2004). The essential aspect of the IR Hall data is the non-Drude frequency dependence observed by Kaplan *et al.* (1996) and substantiated by later experiments.

Drew and Coleman (1997) introduced the sum rule for $\tan\Theta_H = \sigma_{xy}(\omega)/\sigma_{xx}(\omega)$:

$$2\int \frac{d\omega}{\pi} t_H'(\omega) = \omega_H, \tag{31}$$

where $t'(\omega)$ is the real part of $\tan\theta_H$. The sum rule states that the Hall frequency ω_H is unaffected by interactions and in the absence of the lattice corresponds to the bare cyclotron frequency $\omega_c = eH/m$. The significance of this sum rule is that it puts analytical constraints on the frequency dependence of nondiagonal components of conductivity and also allows one to extract a wealth of information through analysis of the spectral weight in ac Hall experiments. Additional sum rules for the nondiagonal components of the conductivity tensor were discussed by Lange and Kotliar (1999).

X. SUMMARY AND OUTLOOK

The puzzle of high-T_c superconductivity is clearly one of the most challenging problems in contemporary physics. Progress in the field is largely driven by a methodical exploration of the properties of superconducting materials using a comprehensive set of experimental tools. Systematic studies of the electromagnetic response discussed in this review have resulted in major advances in our understanding of the underlying concepts and also have inspired innovative theoretical ideas put forward to explain the results. We briefly summarize below those results on the electrodynamics of high-T_c cuprates that have had a profound impact in the field.

- *Electronic structure.* Both the electronic structure and its modification in the process of doping with charge carriers are consistent with the behavior expected for doped Mott-Hubbard insulators. The mobile carriers in the conducting phases cannot be viewed as free electrons/holes but should be regarded as correlated "objects" whose properties are strongly influenced by Coulomb effects and possibly by antiferromagnetic fluctuations. An obvious challenge to any model is to explain the stark contrast between the in-plane and interplane properties of the cuprates, which goes beyond "strong anisotropy," since the two behaviors are qualitatively different. For example, the interplane transport is incoherent at the same time as in-plane properties are at least approximately described by the Drude model. Now that there is evidence for an intricate interconnection between the in-plane and interplane responses, any realistic description of a system must account for these relationships.
- *Charge dynamics.* Already in the early 1990s infrared spectroscopy produced unmistakable evidence for the strong coupling of the charge carriers to some form of magnetic excitations. This issue emerged as a focus of high-T_c research in the second half of the 1990s, when the whole arsenal of spectroscopic tools was applied to investigate electronic self-energy effects. These studies appear to reinforce the notion of coupling between conducting holes and magnetic fluctuations. It is worth pointing out in this context

that this conclusion is based entirely on theory developed to account for interaction of Fermi-liquid quasiparticles with phonons. Needless to say, many properties of cuprates invalidate the applicability of the Fermi-liquid theory and therefore conclusions drawn from strong-coupling analysis can be questioned.

- *Coherence and the pseudogap.* Spectroscopic evidence for the pseudogap state in the underdoped side of the phase diagram is overwhelming; most techniques provide a fairly consistent picture of this enigmatic state. However, IR experiments and ARPES or tunneling techniques do disagree in one important respect. ARPES and tunneling techniques indicate that coherence in the electronic system of underdoped cuprates is established only in the superconducting state, whereas IR methods provide evidence for coherence below the spin-gap temperature $T_s > T_c$. This distinction may be related to fundamental differences between various spectroscopies. Indeed, ARPES and tunneling techniques are believed to probe the single-particle Green's function, whereas IR methods study the complex conductivity. As of today, there is no unified view on the nature of the pseudogap state. None of the proposed scenarios, including preformed pairs, proximity to a quantum critical point, or formation of spin- and/or charge-density wave order are capable of accounting for the full body of experimental data.
- *d-wave symmetry of the order parameter.* Microwave studies of the penetration depth provided some of the earliest indications for a highly anisotropic order parameter with nodes (Hardy *et al.*, 1993). This hypothesis has been proven through direct phase-sensitive measurements (Kirtley *et al.*, 1995; Van Harlingen, 1995). The *d*-wave nature of the superconducting state defines many other characteristics of the cuprates, including the quasiparticle dynamics at low temperature, the nonlinear Meissner effect, and impurity-induced modifications of the low-frequency response.
- *Electronic inhomogeneities.* One difficulty standing in the way of a complete theoretical understanding of the normal-state charge dynamics and superfluid response is the intrinsic tendency of the cuprates to electronic phase separation on diverse length scales. Experimental studies of these effects face formidable technical challenges. In view of the progress achieved in adapting spectroscopic techniques for this task (Sec. VIII.D), it seems feasible to achieve a much more detailed understanding of the impact of inhomogeneities on the electronic transport and on collective effects in phase-segregated systems.
- *Vortex state.* The present experimental picture of this enigmatic state is incomplete, but existing results highlight a rather peculiar situation concerning the interpretation of the data. Spectroscopic experiments in magnetic fields are successfully described by two entirely different perspectives. In one approach it is assumed that gross features of the high-field data are associated with the dynamical properties of vortices, completely ignoring the impact of the *d*-wave order parameter. Another approach suggests that the vortex motion can be ignored, whereas the underlying physics can be understood in terms of nonlinear effects due to the *d*-wave nodes. Despite radically different starting premises, both approaches are able to predict subtle effects confirmed by experiments.
- *Some implications for the pairing mechanism.* The charge dynamics in the normal and superconducting states have been analyzed for Y-123 and Bi-2212 compounds. These analyses suggest that the scattering mechanisms are not due to phonons but are most likely related to the spin degree of freedom. Indirectly, this gives support for the notion of spin fluctuations as the mediator of superconducting pairing (Chubukov, Pines, and Schmalian, 2003). This particular pairing interaction gives rise to a *d*-wave order parameter (Scalapino, 1995). The non-BCS nature of the superconducting state is suggested by experiments indicating lowering of the electronic kinetic energy (Basov *et al.*, 1999; Molengraaf *et al.*, 2002).

ACKNOWLEDGMENTS

The authors are indebted to the many individuals who have contributed to the research discussed in this article. In particular we would like to emphasize the impact of our long-term collaborators: Yoichi Ando, G. Blumberg, D. A. Bonn, J. P. Carbotte, W. N. Hardy, C. C. Homes, R. Liang, and D. B. Tanner. Our special thanks to colleagues who have provided comments on sections of this review: L. N. Bulaevskii, K. S. Burch, S. V. Dordevic, H. D. Drew, T. Hogan, J. Orenstein, W. J. Padilla, and S. Tajima. We also benefited from discussions of many problems presented in this review with A. A. Abrikosov, P. B. Allen, W. Atkinson, A. Balatskii, A. J. Berlinski, A. Chubukov, J. C. Cooper, O. V. Dolgov, R. C. Dynes, V. J. Emery, M. Franz, J. Hirsch, J. Hwang, C. Kallin, S. A. Kivelson, P. A. Lee, A. G. Loeser, J. W. Loram, M. B. Maple, F. Marsiglio, A. J. Millis, M. Norman, M. Pham, D. Pines, J. Preston, Z.-X. Shen, T. Startseva, M. Strongin, M. Reedyk, T. Room, Y. Uemura, and D. van der Marel. The work at UCSD was supported by the U.S. Department of Energy, and the National Science Foundation. The work at McMaster was supported by the Canadian Institute of Advanced Research (CIAR) and Natural Sciences and Engineering Research Council of Canada.

REFERENCES

Abanov, A., and A. V. Chubukov, 2002, Phys. Rev. Lett. **88**, 217001.

Abanov, A., A. V. Chubukov, and J. Schmalian, 2001, Phys. Rev. B **63**, 180510(R).

Abel', E. V., V. S. Bagaev, D. N. Basov, O. V. Dolgov, A. F. Plotnikov, A. G. Poiarkov, and W. Sadovsky, 1991, Solid State Commun. **79**, 931.
Abo-Bakr, M., J. Feikes, K. Holldack, P. Kuske, W. B. Peatman, U. Schade, G. Wüstefeld, and H.-W. Hübers, 2003, Phys. Rev. Lett. **90**, 094801.
Abrahams, E., 1996, J. Phys. I **6**, 2191.
Abrahams, E., and C. M. Varma, 2003, Phys. Rev. B **68**, 094502.
Abrikosov, A. A., L. P. Gorkov, and I. E. Dzyaloshinski, 1975, *Methods of Quantum Field Theory in Statistical Physics* (Dover, New York).
Alexandrov, A. S., A. M. Bratkovky, N. F. Mott, and E. K. H. Salje, 1993, Physica C **215**, 359.
Alexandrov, A. S., V. V. Kabanov, and N. F. Mott, 1996, Phys. Rev. Lett. **77**, 4796.
Alff, L., S. Meyer, S. Kleefisch, U. Schoop, A. Marx, H. Sato, M. Naito, and R. Gross, 1999, Phys. Rev. Lett. **83**, 2644.
Allen, J. W., and J. C. Mikkelsen, 1976, Phys. Rev. B **15**, 2952.
Allen, P., 1992, Comments Condens. Matter Phys. **5-6**, 327.
Allen, P. B., 1971, Phys. Rev. B **3**, 305.
Ambrosch-Draxl, C., P. Süle, H. Auer, and E. Ya. Sherman, 2003, Phys. Rev. B **67**, 100505(R).
Amin, M. H. S., M. Franz, and I. Affleck, 2000, Phys. Rev. Lett. **84**, 5864.
Andersen, O. K., A. I. Liechtenstein, O. Jepsen, and F. Paulsen, 1995, J. Phys. Chem. Solids **56**, 1573.
Anderson, P. W., 1958, Phys. Rev. **109**, 1492.
Anderson, P. W., 1987, Science **51**, 1196.
Anderson, P. W., 1991, Phys. Rev. Lett. **67**, 2092.
Anderson, P. W., 1995, Science **286**, 1154.
Anderson, P. W., 1997, Phys. Rev. B **55**, 11785.
Anderson, P. W., 1998, *The Theory of Superconductivity in the High-T_c Cuprates* (Princeton University Press, Princeton, NJ).
Ando, T., A. B. Fowler, and F. Stern, 1982, Rev. Mod. Phys. **54**, 437.
Ando, Y., Y. Kurita, S. Komiya, S. Ono, and K. Segawa, 2004, Phys. Rev. Lett. **92**, 197001.
Ando, Y., A. N. Lavrov, Seiki Komiya, Kouji Segawa, and X. F. Sun, 2001, Phys. Rev. Lett. **87**, 017001.
Armitage, N. P., D. H. Lu, C. Kim, A. Damascelli, K. M. Shen, F. Ronning, D. L. Feng, P. Bogdanov, X. J. Zhou, W. L. Yang, Z. Hussain, P. K. Mang, N. Kaneko, M. Greven, Y. Onose, Y. Taguchi, Y. Tokura, and Z.-X. Shen, 2003, Phys. Rev. B **68**, 064517.
Atkinson, W. A., and J. P. Carbotte, 1995, Phys. Rev. B **52**, 10601.
Atkinson, W. A., and J. P. Carbotte, 1997, Phys. Rev. B **55**, 3230.
Atkinson, W. A., and P. J. Hirschfeld, 2002, Phys. Rev. Lett. **88**, 187003.
Atkinson, W. A., and A. H. MacDonald, 1999, Phys. Rev. B **60**, 9295.
Averitt, R. D., G. Rodriguez, A. I. Lobad, J. L. W. Siders, S. A. Trugman, and A. J. Taylor, 2001, Phys. Rev. B **63**, 140502(R).
Barabash, S. V., and D. Stroud, 2003, Phys. Rev. B **67**, 144506.
Barabash, S. V., D. Stroud, and I.-J. Hwang, 2000, Phys. Rev. B **61**, R14924.
Baraduc, C., A. El Azrak, and N. Bontemps, 1996, J. Supercond. **9**, 3.
Bardeen, J., L. N. Cooper, and J. R. Schrieffer, 1957, Phys. Rev. **108**, 1175.
Barowski, H. S., A. Arnold, R. Eder, M. Prenninger, A. Vogenauer, E. V. Pechen, K. F. Renk, W. Prusseit, H. Kinder, R. G. Buckley, D. M. Pooke, and K. Kishio, 1996, Proc. SPIE **2696**, 66.
Basov, D. N., B. Dabrowski, and T. Timusk, 1998, Phys. Rev. Lett. **81**, 2132.
Basov, D. N., S. V. Dordevic, E. J. Singley, W. J. Padilla, K. S. Burch, J. E. Elenewski, L. H. Greene, J. Morris, and R. Schickling, 2003, Rev. Sci. Instrum. **74**, 4703.
Basov, D. N., C. C. Homes, E. J. Singley, T. Timusk, M. Strongin, G. Blumberg, and D. van der Marel, 2001, Phys. Rev. B **63**, 134514.
Basov, D. N., R. Liang, D. A. Bonn, W. N. Hardy, B. Dabrowski, M. Quijada, D. B. Tanner, J. P. Rice, D. M. Ginsberg, and T. Timusk, 1995, Phys. Rev. Lett. **74**, 598.
Basov, D. N., R. Liang, B. Dabrowski, D. A. Bonn, W. N. Hardy, and T. Timusk, 1996, Phys. Rev. Lett. **77**, 4090.
Basov, D. N., H. A Mook, B. Dabrowski, and T. Timusk, 1995, Phys. Rev. B **52**, R13141.
Basov, D. N., E. J. Singley, and S. V. Dordevic, 2002, Phys. Rev. B **65**, 054516.
Basov, D. N., and T. Timusk, 2001, in *Handbook on the Physics and Chemistry of Rare Earths*, Vol. 31 (Elsevier Science, Amsterdam), p. 437.
Basov, D. N., T. Timusk, B. Dabrowski, and J. D. Jorgensen, 1994, Phys. Rev. B **50**, 3511.
Basov, D. N., S. I. Woods, A. S. Katz, E. J. Singley, R. C. Dynes, M. Xu, D. G. Hinks, C. C. Homes, and M. Strongin, 1999, Science **283**, 49.
Batlogg, B., and V. J. Emery, 1996, Nature (London) **382**, 20.
Batlogg, B., H. Y. Hwang, H. Takagi, R. J. Cava, H. L. Kao, and J. Kwo, 1994, Physica C **235**, 130.
Bednorz, J. G., and K. A. Müller, 1986, Z. Phys. B: Condens. Matter **64**, 189.
Benfatto, L., and C. M. Smith, 2003, Phys. Rev. B **68**, 184513.
Bernhard, C., R. Henn, A. Wittlin, M. Kläser, Th. Wolf, G. Müller-Vogt, C. T. Lin, and M. Cardona, 1998, Phys. Rev. Lett. **80**, 1762.
Bernhard, C., T. Holden, J. Humlícek, D. Munzar, A. Golnik, M. Kläser, Th. Wolf, L. Carr, C. Homes, B. Keimer, and M. Cardona, 2001, Solid State Commun. **121**, 93.
Bernhard, C., D. Munzar, A. Golnik, C. T. Lin, A. Wittlin, J. Humlícek, and M. Cardona, 2000, Phys. Rev. B **61**, 618.
Bernhard, C., D. Munzar, A. Wittlin, W. König, A. Golnik, C. T. Lin, M. Kläser, Th. Wolf, G. Müller-Vogt, and M. Cardona, 1999, Phys. Rev. B **59**, R6631.
Bidinosti, C. P., W. N. Hardy, D. A. Bonn, and R. Liang, 1999, Phys. Rev. Lett. **83**, 3277.
Birmingham, J. T., S. M. Grannan, P. L. Richards, R. Henn, J. Kircher, M. Cardona, A. Wittlin, V. H. M. Duijn, and A. A. Menovky, 1996, Proc. SPIE **2696**, 56.
Blumberg, G., and M. V. Klein, 1999, J. Low Temp. Phys. **117**, 1001.
Bonn, D. A., P. Dosanjh, R. Liang, and W. N. Hardy, 1992, Phys. Rev. Lett. **68**, 2390.
Bonn, D. A., J. D. Garrett, and T. Timusk, 1988, Phys. Rev. Lett. **61**, 1305.
Bonn, D. A., J. E. Greedan, C. V. Stager, and T. Timusk, 1987, Solid State Commun. **62**, 383.
Bonn, D. A., and W. N. Hardy, 1996, in *Physical Properties of High Temperature Superconductors I*, edited by D. M. Ginsberg (World Scientific, Singapore), p. 7.
Bonn, D. A., S. Kamal, K. Zhang, R. Liang, D. J. Baar, E. Klein, and W. N. Hardy, 1994, Phys. Rev. B **50**, 4051.

Bonn, D. A., R. Liang, T. M. Reisman, D. J. Baar, D. C. Morgan, K. Zhang, P. Dosanjh, T. L. Duty, A. MacFarlane, G. D. Morris, J. H. Brewer, W. N. Hardy, C. Kallin, and A. J. Berlinsky, 1993, Phys. Rev. B **47**, 11314.
Boris, A. V., N. N. Kovaleva, O. V. Dolgov, T. Holden, C. T. Lin, B. Keimer, and C. Bernhard, 2004, Science **304**, 708.
Boris, A. V., D. Munzar, N. N. Kovaleva, B. Liang, C. T. Lin, A. Dubroka, A. V. Pimenov, T. Holden, B. Keimer, Y.-L. Mathis, and C. Bernhard, 2002, Phys. Rev. Lett. **89**, 277001.
Borisenko, S. V., A. A. Kordyuk, S. Legner, T. K. Kim, M. Knupfer, C. M. Schneider, J. Fink, M. S. Golden, M. Sing, R. Claessen, A. Yaresko, H. Berger, C. Grazioli, and S. Turchini, 2004, Phys. Rev. B **69**, 224509.
Borkowski, L. S., and P. J. Hirschfeld, 1994, Phys. Rev. B **49**, 15404.
Bozovic, I., K. Char, S. J. B. Yoo, A. Kapitulnik, M. R. Beasley, T. H. Geballe, Z. Z. Wang, S. Hagen, N. P. Ong, D. E. Aspens, and M. K. Kelly, 1988, Phys. Rev. B **38**, 5077.
Bozovic, I., J. H. Kim, J. S. Harris, Jr., C. B. Eom, J. M. Phillips, and J. T. Cheung, 1994, Phys. Rev. Lett. **73**, 1436.
Brunel, L. C., S. G. Louie, G. Martinez, S. Labdi, and H. Raffy, 1991, Phys. Rev. Lett. **66**, 1346.
Bucher, B., J. Karpinski, E. Kaldis, and P. Wachter, 1992, Phys. Rev. B **45**, 3026.
Buhleier, R., S. D. Brorson, I. E. Trofimov, J. O. White, H.-U. Habermeier, and J. Kuhl, 1994, Phys. Rev. B **50**, 9672(R).
Bulaevskii, L. N., 1973, Sov. Phys. JETP **37**, 1133.
Bulaevskii, L. N., D. Dominguez, M. P. Maley, and A. R. Bishop, 1997, Phys. Rev. B **55**, 8482.
Bulaevskii, L. N., M. Maley, H. Safar, and D. Dominguez, 1996, Phys. Rev. B **53**, 6634.
Bulaevskii, L. N., V. L. Pokrovsky, and M. P. Maley, 1996, Phys. Rev. Lett. **76**, 1719.
Calvani, P., M. Capizzi, S. Lupi, P. Maselli, A. Paolone, and P. Roy, 1996, Phys. Rev. B **53**, 2756.
Cao, N., T. Timusk, and K. Bechgaard, 1996, J. Phys. I **6**, 1719.
Caprara, S., C. Di Castro, S. Fratini, and M. Grilli, 2002, Phys. Rev. Lett. **88**, 147001.
Carbotte, J. P., 1990, Rev. Mod. Phys. **62**, 1027.
Carbotte, J. P., D. N. Basov, and E. Schachinger, 1999, Nature (London) **401**, 354.
Carbotte, J. P., C. Jiang, D. N. Basov, and T. Timusk, 1995, Phys. Rev. B **51**, 11798.
Carr, G. L., M. C. Martin, W. R. McKinney, K. Jordan, G. R. Neil, and G. P. Williams, 2002, Nature (London) **420**, 153.
Carrington, A., R. W. Giannetta, J. T. Kim, and J. Giapinzakis, 1999, Phys. Rev. B **59**, R14173.
Carrington, A., A. P. Mackenzie, C. T. Lin, and J. R. Cooper, 1992, Phys. Rev. Lett. **69**, 2855.
Castellani, C., C. DiCastro, and M. Grilli, 1997, Z. Phys. B: Condens. Matter **103**, 137.
Cerne, J., M. Grayson, D. C. Schmadel, G. S. Jenkins, H. D. Drew, R. Hughes, A. Dabkowski, J. S. Preston, and P.-J. Kung, 2000, Phys. Rev. Lett. **84**, 3418.
Chakravarty, S., 1998, Eur. Phys. J. B **5**, 337.
Chakravarty, S., H.-Y. Kee, and E. Abrahams, 1999, Phys. Rev. Lett. **82**, 2366.
Chakravarty, S., S. P. Strong, and P. W. Anderson, 1994, Phys. Rev. Lett. **72**, 3218.
Chakravarty, S., A. Sudbo, P. W. Anderson, and S. P. Strong, 1993, Science **261**, 337.
Chernyshev, A. L., A. H. Castro Neto, and A. R. Bishop, 2000, Phys. Rev. Lett. **84**, 4922.
Chien, T. R., D. A. Brawner, Z. Z. Wang, and N. P. Ong, 1991, Phys. Rev. B **43**, R6242.
Choi, E.-J., H.-T. S. Lihn, H. D. Drew, and T. C. Hsu, 1994, Phys. Rev. B **49**, 13271.
Choi, E.-J., K. P. Stewart, S. K. Kaplan, H. D. Drew, S. N. Mao, and T. Venkatessan, 1996, Phys. Rev. B **53**, R8859.
Chuang, Y.-D., A. D. Gromko, A. Fedorov, Y. Aiura, K. Oka, Y. Ando, H. Eisaki, S. I. Uchida, and D. S. Dessau, 2001, Phys. Rev. Lett. **87**, 117002.
Chubukov, A. V., A. Abanov, and D. N. Basov, 2003, Phys. Rev. B **68**, 024504.
Chubukov, A. V., D. Pines, and J. Schmalian, 2003, in *The Physics of Superconductors*, edited by K. H. Bennemann and J. B. Ketterson (Springer, Berlin), Vol. 1, p. 495.
Clarke, D. G., S. P. Strong, and P. W. Anderson, 1995, Phys. Rev. Lett. **74**, 4499.
Coleman, P., A. J. Schofield, and A. M. Tsvelik, 1996, J. Phys.: Condens. Matter **9**, 345.
Collins, R. T., Z. Schlesinger, G. V. Chandrashekhar, and M. W. Shafer, 1989, Phys. Rev. B **39**, 2251.
Collins, R. T., Z. Schlesinger, F. Holtzberg, P. Chaudhari, and C. Feild, 1990, Phys. Rev. B **39**, 6571.
Cooper, J. R., L. Forro, and B. Keszei, 1989, Nature (London) **343**, 444.
Cooper, S. L., and K. E. Gray, 1994, in *Physical Properties of High-Temperature Superconductors IV*, edited by D. M. Ginsberg (World Scientific, Singapore), p. 61.
Cooper, S. L., A. L. Kotz, M. A. Karlow, M. V. Klein, W. C. Lee, J. Giapintzakis, and D. M. Ginsberg, 1992, Phys. Rev. B **45**, 2549.
Cooper, S. L., D. Reznik, A. L. Kotz, M. A. Karlow, R. Liu, M. V. Klein, W. C. Lee, J. Giapintzakis, D. M. Ginsberg, B. W. Veal, and A. P. Paulikas, 1993, Phys. Rev. B **47**, 8233.
Cooper, S. L., G. A. Thomas, J. Orenstein, D. H. Rapkine, A. J. Millis, S. W. Cheong, A. S. Cooper, and Z. Fisk, 1990, Phys. Rev. B **41**, 11605.
Corson, J., R. Mallozzi, J. Orenstein, J. N. Eckstein, and I. Bozovic, 1999, Nature (London) **398**, 221.
Corson, J., J. Orenstein, S. Oh, J. O'Donnell, and J. N. Eckstein, 2000, Phys. Rev. Lett. **85**, 2569.
Dagotto, E., 1994, Rev. Mod. Phys. **66**, 763.
Dahne, U., Y. Goncharov, N. Klein, N. Tellmann, G. Kozlov, and K. Urban, 1995, J. Supercond. **8**, 129.
Damascelli, A., Z. Hussain, and Z.-X. Shen, 2003, Rev. Mod. Phys. **68**, 473.
Degiorgi, L., 1999, Rev. Mod. Phys. **71**, 687.
Degiorgi, L., B. Alavi, G. Mihály, and G. Grüner, 1991, Phys. Rev. B **44**, 7808.
de Vaulchier, L. A., J. P. Vieren, Y. Guldner, N. Bontemps, R. Combescot, Y. Lemaitre, and J. C. Mage, 1996, Europhys. Lett. **33**, 153.
Devereaux, T. P., 2003, Phys. Rev. B **68**, 094503.
Dewing, H. L., and E. K. H. Salje, 1992, Supercond. Sci. Technol. **5**, 50.
Ding, H., M. Norman, T. Yokoya, T. Takeuchi, M. Randera, J. C. Campuzano, T. Takahashi, T. Mochiku, and K. Kadowaki, 1997, Phys. Rev. Lett. **78**, 2628.
Ding, H., T. Yokoya, J. C. Campuzano, T. Takahashi, M. Randeria, M. R. Norman, T. Mochiku, K. Kadowaki, and J. Giapintzakis, 1996, Nature (London) **382**, 51.
Dolgov, O. V., and S. V. Shulga, 1995, J. Supercond. **8**, 611.
Dordevic, S. V., D. N. Basov, N. R. Dilley, E. D. Bauer, and M. B. Maple, 2001, Phys. Rev. Lett. **86**, 684.

Dordevic, S. V., C. C. Homes, J. J. Tu, T. Valla, M. Strongin, P. D. Johnson, G. D. Gu, and D. N. Basov, 2005a, Phys. Rev. B **71**, 104529.
Dordevic, S. V., Seiki Komiya, Yoichi Ando, and D. N. Basov, 2003a, Phys. Rev. Lett. **91**, 167401.
Dordevic, S. V., Seiki Komiya, Yoichi Ando, Y. J. Wang, and D. N. Basov, 2003b, Europhys. Lett. **61**, 122.
Dordevic, S. V., Seiki Komiya, Yoichi Ando, Y. J. Wang, and D. N. Basov, 2005b, Phys. Rev. B **71**, 054503.
Dordevic, S. V., E. J. Singley, D. N. Basov, S. Komiya, Y. Ando, E. Bucher, C. C. Homes, and M. Strongin, 2002, Phys. Rev. B **65**, 134511.
Dordevic, S. V., E. J. Singley, J. H. Kim, M. B. Maple, S. Komiya, O. Shimpei, Y. Ando, T. Room, R. Liang, D. A. Bonn, W. N. Hardy, J. P. Carbotte, C. C. Homes, M. Strongin, and D. N. Basov, 2004, Phys. Rev. B **69**, 094511.
Dressel, M., and G. Grüner, 2002, *Electrodynamics of Solids: Optical Properties of Electrons in Matter* (Cambridge University, Cambridge, UK).
Drew, H. D., and P. Coleman, 1997, Phys. Rev. Lett. **78**, 1572.
Drew, H. D., and H. C. Hsu, 1995, Phys. Rev. B **52**, 9178.
Drew, H. D., S. Wu, and H.-T. S. Lihn, 1996, J. Phys.: Condens. Matter **8**, 10037.
Dulic, D., A. Pimenov, D. van der Marel, D. M. Broun, S. Kamal, W. N. Hardy, A. A. Tsvetkov, I. M. Sutjaha, R. Liang, A. A. Menovsky, A. Loidl, and S. S. Saxena, 2001, Phys. Rev. Lett. **86**, 4144.
Dumm, M., D. N. Basov, S. Komiya, Y. Abe, and Y. Ando, 2002, Phys. Rev. Lett. **88**, 147003.
Dumm, M., S. Komiya, Y. Ando, and D. N. Basov, 2003, Phys. Rev. Lett. **91**, 077004.
Eckl, T., W. Hanke, and E. Arrigoni, 2003, Phys. Rev. B **68**, 014505.
Eder, R., Y. Ohta, and S. Maekawa, 1995, Phys. Rev. B **51**, 3265.
El Azrak, A., R. Nahoum, N. Bontemps, M. Guilloux-Viry, C. Thivet, A. Perrin, S. Labdi, Z. Z. Li, and H. Raffy, 1994, Phys. Rev. B **49**, 9846.
Eldridge, J. E., M. Dressel, D. J. Matz, B. Gross, Q. Y. Ma, and W. N. Hardy, 1995, Phys. Rev. B **52**, 4462.
Emery, V. J., and S. A. Kivelson, 1993, Physica C **209**, 597.
Emery, V. J., and S. A. Kivelson, 1995a, Phys. Rev. Lett. **74**, 3253.
Emery, V. J., and S. A. Kivelson, 1995b, Nature (London) **374**, 434.
Emery, V. J., S. A. Kivelson, and O. Zachar, 1997, Phys. Rev. B **56**, 6120.
Falck, J. P., A. Levy, M. A. Kastner, and R. J. Birgeneau, 1992, Phys. Rev. Lett. **69**, 1109.
Farnworth, B., and T. Timusk, 1974, Phys. Rev. B **10**, 2799.
Fehrenbacher, R., and M. R. Norman, 1994, Phys. Rev. B **50**, 3495.
Feng, D. L., N. P. Armitage, D. H. Lu, A. Damascelli, J. P. Hu, P. Bogdanov, A. Lanzara, F. Ronning, K. M. Shen, H. Eisaki, C. Kim, Z.-X. Shen, J.-i. Shimoyama, and K. Kishio, 2001, Phys. Rev. Lett. **86**, 5550.
Ferrell, R. A., and R. E. Glover III, 1958, Phys. Rev. **109**, 1398.
Fleck, M., A. I. Lichtenstein, A. M. Oles, and L. Hedin, 1999, Phys. Rev. B **60**, 5224.
Forro, L., G. L. Carr, G. P. Williams, D. Mandrus, and L. Mihaly, 1990, Phys. Rev. Lett. **65**, 1941.
Friedmann, T. A., M. W. Rabin, J. Giapintzakis, J. P. Rice, and D. M. Ginsberg, 1990, Phys. Rev. B **42**, 6217.
Fudamoto, Y., S. Tajima, B. Gorshunov, M. Dressel, T. Kakeshita, K. M. Kojima, and S. Uchida, 2003, J. Low Temp. Phys. **131**, 761.
Fujimori, A., E. Takayama-Muromachi, Y. Uchida, and B. Okai, 1987, Phys. Rev. B **35**, 8814.
Gaifullin, M. B., Y. Matsuda, N. Chikumoto, J. Shimoyama, and K. Kishio, 2000a, Phys. Rev. Lett. **84**, 2945.
Gaifullin, M. B., Y. Matsuda, N. Chikumoto, J. Shimoyama, K. Kishio, R. Yoshizaki, J. Cerne, D. C. Schmadel, M. Grayson, G. S. Jenkins, J. R. Simpsaon, and H. D. Drew, 2000b, Phys. Rev. B **61**, 8133.
Gao, F., J. W. Kruse, C. E. Platt, M. Feng, and M. V. Klein, 1993, Appl. Phys. Lett. **63**, 2274.
Georges, A., G. Kotliar, W. Krauth, and M. J. Rozenberg, 1996, Rev. Mod. Phys. **68**, 13.
Gerrits, A. M., M. E. J. Boonman, A. Wittlin, P. J. M. van Bentum, V. H. M. Duijn, and A. A. Menovsky, 1995, Phys. Rev. B **51**, R12049.
Gerrits, A. M., T. J. B. M. Janssen, A. Wittlin, N. Y. Chen, and P. J. M. van Bentum, 1994, Physica C **235**, 1115.
Giamarchi, T., 1997, Physica B **230-232**, 975.
Gittleman, J. I., and B. Rosenblum, 1966, Phys. Rev. Lett. **16**, 734.
Glover, R. E., and M. Tinkham, 1956, Phys. Rev. **104**, 844.
Gold, A., S. J. Allen, B. A. Wilson, and D. C. Tsui, 1982, Phys. Rev. B **25**, 3519.
Gorshunov, B. P., A. V. Pronin, A. A. Volkov, H. S. Somal, D. van der Marel, B. J. Feenstra, Y. Jaccard, and J.-P. Locquet, 1998, Physica B **244**, 15.
Götze, W., 1981, Philos. Mag. B **43**, 219.
Graf, M. J., D. Rainer, and J. A. Sauls, 1995, Phys. Rev. B **47**, 12089.
Grayson, M., L. B. Rigal, D. C. Schmadel, H. D. Drew, and P.-J. Kung, 2002, Phys. Rev. Lett. **89**, 037003.
Grishkovky, D., S. Keiding, M. van Exter, and Ch. Fattinger, 1990, J. Opt. Soc. Am. A **7**, 2006.
Grüninger, M., 1999, Ph.D. thesis (University of Groningen).
Grüninger, M., J. Münzel, J. Gaymann, A. Zibold, and H. P. Geserich, 1996, Europhys. Lett. **35**, 55.
Grüninger, M., D. van der Marel, A. Damascelli, A. Erb, T. Nunner, and T. Kopp, 2000a, Phys. Rev. B **62**, 12422.
Grüninger, M., D. van der Marel, A. A. Tsvetkov, and A. Erb, 2000b, Phys. Rev. Lett. **84**, 1575.
Gunnarsson, O., M. Calandra, and J. E. Han, 2003, Rev. Mod. Phys. **75**, 1085.
Gurvitch, M., and A. T. Fiory, 1987, Phys. Rev. Lett. **59**, 1337.
Halterman, K., O. T. Valls, and I. Zutic, 2001, Phys. Rev. B **64**, 180405(R).
Hanaguri, T., T. C. Lupien, Y. Kohsaka, D.-H. Lee, M. Azuma, M. Takano, H. Takagi, and J. C. Davis, 2004, Nature (London) **430**, 1001.
Hardy, W. N., and D. A. Bonn, 1996, in *Physical Properties of High Temperature Superconductors V*, edited by D. M. Ginsberg (World Scientific, Singapore).
Hardy, W. N., D. A. Bonn, D. C. Morgan, R. Liang, and K. Zhang, 1993, Phys. Rev. Lett. **70**, 3999.
Hardy, W. N., S. Kamal, R. Liang, D. A. Bonn, C. C. Homes, D. N. Basov, and T. Timusk, 1996, in *Proceedings of the 10th Anniversary of High-T_c Workshop*, edited by B. Batlogg, C. W. Chu, W. K. Chu, D. U. Gubser, and K. A. Müller (World Scientific, Singapore), p. 263.
Haslinger, R., and A. V. Chubukov, 2003, Phys. Rev. B **67**, 140504(R).

Helm, Ch., L. N. Bulaevskii, E. M. Chudnovsky, and M. P. Maley, 2002, Phys. Rev. Lett. **89**, 057003.
Henn, R., J. Kircher, M. Cardona, A. Wittlin, V. H. M. Duijn, and A. A. Menovsky, 1996, Phys. Rev. B **53**, 9353.
Hildebrand, M. G., M. Reedyk, T. Katsufuji, and Y. Tokura, 2001, Phys. Rev. Lett. **87**, 227002.
Hirsch, J. E., 1992, Physica C **199**, 305.
Hirsch, J. E., 2002, Science **295**, 2226.
Hirschfeld, P. J., W. O. Putikka, and D. J. Scalapino, 1993, Phys. Rev. Lett. **71**, 3705.
Hirschfeld, P. J., W. O. Putikka, and D. J. Scalapino, 1994, Phys. Rev. B **50**, 10250.
Hirschfeld, P. J., S. M. Quinlan, and D. J. Scalapino, 1997, Phys. Rev. B **55**, 12742.
Hoffman, J. E., E. W. Hudson, K. M. Lang, V. Madhavan, H. Eisaki, S. Uchida, and J. C. Davis, 2002, Science **95**, 466.
Holcomb, M. J., J. P. Collman, and W. A. Little, 1994, Phys. Rev. Lett. **73**, 2360.
Homes, C. C., D. A. Bonn, R. Liang, W. N. Hardy, D. N. Basov, T. Timusk, and B. P. Clayman, 1999, Phys. Rev. B **60**, 9782.
Homes, C. C., B. P. Clayman, J. L. Peng, and R. L. Greene, 1997, Phys. Rev. B **56**, 5525.
Homes, C. C., S. V. Dordevic, M. Strongin, D. A. Bonn, R. Liang, W. N. Hardy, S. Koymia, Y. Ando, G. Yu, X. Zhao, M. Greven, D. N. Basov, and T. Timusk, 2004, Nature (London) **430**, 539.
Homes, C. C., M. A. Reedyk, D. A. Crandles, and T. Timusk, 1993, Appl. Opt. **32**, 2976.
Homes, C. C., T. Timusk, D. A. Bonn, R. Liang, and W. N. Hardy, 1993, Phys. Rev. Lett. **71**, 1645.
Homes, C. C., T. Timusk, D. A. Bonn, R. Liang, and W. N. Hardy, 1995a, Physica C **254**, 265.
Homes, C. C., T. Timusk, D. A. Bonn, R. Liang, and W. N. Hardy, 1995b, Can. J. Phys. **73**, 663.
Homes, C. C., J. M. Tranquada, Q. Li, A. R. Moodenbaugh, and D. J. Buttrey, 2003, Phys. Rev. B **67**, 184516.
Hosseini, A., D. M. Broun, D. E. Sheehy, T. P. Davis, M. Franz, W. N. Hardy, Ruixing Liang, and D. A. Bonn, 2004, Phys. Rev. Lett. **93**, 107003.
Hosseini, A., R. Harris, S. Kamal, P. Dosanjh, J. Preston, R. Liang, W. N. Hardy, and D. A. Bonn, 1999, Phys. Rev. B **60**, 1349.
Hosseini, A., S. Kamal, D. A. Bonn, R. Liang, and W. N. Hardy, 1998, Phys. Rev. Lett. **81**, 1298.
Hsu, T. C., 1992, Phys. Rev. B **46**, 3680.
Hsu, T. C., 1993, Physica C **213**, 305.
Hussey, N. E., K. Takenaka, and H. Takagi, 2004, Philos. Mag. **84**, 2847.
Hwang, J., T. Timusk, and G. D. Gu, 2004, Nature (London) **427**, 714.
Hwang, J., T. Timusk, A. V. Puchkov, N. L. Wang, G. D. Gu, C. C. Homes, J. J. Tu, and H. Eisaki, 2004, Phys. Rev. B **69**, 094520.
Imada, M., A. Fujimori, and Y. Tokura, 1998, Rev. Mod. Phys. **70**, 1039.
Ioffe, L. B., A. I. Larkin, A. A. Varlamov, and L. Yu, 1993, Phys. Rev. B **47**, 8936.
Ioffe, L. B., and A. J. Millis, 1998, Phys. Rev. B **58**, 11631.
Ioffe, L. B., and A. J. Millis, 1999, Science **285**, 1241.
Ito, T., K. Takenaka, and S. Uchida, 1993, Phys. Rev. Lett. **70**, 3995.
Iyengar, A., J. Stajic, Ying-Jer Kao, and K. Levin, 2003, Phys. Rev. Lett. **90**, 187003.
Jacobs, T., S. Sridhar, Q. Li, G. D. Gu, and N. Koshizuka, 1995, Phys. Rev. Lett. **75**, 4516.
Jacobsen, C. S., D. B. Tanner, and K. Bechgaard, 1981, Phys. Rev. Lett. **46**, 1142.
Jaklic, J., and P. Prelovsek, 2000, Adv. Phys. **49**, 1.
Jang, H. F., G. Cripps, and T. Timusk, 1990, Phys. Rev. B **41**, 5152.
Jarrel, M., J. K. Freericks, and Th. Pruschke, 1995, Phys. Rev. B **51**, 11704.
Johnson, P. D., T. Valla, A. V. Fedorov, Z. Yusof, B. O. Wells, Q. Li, A. R. Moodenbaugh, G. D. Gu, N. Koshizuka, C. Kendziora, S. Jian, and D. G. Hinks, 2001, Phys. Rev. Lett. **87**, 177007.
Joyce, R. R., and P. L. Richards, 1970, Phys. Rev. Lett. **24**, 1007.
Julien, M.-H., 2003, Physica B **329**, 693.
Julien, M.-H., P. Caretta, M. Horovatić, C. Berthier, Y. Berthier, P. Ségransan, A. Carrington, and D. Colson, 1996, Phys. Rev. Lett. **76**, 4238.
Kajueter, H., G. Kotliar, and G. Moeller, 1996, Phys. Rev. B **53**, 16214.
Kakeshita, T., S. Uchida, K. M. Kojima, S. Adachi, S. Tajima, B. Gorshunov, and M. Dressel, 2001, Phys. Rev. Lett. **86**, 4140.
Kamaras, K., S. L. Herr, C. D. Porter, N. Tache, D. B. Tanner, S. Etemad, T. Venakatesan, E. Chase, A. Inam, X. D. Wu, M. S. Hegde, and B. Dutta, 1990, Phys. Rev. Lett. **64**, 84.
Kaminski, A., J. Mesot, H. Fretwell, J. C. Campuzano, M. R. Norman, M. Randeria, H. Ding, T. Sato, T. Takahashi, T. Mochiku, K. Kadowaki, and H. Hoechst, 2000, Phys. Rev. Lett. **84**, 1788.
Kane, C. L., P. A. Lee, and N. Read, 1989, Phys. Rev. B **39**, 6880.
Kaplan, S. G., S. Wu, H.-T. S. Lihn, H. D. Drew, Q. Li, D. B. Fenner, J. M. Phillips, and S. Y. Hou, 1996, Phys. Rev. Lett. **76**, 696.
Karrai, K., E. Choi, F. Dunmore, S. Liu, X. Xingg, Qi Li, T. Venkatesan, and H. D. Drew, 1992, Phys. Rev. Lett. **69**, 355.
Katsufuji, T., M. Kasai, and Y. Tokura, 1996, Phys. Rev. Lett. **76**, 126.
Katz, A. S., S. I. Woods, E. J. Singley, T. W. Li, M. Xu, D. G. Hinks, R. C. Dynes, and D. N. Basov, 2000, Phys. Rev. B **61**, 5930.
Kendziora, C., M. C. Martin, L. Forro, D. Mandrus, and L. Mihaly, 1997, Phys. Rev. Lett. **79**, 4935.
Kim, M.-S., J. A. Skinta, T. R. Lemberger, A. Tsukada, and M. Naito, 2003, Phys. Rev. Lett. **91**, 087001.
Kim, W., and J. P. Carbotte, 2000, Phys. Rev. B **61**, R11886.
Kim, W., and J. P. Carbotte, 2001a, Phys. Rev. B **63**, 140505(R).
Kim, W., and J. P. Carbotte, 2001b, Phys. Rev. B **64**, 104501.
Kimura, H., K. Hirota, H. Matsushita, K. Yamada, Y. Endoh, S-H. Lee, C. F. Majkrzak, R. Erwin, G. Shirane, M. Greven, Y. S. Lee, M. A. Kastner, and R. J. Birgeneau, 1999, Phys. Rev. B **59**, 6517.
Kircher, J., R. Henn, M. Cardona, P. L. Richards, and G. R. Williams, 1997, J. Opt. Soc. Am. B **14**, 705.
Kirtley, J. R., K. A. Moler, G. Villard, and A. Maignan, 1998, Phys. Rev. Lett. **81**, 2140.
Kirtley, J. R., C. C. Tsuei, J. Z. Sun, C. C. Chi, L. S. Yu-Jahnes, A. Gupta, M. Rupp, and M. B. Ketchen, 1995, Nature (London) **373**, 225.

Kivelson, S. A., E. Fradkin, and V. J. Emery, 1998, Nature (London) **393**, 550.
Kivelson, S. A., E. Fradkin, V. Oganesyan, I. P. Bindloss, J. M. Tranquada, A. Kapitulnik, and C. Howald, 2003, Rev. Mod. Phys. **75**, 1201.
Kohn, W., 1961, Phys. Rev. **123**, 1242.
Kojima, K. M., S. Uchida, Y. Fudamoto, and S. Tajima, 2002, Phys. Rev. Lett. **89**, 247001.
Kokales, J. D., P. Fournier, L. V. Mercaldo, V. V. Talanov, R. L. Greene, and S. M Anlage, 2000, Phys. Rev. Lett. **85**, 3696.
Kopnin, N. B., 1998, Phys. Rev. B **57**, 11775.
Kopnin, N. B., and V. M. Vinokur, 2001, Phys. Rev. Lett. **87**, 017003.
Koshelev, A. E., and L. N. Bulaevskii, 1999, Phys. Rev. B **60**, R3743.
Kovaleva, N. N., A. V. Boris, D. Munzar, T. Holden, C. Ulrich, J. L. Tallon, B. Liang, C. T. Lin, A. M. Stoneham, B. Keimer, and C. Bernhard, 2004, Phys. Rev. B **69**, 054511.
Kozlov, G., and A. Volkov, 1998, in *Millimeter and Submillimeter Wave Spectroscopy of Solids*, edited by G. Grüner (Springer, New York), p. 51.
Krasnov, V. M., A. Yurgens, D. Winkler, P. Delsing, and T. Claeson, 2000, Phys. Rev. Lett. **84**, 5860.
Kresin, V. Z., and S. A. Wolf, 1992, Phys. Rev. B **46**, 6458.
Kumar, N., P. A. Lee, and B. Shapiro, 1990, Physica A **168**, 447.
Kuzmenko, A. B., H. J. A. Molegraaf, F. Carbone, and D. van der Marel, 2005, e-print cond-mat/0503768.
Kuzmenko, A. B., N. Tombros, H. J. A. Molegraaf, M. Grüninger, D. van der Marel, and S. Uchida, 2003, Phys. Rev. Lett. **91**, 037004.
Lake, B., G. Aeppli, K. N. Clausen, D. F. McMorrow, K. Lefmann, N. E. Hussey, N. Mangkorntong, M. Nohara, H. Takagi, T. E. Mason, and A. Schröder, 2001, Science **291**, 1759.
Lange, E., and G. Kotliar, 1999, Phys. Rev. Lett. **82**, 1317.
Latyshev, Yu. I., T. Yamashita, L. N. Bulaevskii, M. J. Graf, A. V. Balatsky, and M. P. Maley, 1999, Phys. Rev. Lett. **82**, 5345.
Lawrence, W. E., and S. Doniach, 1971, in *Proceedings of the 12th International Conference on Low Temperature Physics*, edited by E. Kanda (Academic Press, Kyoto), p. 361.
Lee, P. A., 1993, Phys. Rev. Lett. **71**, 1887.
Lee, P. A., 2005, private communication.
Lee, Y. S., K. Segawa, Y. Ando, and D. N. Basov, 2004, Phys. Rev. B **70**, 014518.
Lee, Y. S., K. Segawa, Y. Ando, and D. N. Basov, 2005a, Phys. Rev. Lett. **94**, 137004.
Lee, Y. S., K. Segawa, Y. Ando, and D. N. Basov, 2005b, Phys. Rev. B (to be published).
Leggett, A. J., 1996, Science **274**, 587.
Leplae, L., 1983, Phys. Rev. B **27**, 1911.
Li, M.-R., P. J. Hirschfeld, and P. Wölfle, 1998, Phys. Rev. Lett. **81**, 5640.
Liechtenstein, A. I., O. Gunnarsson, O. K. Andersen, and R. M. Martin, 1996, Phys. Rev. B **54**, 12505.
Lihn, H.-T. S., and H. D. Drew, 1997, Phys. Rev. B **56**, 5559.
Lihn, H.-T., S. Wu, H. D. Drew, S. Kaplan, Q. Li, and D. B. Fenner, 1996, Phys. Rev. Lett. **76**, 3810.
Littlewood, P. B., and C. M. Varma, 1991, J. Appl. Phys. **69**, 4979.
Litvinchuk, A. P., C. Thomsen, and M. Cardona, 1994, in *Physical Properties of High Temperature Superconductors IV*, edited by D. M. Ginsberg (World Scientific, Singapore), p. 375.
Liu, H. L., M. A. Quijada, A. M. Zibold, Y.-D. Yoon, D. B. Tanner, G. Cao, J. E. Crow, H. Berger, G. Margaritondo, L. Forro, K. Beom-Hoan, J. T. Markert, R. J. Kelly, and M. Onellion, 1999, J. Phys.: Condens. Matter **11**, 239.
Liu, H. L., A. Zibold, D. B. Tanner, Y. J. Wang, M. J. Burns, K. A. Delin, M. Y. Li, and M. K. Wu, 1998, Solid State Commun. **109**, 7.
Lobo, R. P. S. M., F. J. Gotor, P. Odier, and F. Gervais, 1996, Phys. Rev. B **53**, 410.
Lobo, R. P. S. M., E. Ya. Sherman, D. Racah, Y. Dagan, and N. Bontemps, 2002, Phys. Rev. B **65**, 104509.
Loeser, A. G., Z.-X. Shen, D. S. Dessau, D. S. Marshall, C. H. Park, P. Fournier, and A. Kapitulnik, 1996, Science **273**, 325.
Loram, J. W., J. Luo, J. R. Cooper, W. Y. Liang, and J. L. Tallon, 2001, J. Phys. Chem. Solids **62**, 59.
Lorenzana, J., and G. A. Sawatzky, 1995, Phys. Rev. Lett. **74**, 1867.
Lorenzana, J., and G. Seibold, 2003, Phys. Rev. Lett. **90**, 066404.
Lupi, S., P. Calvani, M. Capizzi, P. Maselli, W. Sadowski, and E. Walker, 1992, Phys. Rev. B **45**, 12470.
Ma, Z., 1995, Ph.D. thesis (Stanford University).
Maeda, A., Y. Iino, T. Hanaguri, N. Motohira, K. Kishio, and T. Fukase, 1995, Phys. Rev. Lett. **74**, 1202.
Mallozzi, R., J. Orenstein, J. N. Eckstein, and I. Bozovic, 1998, Phys. Rev. Lett. **81**, 1485.
Mandrus, D., M. C. Martin, C. Kendziora, D. Koller, L. Forro, and L. Mihaly, 1993, Phys. Rev. Lett. **70**, 2629.
Mao, J., D. H. Wu, J. L. Peng, R. L. Greene, and S. Anlage, 1995, Phys. Rev. B **51**, R3316.
Marshall, D. S., D. S. Dessau, A. G. Loeser, C. H. Park, Z.-X. Shen, A. Y. Matsuura, J. N. Eckstein, I. Bozovik, P. Fornier, A. Kapitulnik, W. E. Spicer, and Z.-X. Shen, 1996, Phys. Rev. Lett. **76**, 4841.
Marsiglio, F., 1998, Phys. Lett. A **245**, 172.
Massidda, S., J. Yu, and A. J. Freeman, 1988, Physica C **152**, 251.
Matsuda, Y., M. B. Gaifullin, K. Kumagai, K. Kadowaki, and T. Mochiku, 1995, Phys. Rev. Lett. **75**, 4512.
Matsuda, M., S. Katano, T. Uefuji, M. Fujita, and K. Yamada, 2002, Phys. Rev. B **66**, 172509.
Mattis, D. C., and J. Bardeen, 1958, Phys. Rev. **111**, 412.
Mazin, I. I., S. N. Rashkeev, A. I. Liechtenstein, and O. K. Andersen, 1992, Phys. Rev. B **46**, R11232.
McGuire, J. J., M. Windt, T. Startseva, T. Timusk, D. Colson, and V. Viallet-Guillen, 2000, Phys. Rev. B **62**, 8711.
Millis, A. J., and H. D. Drew, 2003, Phys. Rev. B **67**, 214517.
Millis, A. J., H. Monien, and D. Pines, 1990, Phys. Rev. B **42**, 167.
Millis, A. J., S. Sachdev, and C. M. Varma, 1988, Phys. Rev. B **37**, 4975.
Mitrovic, V. F., E. E. Sigmund, M. Eschrig, H. N. Bachman, W. P. Halperin, A. P. Reyes, P. Kuhns, and W. G. Moulton, 2001, Nature (London) **413**, 501.
Molegraaf, H. J. A., C. Presura, D. van der Marel, P. H. Kes, and M. Li, 2002, Science **295**, 2239.
Moler, K. A., J. R. Kirtley, D. G. Hinks, T. W. Li, and M. Xu, 1998, Science **279**, 1193.
Monthoux, P., and D. Pines, 1993, Phys. Rev. B **47**, 6069.
Monthoux, P., and D. Pines, 1994a, Phys. Rev. B **49**, 4261.
Monthoux, P., and D. Pines, 1994b, Phys. Rev. B **50**, 16015.

Mori, H., 1965, Prog. Theor. Phys. **34**, 399.
Morr, D. K., and A. V. Balatsky, 2001, Phys. Rev. Lett. **87**, 247002.
Munzar, D., C. Bernhard, and M. Cardona, 1999a, Physica C **312**, 121.
Munzar, D., C. Bernhard, A. Golnik, J. Humlicek, and M. Cardona, 1999b, Solid State Commun. **112**, 365.
Munzar, D., C. Bernhard, T. Holden, A. Golnik, J. Humilíček, and M. Cardona, 2001, Phys. Rev. B **64**, 024523.
Munzar, D., T. Holden, and C. Bernhard, 2003, Phys. Rev. B **67**, 020501.
Nachumi, B., A. Keren, K. Kojima, M. Larkin, G. M. Luke, J. Merrin, O. Tchernyshov, Y. J. Uemura, N. Ichikawa, M. Goto, and S. Uchida, 1996, Phys. Rev. Lett. **77**, 5421.
Naeini, J. G., X. K. Chen, K. C. Hewitt, J. C. Irwin, T. P. Devereaux, M. Okuya, T. Kimura, and K. Kishio, 1998, Phys. Rev. B **57**, R11077.
Nakamura, Y., and S. Uchida, 1993, Phys. Rev. B **47**, R8369.
Nemetschek, R., M. Opel, C. Hoffmann, P. F. Müller, R. Hackl, H. Berger, L. Forró, A. Erb, and E. Walker, 1997, Phys. Rev. Lett. **78**, 4837.
Ng, H. K., M. Capizzi, G. A. Thomas, R. N. Bhatt, and A. C. Gossard, 1986, Phys. Rev. B **33**, 7329.
Nicol, E. J., J. P. Carbotte, and T. Timusk, 1991, Phys. Rev. B **43**, 473.
Noh, T., W. S. G. Kaplan, and A. J. Sievers, 1989, Phys. Rev. Lett. **62**, 599.
Norman, M. R., and H. Ding, 1998, Phys. Rev. B **57**, 11089.
Norman, M. R., and C. Pepin, 2000, Phys. Rev. B **66**, 100506(R).
Norman, M. R., M. Randeria, B. Janko, and J. C. Campuzano, 2000, Phys. Rev. B **61**, 14742.
Nuss, M. C., P. M. Mankiewich, M. L. O'Malley, E. H. Westerwick, and P. B. Littlewood, 1991, Phys. Rev. Lett. **66**, 3305.
Nyhus, P., M. A. Karlow, S. L. Cooper, B. Veal, and A. P. Paulikas, 1994, Phys. Rev. B **50**, R13898.
Ohashi, Y., 2000, J. Phys. Soc. Jpn. **69**, 659.
Onose, Y., Y. Taguchi, K. Ishizaka, and Y. Tokura, 2001, Phys. Rev. Lett. **87**, 217001.
Opel, M., R. Nemetschek, C. Hoffmann, R. Philipp, P. F. Müller, R. Hackl, I. Tüttö, A. Erb, B. Revaz, E. Walker, H. Berger, and L. Forró, 2000, Phys. Rev. B **61**, 9752.
Orenstein, J., 1990, in *Electronic Properties of High-T_c Superconductors*, edited by H. Kuzmany (Springer, Berlin), p. 254.
Orenstein, J., 2003, Physica C **390**, 243.
Orenstein, J., J. Bokor, E. Budiarto, J. Corson, R. Mallozzi, I. Bozovic, and J. N. Eckstein, 1997, Physica C **282**, 252.
Orenstein, J., and D. H. Rapkine, 1988, Phys. Rev. Lett. **60**, 968.
Orenstein, J., G. A. Thomas, A. J. Millis, S. L. Cooper, D. Rapkine, T. Timusk, L. F. Schneemeyer, and J. V. Waszczak, 1990, Phys. Rev. B **42**, 6342.
Osafune, T., N. Motoyama, H. Eisaki, S. Uchida, and S. Tajima, 1999, Phys. Rev. Lett. **82**, 1313.
Padilla, W. J., Y. S. Lee, M. Dumm, S. Komiya, Y. Ando, and D. N. Basov, 2005a, e-print cond-mat/0505094.
Padilla, W. J., Y. S. Lee, M. Dumm, S. Komiya, Y. Ando, and D. N. Basov, 2005b, unpublished.
Palumbo, M., and M. J. Graf, 1996, Phys. Rev. B **53**, 2261.
Pan, S. H., J. P. O'Neal, R. L. Badzey, C. Chamon, H. Ding, J. R. Engelbrecht, Z. Wang, H. Eisaki, S. Uchida, A. K. Gupta, K.-W. Ng, E. W. Hudson, K. M. Lang, and J. C. Davis, 2001, Nature (London) **413**, 282.
Panagopoulos, C., J. R. Cooper, T. Xiang, G. B. Peacock, I. Gameson, and P. P. Edwards, 1997, Phys. Rev. Lett. **79**, 2320.
Panagopoulos, C., A. P. Petrovic, A. D. Hillier, J. L. Tallon, C. A. Scott, and B. D. Rainford, 2004, Phys. Rev. B **69**, 144510.
Paramekanti, A., M. Randeria, and N. Trivedi, 2001, Phys. Rev. Lett. **87**, 217002.
Parks, B., S. Spielman, and J. Orenstein, 1997, Phys. Rev. B **56**, 115.
Parks, B., S. Spielman, J. Orenstein, D. T. Nemeth, F. Ludwig, J. Clarke, P. Merchant, and D. J. Lew, 1995, Phys. Rev. Lett. **74**, 3265.
Pereg-Barnea T., P. J. Turner, R. Harris, G. K. Mullins, J. S. Bobowski, M. Raudsepp, R. Liang, D. A. Bonn, and W. N. Hardy, 2004, Phys. Rev. B **69**, 184513.
Perkins, J. D., D. S. Kleinberg, M. A. Kastner, R. J. Birgebeau, Y. Endoh, K. Yamada, and S. Hosoya, 1995, Phys. Rev. B **52**, R9863.
Perkins, J. D., J. M. Graybeal, M. A. Kastner, R. J. Birgeneau, J. P. Falck, and M. Greven, 1993, Phys. Rev. Lett. **71**, 1621.
Pham, T., M. W. Lee, H. D. Drew, U. Welp, and Y. Fang, 1991, Phys. Rev. B **44**, 5377.
Pickett, W. E., 1989, Rev. Mod. Phys. **61**, 433.
Pickett, W. E., H. Krakauer, R. E. Cohen, and D. J. Singh, 1992, Science **255**, 46.
Pimenov, A., A. Loidl, D. Dulic, D. van der Marel, I. M. Sutjahja, and A. A. Menovsky, 2001, Phys. Rev. Lett. **87**, 177003.
Pimenov, A., A. Loidl, G. Jakob, and H. Adrian, 1999, Phys. Rev. B **59**, 4390.
Pimenov, A., A. V. Pronin, A. Loidl, A. Tsukada, and M. Naito, 2002, Phys. Rev. B **66**, 212508.
Pimenov, A., A. V. Pronin, A. Loidl, A. Tsukada, and M. Naito, 2003, Europhys. Lett. **64**, 246.
Pines, D., and P. Nozières, 1996, *The Theory of Quantum Liquids* (Benjamin, New York).
Pippard, A. B., 1953, Proc. R. Soc. London, Ser. A **216**, 547.
Preosti, G., H. Kim, and P. Muzikar, 1994a, Phys. Rev. B **50**, 1259.
Preosti, G., H. Kim, and P. Muzikar, 1994b, Phys. Rev. B **50**, 13638.
Presland, M. R., J. L. Tallon, R. G. Buckley, R. S. Liu, and N. E. Flower, 1991, Physica C **176**, 95.
Prohammer, M., and J. P. Carbotte, 1991, Phys. Rev. B **43**, 5370.
Pronin, A. V., M. Dressel, A. Pimenov, A. Loidl, I. V. Roshchin, and L. H. Greene, 1998, Phys. Rev. B **57**, 14416.
Pronin, A. V., A. Pimenov, A. Loidl, A. Tsukada, and M. Naito, 2003, Phys. Rev. B **68**, 054511.
Prozorov, R., R. W. Giannetta, P. Fournier, and R. L. Greene, 2000, Phys. Rev. Lett. **85**, 3700.
Puchkov, A. V., D. N. Basov, and T. Timusk, 1996, J. Phys.: Condens. Matter **8**, 10049.
Puchkov, A. V., P. Fournier, T. Timusk, and N. N. Kolesnikov, 1996, Phys. Rev. Lett. **77**, 1853.
Puchkov, A. V., T. Timusk, S. Doyle, and A. M. Herman, 1995, Phys. Rev. B **51**, 3312.
Quijada, M. A., D. B. Tanner, F. C. Chou, D. C. Johnston, and S. W. Cheong, 1995, Phys. Rev. B **52**, 15485.
Quijada, M. A., D. B. Tanner, R. J. Kelley, M. Onellion, H. Berger, and G. Margaritondo, 1999, Phys. Rev. B **60**, 14917.
Quinlan, S. M., P. J. Hirschfeld, and D. J. Scalapino, 1996, Phys. Rev. B **53**, 8575.
Quinlan, S. M., D. J. Scalapino, and N. Bulut, 1994, Phys. Rev. B **49**, 1470.

Radtke, R. J., K. Levin, H.-B. Shuttler, and M. R. Norman, 1993, Phys. Rev. B **48**, 15957.
Reedyk, M., 1992, Ph.D. thesis (McMaster University).
Reedyk, M., D. A. Bonn, J. D. Garrett, J. E. Greedan, C. V. Stager, T. Timusk, K. Kamarás, and D. B. Tanner, 1988, Phys. Rev. B **38**, 11981.
Reedyk, M., and T. Timusk, 1992, Phys. Rev. Lett. **69**, 2705.
Reedyk, M., T. Timusk, J. S. Xue, and J. E. Greedan, 1994, Phys. Rev. B **49**, 15984.
Renner, Ch., B. Revaz, J.-Y. Genoud, K. Kadowaki, and O. Fischer, 1998, Phys. Rev. Lett. **80**, 149.
Rice, J. P., J. Giapintzakis, D. M. Ginsberg, and J. M. Mochel, 1991, Phys. Rev. B **44**, 10158.
Rieck, C. T., W. A. Little, J. Ruvalds, and A. Virosztek, 1995, Phys. Rev. B **51**, 3772.
Rigal, L. B., D. C. Schmadel, H. D. Drew, B. Maiorov, E. Osquigil, J. S. Preston, R. Hughes, and G. D. Gu, 2004, Phys. Rev. Lett. **93**, 137002.
Rojo, A. G., and K. Levin, 1993, Phys. Rev. B **48**, 16861.
Romero, D. B., C. D. Porter, D. B. Tanner, L. Forro, D. Mandrus, L. Mihaly, G. L. Carr, and G. P. Williams, 1992, Phys. Rev. Lett. **68**, 1590.
Rotter, L. D., *et al.*, 1991, Phys. Rev. Lett. **67**, 2741.
Rübhausen, M., A. Gozar, M. V. Klein, P. Guptasarma, and D. G. Hinks, 2001, Phys. Rev. B **63**, 224514.
Sachdev, S., 1989, Phys. Rev. B **39**, 12232.
Sachdev, S., 2003, Rev. Mod. Phys. **75**, 913.
Sacuto, A., R. Combescot, N. Bontemps, C. A. Müller, N. Vialett, and D. Colson, 1998, Phys. Rev. B **58**, 11721.
Santander-Syro, A., R. P. S. M. Lobo, N. Bontemps, Z. Konstantinovic, Z. Z. Li, and H. Raffy, 2003, Europhys. Lett. **62**, 568.
Santander-Syro, A., R. P. S. M. Lobo, N. Bontemps, W. Lopera, D. Girata, Z. Konstantinovic, Z. Z. Li, and H. Raffy, 2004, Phys. Rev. B **70**, 134504.
Scalapino, D., 1995, Phys. Rep. **250**, 329.
Schachinger, E., and J. P. Carbotte, 2001, Phys. Rev. B **64**, 094501.
Schachinger, E., J. J. Tu, and J. P. Carbotte, 2003, Phys. Rev. B **67**, 214508.
Schlesinger, Z., R. T. Collins, F. Holtzberg, C. Feild, S. H. Blanton, U. Welp, G. W. Crabtree, Y. Fang, and J. Z. Liu, 1990, Phys. Rev. Lett. **65**, 801.
Schützmann, J., B. Gorshunov, K. F. Renk, J. Münzel, A. Zibold, H. P. Geserich, A. Erb, and G. Muller-Vogt, 1992, Phys. Rev. B **46**, 512.
Schützmann, J., H. Somal, A. A. Tsevetkov, D. van der Marel, G. E. J. Koops, N. Kolesnikov, Z. F. Ren, J. H. Wang, E. Bruk, and A. A. Menovsky, 1997, Phys. Rev. B **55**, 11118.
Schützmann, J., S. Tajima, S. Miyamoto, and S. Tanaka, 1994, Phys. Rev. Lett. **73**, 174.
Schwartz, A., M. Dressel, G. Grüner, V. Vescoli, L. Degiorgi, and T. Giamarchi, 1998, Phys. Rev. B **58**, 1261.
Segre, G. P., N. Gedik, J. Orenstein, D. A. Bonn, R. Liang, and W. N. Hardy, 2002, Phys. Rev. Lett. **88**, 137001.
Shah, N., and A. J. Millis, 2001, Phys. Rev. B **64**, 174506.
Shibata, H., 2001, Phys. Rev. Lett. **86**, 2122.
Shibata, H., and T. Yamada, 1998, Phys. Rev. Lett. **81**, 3519.
Shibauchi, T., H. Kitano, A. Maeda, H. Asaoka, H. Takei, I. Chigaki, T. Kimura, K. Kishio, K. Izumi, T. Suzuki, and K. Uchinokura, 1996, J. Phys. Soc. Jpn. **65**, 3266.
Shibauchi, T., H. Kitano, K. Uchinokura, A. Maeda, T. Kimura, and K. Kishio, 1994, Phys. Rev. Lett. **72**, 2263.
Shibauchi, T., L. Krusin-Elbaum, Ming Li, M. P. Maley, and P. H. Kes, 2001, Phys. Rev. Lett. **86**, 5763.
Shibauchi, T., T. Nakano, M. Sato, T. Kisu, N. Kameda, N. Okuda, S. Ooi, and T. Tamegai, 1999, Phys. Rev. Lett. **83**, 1010.
Shulga, S. V., O. V. Dolgov, and E. G. Maksimov, 1991, Physica C **178**, 266.
Singley, E. J., M. Abo-Bakr, D. N. Basov, G. Blumberg, J. Feikes, P. Guptasarma, K. Holldack, H. W. Hübers, P. Kuske, M. C. Martin, W. B. Peatman, U. Schade, and G. Wüstefeld, 2004, unpublished.
Singley, E. J., D. N. Basov, K. Kurahashi, T. Uefuji, and K. Yamada, 2001, Phys. Rev. B **64**, 224503.
Skinta, J. A., M.-S. Kim, T. R. Lemberger, T. Greibe, and M. Naito, 2002, Phys. Rev. Lett. **88**, 207005.
Skinta, J. A., T. R. Lemberger, T. Greibe, and M. Naito, 2002, Phys. Rev. Lett. **88**, 207003.
Smith, D. Y., 1976, J. Opt. Soc. Am. **66**, 547.
Smith, D. Y., 1998, in *Handbook of Optical Constants of Solids*, edited by E. D. Palik (Academic Press, New York), p. 35.
Smith, D. Y., and E. Shiles, 1978, Phys. Rev. B **17**, 4689.
Smith, R. A., and V. Ambegaokar, 1992, Phys. Rev. B **45**, 2463.
Sondhi, S. L., S. M. Girvin, J. P. Carini, and D. Shahar, 1997, Rev. Mod. Phys. **69**, 315.
Spielman, S., B. Parks, J. Orenstein, D. T. Nemeth, F. Ludwig, J. Clarke, P. Merchant, and D. J. Lew, 1994, Phys. Rev. Lett. **73**, 1537.
Statt, B. W., and A. Griffin, 1992, Phys. Rev. B **46**, 3199.
Stojkovic, B. P., and D. Pines, 1996, Phys. Rev. Lett. **76**, 811.
Sun, A. G., S. H. Han, A. S. Katz, D. A. Gajewski, M. B. Maple, and R. C. Dynes, 1995, Phys. Rev. B **52**, R15731.
Sun, A. G., L. M. Paulius, D. A. Gajewskim, M. B. Maple, and R. C. Dynes, 1994, Phys. Rev. B **50**, 3266.
Suzuki, M., and T. Watanabe, 2000, Phys. Rev. Lett. **85**, 4787.
Taillefer, L., B. Lussier, R. Gagnon, K. Behnia, and H. Aubin, 1997, Phys. Rev. Lett. **79**, 483.
Tajima, S., J. Schützmann, S. Miyamoto, I. Terasaki, Y. Sato, and R. Hauff, 1997, Phys. Rev. B **55**, 6051.
Tajima, S., S. Uchida, D. van der Marel, and D. N. Basov, 2003, Phys. Rev. Lett. **91**, 129701.
Tajima, S., N. L. Wang, N. Ichikawa, H. Eisaki, S. Uchida, H. Kitano, T. Hanaguri, and A. Maeda, 1999, Europhys. Lett. **47**, 715.
Takenaka, K., K. Mizuhashi, H. Takagi, and S. Uchida, 1994, Phys. Rev. B **50**, R6534.
Takenaka, K., K. Nakada, A. Osuka, S. Horii, H. Ikuta, I. Hirabayashi, S. Sugai, and U. Mizutani, 2000, Phys. Rev. Lett. **85**, 5428.
Takenaka, K., J. Nohara, R. Shiozaki, and S. Sugai, 2003, Phys. Rev. B **68**, 134501.
Tallon, J. L., C. Bernhard, U. Binninger, A. Hofer, G. V. M. Williams, E. J. Ansaldo, J. I. Budnick, and Ch. Niedermayer, 1995, Phys. Rev. Lett. **74**, 1008.
Tamasaku, K., Y. Nakamura, and S. Uchida, 1992, Phys. Rev. Lett. **69**, 1455.
Tanner, D. B., F. Gao, M. Quijada, D. B. Romero, J. P. Rice, D. M. Ginsberg, J. Talivacchio, M. G. Forrester, L. Forro, D. Mandrus, L. Mihaly, G. L. Carr, and G. P. Williams, 1992, J. Phys. Chem. Solids **53**, 1611.
Tanner, D. B., and T. Timusk, 1992, in *Physical Properties of High Temperature Superconductors III*, edited by D. M. Ginsberg (World Scientific, Singapore), p. 363.
Tanner, D. B., Y. Yoon, A. Zibold, H. L. Liu, M. A. Quijada, S.

W. Moore, J. M. Graubeal, Beom-Hoan O, J. T. Market, R. J. Kelly, M. Onellion, and J.-H. Cho, 1996, Proc. SPIE **2696**, 13.
Tao, H. J., F. Lu, and E. L. Wolf, 1997, Physica C **282**, 1507.
Thomas, G. A., J. Orenstein, D. H. Rapkine, M. Capizzi, A. J. Millis, R. N. Bhatt, L. F. Schneemeyer, and J. V. Waszczak, 1988, Phys. Rev. Lett. **61**, 1313.
Thomsen, C., and M. Cardona, 1989, in *Physical Properties of High Temperature Superconductors I*, edited by D. M. Ginsberg (World Scientific, Singapore).
Thorsmølle, V. K., R. D. Averitt, M. P. Maley, M. F. Hundley, A. E. Koshelev, L. N. Bulaevskii, and A. J. Taylor, 2002, Phys. Rev. B **66**, 012519.
Timusk, T., 2003, Solid State Commun. **127**, 337.
Timusk, T., and C. C. Homes, 2003, Solid State Commun. **126**, 63.
Timusk, T., C. C. Homes, and W. Reichardt, 1995, in *International Workshop on the Anharmonic Properties of High T_c Cuprates*, Bled, Slovenia, edited by G. Ruani (World Scientific, Singapore), p. 121.
Timusk, T., and B. Statt, 1999, Rep. Prog. Phys. **62**, 61.
Timusk, T., and D. B. Tanner, 1989, in *Physical Properties of High Temperature Superconductors I*, edited by M. Ginsberg (World Scientific, Singapore), p. 339.
Tinkham, M., 1974, Rev. Mod. Phys. **46**, 587.
Tinkham, M., and R. A. Ferrell, 1959, Phys. Rev. Lett. **2**, 331.
Tokura, Y., S. Koshinara, T. Arima, H. Takagi, S. Ishibashi, and S. Uchida, 1990, Phys. Rev. B **41**, 11657.
Toll, J. S., 1956, Phys. Rev. **104**, 1760.
Toplygo, S. K., J.-Y. Lin, M. Gurvitch, S. Y. Hou, and J. Phillips, 1996, Phys. Rev. B **53**, 12454.
Tranquada, J. M., J. D. Axe, N. Ichikawa, Y. Nakamura, S. Uchida, and B. Nachumi, 1996, Phys. Rev. B **54**, 7489.
Tranquada, J. M., B. J. Sternlieb, J. D. Axe, Y. Nakamura, and S. Uchida, 1995, Nature (London) **373**, 561.
Trugman, S. A., 1988, Phys. Rev. B **37**, 1597.
Tsui, O. K. C., N. P. Ong, and J. B. Peterson, 1996, Phys. Rev. Lett. **76**, 819.
Tsvetkov, A. A., D. van der Marel, K. A. Moler, J. R. Kirtley, J. L. de Boer, A. Meetsma, Z. F. Ren, N. Koleshnikov, D. Dulic, A. Damascelli, M. Grüninger, J. Schützmann, J. W. van der Eb, H. S. Somal, and J. H. Wang, 1998, Nature (London) **395**, 360.
Tu, J. J., C. C. Homes, G. D. Gu, D. N. Basov, and M. Strongin, 2002, Phys. Rev. B **66**, 144514.
Turner, P. J., *et al.*, 2003, Phys. Rev. Lett. **90**, 237005.
Uchida, S., T. Ido, H. Takagi, T. Arima, Y. Tokura, and S. Tajima, 1991, Phys. Rev. B **43**, 7942.
Uchida, S., K. Tamasaku, and S. Tajima, 1996, Phys. Rev. B **53**, 1.
Uemura, Y. J., 1996, in *Proceedings of the 10th Aniversary HTS Workshop*, edited by B. Batlogg, C. W. Chu, W. K. Chu, D. U. Gubser, and K. A. Müller (World Scientific, Singapore), p. 68.
Uemura, Y. J., L. P. Le, G. M. Luke, B. J. Sternlieb, W. D. Wu, J. H. Brewer, T. M. Riseman, C. L. Seamen, M. B. Maple, M. Ishikawa, D. G. Hinks, J. D. Jorgensen, G. Saito, and H. Yamochi, 1991, Phys. Rev. Lett. **66**, 2665.
Uemura, Y. J., G. M. Luke, B. J. Sternlieb, J. H. Brewer, J. F. Carolan, W. N. Hardy, R. Kadono, J. R. Kempton, R. F. Kiefl, S. R. Kreitzman, P. Mulhern, T. M. Riseman, D. L. Williams, B. X. Yang, S. Uchida, H. Takagi, J. Gopalakrishnan, A. W. Sleight, M. A. Subramanian, C. L. Chien, M. Z. Cieplak, G. Xiao, V. Y. Lee, B. W. Statt, C. E. Stronach, W. J. Kossler, and X. H. Yu, 1989, Phys. Rev. Lett. **62**, 2317.
Valles, J. M., A. E. White, K. T. Short, R. C. Dynes, J. P. Garno, A. F. J. Levi, M. Anzlowar, and K. Baldwin, 1989, Phys. Rev. B **39**, 11599.
van Bentum, P. J. M., A. M. Gerrits, M. E. J. Boonman, A. Wittlin, V. H. M. Duijn, and A. A. Menovsky, 1995, Physica B **211**, 260.
van der Eb, J. W., A. B. Kuz'menko, and D. van der Marel, 2001, Phys. Rev. Lett. **86**, 3407.
van der Marel, D., 2003, in *Physics and Chemistry of Materials with Low-Dimensional Structures*, Interaction Electrons in Low Dimensions (Kluwer Academic, Dordrecht).
van der Marel, D., 2004, J. Supercond. **17**, 559.
van der Marel, D., and J. H. Kim, 1995, J. Phys. Chem. Solids **56**, 1825.
van der Marel, D., H. J. A. Molegraaf, J. Zaanen, Z. Nussinov, F. Carbone, A. Damascelli, H. Eisaki, M. Greven, P. H. Kes, and M. Li, 2003, Nature (London) **425**, 271.
van der Marel, D., and A. Tsvetkov, 1996, Czech. J. Phys. **46**, 3165.
van der Marel, D., and A. A. Tsvetkov, 2001, Phys. Rev. B **64**, 024530.
Van Harlingen, D. J., 1995, Rev. Mod. Phys. **67**, 515.
Varma, C. M., and E. Abrahams, 2001, Phys. Rev. Lett. **86**, 4652.
Varma, C. M., P. B. Littlewood, S. Schmitt-Rink, E. Abrahams, and A. E. Ruckenstein, 1989, Phys. Rev. Lett. **63**, 1996.
Varma, C. M., Z. Nussinov, and W. von Saarlos, 2002, Phys. Rep. **361**, 267.
Vescoli, V., L. Degiorgi, W. Henderson, G. Grner, K. P. Starkey, and L. K. Montgomery, 1998, Science **281**, 1181.
Vinokur, V. M., V. B. Geshkenbein, M. V. Feigel'man, and G. Blatter, 1993, Phys. Rev. Lett. **71**, 1242.
Virosztek, A., and J. Ruvalds, 1990, Phys. Rev. B **42**, 4064.
Waku, K., T. Katsufuji, Y. Kohsaka, T. Sasagawa, H. Takagi, H. Kishida, H. Okamoto, M. Azuma, and M. Takano, 2004, Phys. Rev. B **70**, 134501.
Walker, M. B., and M. F. Smith, 2000, Phys. Rev. B **61**, 11285.
Wang, N. L., G. Li, Dong Wu, X. H. Chen, C. H. Wang, and H. Ding, 2004, e-print cond-mat/0410242.
Wang, N. L., S. Tajima, A. I. Rykov, and K. Tomimoto, 1998, Phys. Rev. B **57**, R11081.
Wang, N. L., P. Zheng, J. L. Luo, Z. J. Chen, S. L. Yan, L. Fang, and Y. C. Ma, 2003, Phys. Rev. B **68**, 054516.
Wang, Y., and A. H. MacDonald, 1999, Solid State Commun. **64**, 289.
Wang, Y., Z. A. Xu, T. Kakeshita, S. Uchida, S. Ono, Y. Ando, and N. P. Ong, 2001, Phys. Rev. B **64**, 224519.
Warren, W. W., R. E. Walstedt, G. F. Brennert, R. J. Cava, R. Tycko, R. F. Bell, and G. Dabbagh, 1989, Phys. Rev. Lett. **62**, 1193.
Webb, B. C., A. J. Sievers, and T. Mihalisin, 1986, Phys. Rev. Lett. **57**, 1951.
Welp, U., S. Fleshler, W. K. Kwok, J. Downey, Y. Fang, and G. W. Crabtree, 1990, Phys. Rev. B **42**, 10189.
Wheatley, J. M., T. C. Hsu, and P. W. Anderson, 1988, Phys. Rev. B **37**, 5897.
White, S. R., and D. J. Scalapino, 1998, Phys. Rev. Lett. **81**, 3227.
Wiesmann, H., M. Gurvitch, H. Lutz, A. Ghosh, B. Schwarz, M. Strongin, P. B. Allen, and J. W. Halley, 1977, Phys. Rev. Lett. **38**, 782.
Williams, G. P., R. C. Budhani, C. J. Hirschmugl, G. L. Carr, S. Perkowitz, B. Lou, and T. R. Yang, 1990, Phys. Rev. B **41**,

4752.
Won, H., H. Jang, and K. Maki, 2000, Physica B **281**, 944.
Wooten, F., 1972, *Optical Properties of Solids* (Academic, New York/London).
Wu, D. H., J. Mao, S. N. Mao, J. L. Peng, X. X. Xi, T. Venkatesan, R. L. Greene, and S. M. Anlage, 1993, Phys. Rev. Lett. **70**, 85.
Xiang, T., and J. M. Wheatley, 1995, Phys. Rev. B **51**, 11721.
Xu, D., S. K. Yip, and J. A. Sauls, 1995, Phys. Rev. B **51**, 16233.
Xu, Z. A., N. P. Ong, Y. Wang, T. Kakeshita, and S. Uchida, 2000, Nature (London) **405**, 486.
Yamada, K., C. H. Lee, K. Kurahashi, J. Wada, S. Wakimoto, S. Ueki, H. Kimura, Y. Endoh, S. Hosoya, G. Shirane, R. J. Birgeneau, M. Greven, M. A. Kastner, and Y. J. Kim, 1998, Phys. Rev. B **57**, 6165.
Yang, K., and S. L. Sondhi, 1998, Phys. Rev. B **57**, 8566.
Yip, S. K., and J. A. Sauls, 1992, Phys. Rev. Lett. **69**, 2264.
Yoshida, T., *et al.*, 2003, Phys. Rev. Lett. **91**, 027001.
Yoshinari, Y., H. Yasuoka, Y. Ueda, K. Koga, and K. Kosuge, 1990, J. Phys. Soc. Jpn. **59**, 3698.
Zaanen, J., 2004, Nature (London) **430**, 512.
Zaanen, J., G. A. Sawatzky, and J. W. Allen, 1985, Phys. Rev. Lett. **55**, 418.
Zelezny, V., S. Tajima, D. Munzar, T. Motohashi, J. Shimoyama, and K. Kishio, 2001, Phys. Rev. B **63**, 060502(R).
Zhang, K., D. A. Bonn, S. Kamal, R. Liang, D. J. Baar, W. N. Hardy, D. Basov, and T. Timusk, 1994, Phys. Rev. Lett. **73**, 2484.
Zheleznyak, A. T., V. M. Yakovenko, H. D. Drew, and I. I. Mazin, 1998, Phys. Rev. B **57**, 3089.
Zheng, X. C., P. M. Hui, and D. Stroud, 1989, Phys. Rev. B **39**, 1063.
Zhou, X. J., P. Bogdanov, S. A. Kellar, T. Noda, H. Eisaki, S. Uchida, Z. Hussain, and Z.-X. Shen, 1999, Science **286**, 268.
Zhou, X. J., T. Yoshida, S. A. Kellar, P. V. Bogdanov, E. D. Lu, A. Lanzara, M. Nakamura, T. Noda, T. Kakeshita, H. Eisaki, S. Uchida, A. Fujimori, Z. Hussain, and Z.-X. Shen, 2001, Phys. Rev. Lett. **86**, 5578.
Zhou, X. J., T. Yoshida, A. Lanzara, P. V. Bogdanov, S. A. Kellar, M. Shen, W. L. Yang, F. Ronning, T. Sasagawa, T. Kakeshita, T. Noda, H. Eisaki, S. Uchida, C. T. Lin, F. Zhou, J. W. Xiong, W. X. Ti, Z. X. Zhao, A. Fujimori, Z. Hussain, and Z.-X. Shen, 2003, Nature (London) **423**, 398.
Zimmermann, W., E. H. Brandt, M. Bauer, E. Seider, and L. Genzel, 1991, Physica C **183**, 99.
Zimmers, A., J. M. Tomczak, R. P. S. M. Lobo, N. Bontemps, C. P. Hill, M. C. Barr, Y. Dagan, R. L. Greene, A. J. Millis, and C. C. Homes, 2004, e-print cond-mat/0406204.
Zutic, I., and O. T. Valls, 1997, Phys. Rev. B **56**, 11279.